1-1-2022

Exploring the Standard Model and Beyond using B and D meson decays

John Waite

EXPLORING THE STANDARD MODEL AND BEYOND WITH B AND D MESON DECAYS

John Vincent Waite

A dissertation presented for the degree of

Doctor of Philosophy

Department of Physics and Astronomy

University of Mississippi

May 2022

Abstract

In this research, I have tested the standard model(SM) and various new physics (NP) models using B and D meson decays. In D meson decays, the $SU(3)$ flavor symmetry of the SM for Cabibbo favored decays is tested against experimental measurements. The $SU(3)$ analysis with η and η' are considered in a general and consistent way for the first time. In B decays, a fit to the data for four $B \to \pi K$ decays is performed, within the SM and with NP. The fit confirms that the SM gives a poor fit to the $B \to \pi K$ data which is known as the $B \to \pi K$ "puzzle". A solution to the $B \to \pi K$ "puzzle" is presented in terms of an axion like particle (ALP) with a mass near the neutral pion mass. Several search strategies to observe this particle in various experiments have also been explored. Finally, an explanation of the $B \to \pi K$ "puzzle" via the presence of diquarks is considered. The possibility to generate neutrino masses and mixing via a combination of diquarks and leptoquarks is also discussed. The leptoquark can account for the lepton universality violating anomalies in semileptonic B decays.

Acknowledgements

I would like to thank my advisor, Alakabha Datta, for his guidance and support to complete this work. I would also like to thank the various collaborators on the papers that went into this dissertation. Finally, I would like to thank my wife, Kelly, for the sacrifices she has had to make over the years.

Contents

List of Tables

List of Figures

1 Introduction

The Standard Model as presently constituted does an excellent job of describing the phenomena we observe in the universe. Over the past century the SM has been created, modified and amended as more observations have been made. As a fundamental theory it is highly successful, but as more data has been accumulated some discrepancies between the theory and certain observables have emerged; and as has happened throughout the history of science, we recognize the need to again either modify or expand the model. Care must be taken when doing so due to the high level of agreement between theory and experiment that does exist. We don't want those aspects of the theory that work to be significantly altered by anything we change or add. The motivation for the work that follows comes from the following shortcomings in the Standard Model:

- CP asymmetry in the Charm decay sector
- CP asymmetry in the Bottom decay sector
- Origin of neutrino masses
- The question of lepton universality

The research that I have carried out deals with addressing these areas testing the effectiveness of the Standard Model, and presenting physics Beyond the Standard Model, as well as informing some future experimental search strategies for distinguishing signals indicating New Physics.

The research is presented as follows: A brief introduction of the SM will comprise Section 2. Section 3 explores the connection between $SU(3)$ matrix elements and flavor flow diagrams in the D system. Section 4 considers R-parity violating supersymmetry to explain CP asymmetry, also in the D system. Section 5 transitions to the B

system and introduces diquarks and leptoquarks. Section 6 discusses the introduction of an axion-like particle (ALP) to resolve the $B \to \pi K$ puzzle. Section 7 is an attempt to created detector signals of the ALP that could potentially be measured at various experiments.

2 The Standard Model

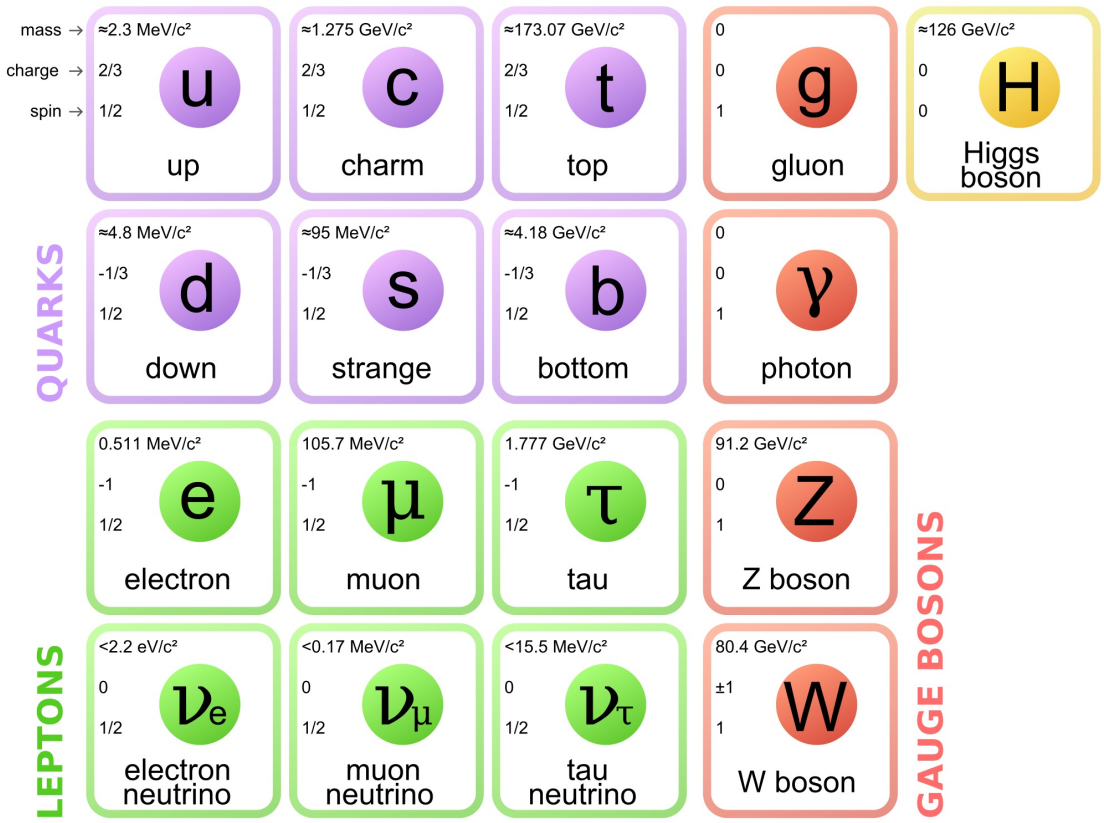

Figure 1: The Standard Model, as presently constituted.

The Standard Model currently consists of classes of fermions (spin 1/2, matter particles) and bosons (spin 1 force carriers). The fermions are further classified into leptons and quarks. The leptons come in two separate classes and three different flavors. The class of charged leptons consist of electrons (e), muon (μ), and tau (τ) particles, each carrying an electric charge of $q = -1\ e$ (where e is the fundamental electric charge). The flavors are listed here in order of increasing mass. Each of these leptons has an associated neutrino that is electrically neutral. The neutrinos constitute the second class of leptons. The quarks are similarly separated into two classes and three flavors. The up-type quarks carry a charge of $q = +2/3\ e$ and the down-type quarks carry a charge of $q = -1/3\ e$. The three flavors for the up-type class are

the up (u), charm (c), and top (t). The down-type quarks are the down (d), strange (s), and bottom (b). These are again listed in order of increasing mass. The quarks furthermore possess a color charge, similar to electric charge but more complicated. The electric charge comes in a single type, whereas the color charge comes in three types referred to as red, green and blue. These particle constitute all of the known matter in the universe. Since decay processes proceed in the direction of decreasing mass, the only stable fermions that we observe in nature are the up and down quarks, the neutrinos, and the electron. All of the other fermions are unstable and decay into lighter particles.

The bosons of the Standard Model mediate the different forces that particles feel. The known forces in the universe are the gravitational, electromagnetic, weak and strong forces. These forces cause particles to interact that possess the specific property that couples the fermion field to the boson field. Particles that possess mass interact via the gravitational force, which is mediated by the graviton (predicted but not yet observed). Particles that possess electric charge interact through the electromagnetic force mediated by the photon. Particles that possess flavor interact through the weak force mediated by the $W^{\pm}$, and Z bosons. Particles that possess color interact through the strong force mediated by gluons. While the gravitational and electromagnetic forces have been observed and studied for centuries, the weak and strong forces are less familiar. The weak interaction was first observed in the 1930s and is the process that is responsible for radioactive decay of atoms and nuclear reactions. The strong interaction, first formalized in the 1970s, is responsible for binding protons and neutrons in the nucleus of an atom as well as binding the quarks that protons and neutrons are composed of.

The strong force is responsible for binding quarks together and within the SM this binding occurs between 3 quarks (baryons) or a quark/anti-quark pair (mesons). Quarks have never been observed by themselves, they only exist as components of baryons or mesons. This is due to what is referred to as color confinement (the overall color charge of all existing matter is neutral).

The weak force is responsible for the decay of atomic nuclei. There are three separate regimes in which this interaction occurs: leptonic, semi-leptonic and non-leptonic. All of these interactions are flavor changing. These interactions occur through the following basic vertices.

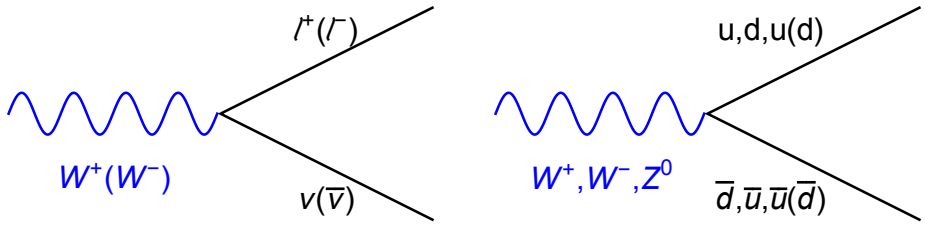

Figure 2: The Standard Model vertices for the weak interaction. The figure on the left is the leptonic vertex, the figure on the right shows the quark vertex. The vertex factors are given in Section 3. The quark vertex has an additional factor from the CKM matrix due to quark mixing.

2.1 Symmetries

It is common when discussing the fundamental interactions within the SM to frame the analysis in terms of symmetries. The main symmetries that come under consideration are referred to as C (charge conjugation), P (parity), and T (time inversion). The charge conjugation operation transforms a particle into its anti-particle without affecting the chirality or spin of the particle. This means that a left-handed particle will transform into a left-handed anti-particle. The parity transformation inverts space which does change chirality. The time inversion operation reverses the direction of the flow of time. Violations of these symmetries have been investigated for many years. The charge conjugation and parity symmetries are broken by the weak interaction since these processes are chiral in nature, transforming left(right)-handed particles to right(left)-handed anti-particles. While the weak interaction breaks each of these symmetries individually, taking them both together, (CP symmetry), it was thought for many years that this was a preserved symmetry. In a model that preserves this CP symmetry the decay of particles would proceed at the same rate as the decay of the corresponding anti-particles. The first bit of evidence that there is some disagreement

between the two decay rates is that the observed universe contains an abundance of matter and essentially no anti-matter. As experiments became more sophisticated and large numbers of decays were measured, CP asymmetries have become more pronounced. While there are mechanisms within the SM that allow CP asymmetry, the degree of the violation of this symmetry is as yet unexplained.

3 Flavor $SU(3)$ in Cabibbo-favored D meson decays

Studies of non-leptonic decays of charmed mesons constitute a primary method of investigations into direct CP-violation in that system. Even though the experimental precision for studying D decays has steadily improved over the past decade, theory calculations have faced severe challenges. Precise numerical predictions of CP-violating observables are not possible at the moment due to large non-perturbative contributions from strong interactions affecting weak-decay amplitudes. A way out in such a situation involves phenomenological fits of decay amplitudes to experimentally measured decay widths of charmed mesons. If the number of fit parameters is smaller than the number of experimentally measured observables, then predictions are possible. Such fits require a defined procedure on how to parametrize complex-valued decay amplitudes [1].

One way to approach the problem is to note that the light-quark operators in the weak effective Hamiltonian governing heavy-quark decays, as well as the initial and final states form product representations of a flavor $SU(3)_F$ group. These product representations can be reduced with the help of the Wigner-Eckart theorem. This way, a basis is chosen, in which all decay amplitudes can be expanded in terms of the reduced matrix elements. Such an approach was applied to both B-decays [2, 3, 4, 5] and D-decays [6, 7, 8, 4, 5]. In the limit of exact $SU(3)_F$ symmetry, all decays of a triplet of D-mesons, D^0, D^+, and D_s^+, into two light octet meson states can be parametrized in terms of five independent complex parameters [6]. We will refer to this approach as the "$SU(3)_F$ matrix-elements approach."

Alternatively, a topological flavor-flow approach can be used. Developed in the study of B-decays [9, 10, 11, 4, 5], it has been applied to the charm sector [12, 13, 4, 5]. The flavor-flow approach postulates a basis of universal flavor topologies for various

decay amplitudes.[1] $SU(3)_F$ symmetry can be used to relate decay amplitudes, as both the light-quark final states and initial D-mesons transform under it. These universal topological amplitudes can be fitted to the existing experimental data. Due to long-distance effects, particularly rescattering among hadronic final states, often multiple flavor-flow diagrams contribute to the same process. A subset of *linear combinations* of flavor-flow amplitudes can then be identified as the basis set for the flavor-flow approach.

The two approaches described above are equivalent if the number of reduced matrix elements in the $SU(3)_F$ matrix-elements approach is equal to the number of diagrammatic combinations in the flavor-flow approach, both describing the same set of decay amplitudes. Such an equivalence has been shown in the of exact $SU(3)_F$ symmetry [9, 14], as well as when first-order $SU(3)_F$-breaking corrections are taken into account [15]. Here we revisit the question of equivalence of the two descriptions and discuss the fit quality of the available data in both approaches.

Non-leptonic decays of charmed mesons can be additionally classified according to the rate of suppression of the (leading-order) weak-decay amplitudes by the Wolfenstein parameter, $\lambda = \sin\theta \simeq 0.2$ [16], where θ is the Cabibbo angle. Such amplitudes may contain zero, one, or two powers of λ. Weak-hadronic decays of charm are, therefore, categorized into Cabibbo-favored (CF) decays ($\mathcal{A} \propto V_{cs}^* V_{ud} \sim \mathcal{O}(1)$), singly-Cabibbo-suppressed (SCS) decays ($\mathcal{A} \propto V_{cq}^* V_{uq} \sim \mathcal{O}(\lambda)$ where $q = d, s$), and doubly-Cabibbo-suppressed (DCS) decays ($\mathcal{A} \propto V_{cd}^* V_{us} \sim \mathcal{O}(\lambda^2)$). Since such classification is external to QCD, both the flavor $SU(3)_F$ and topological flavor-flow approaches can, in principle, be used to parametrize all CF, SCS, and DCS amplitudes. This can be considered as an advantage, as some fit parameters can be obtained from the CF and/or DCS transitions and then used to predict CP-violating asymmetries in SCS decays [17, 18, 19, 20, 21]. This is so because the quark-level transitions for CF ($c \to sud\bar{}$) and DCS ($c \to du\bar{s}$) modes involve four distinct quark flavors that be-

[1] We remind the reader that while the flavor-flow diagrams do resemble Feynman graphs, they are not computed in perturbative field theory due to large non-perturbative QCD effects.

long to the first two generations and therefore do not generate CP-asymmetries in the Standard Model at leading order in λ. To execute this program one needs to control $SU(3)_F$-breaking corrections in both approaches [7, 8, 15, 22, 23].

Here we take a different look at the equivalency of the flavor $SU(3)_F$ and the topological flavor-flow approaches. Since the Wolfenstein parameter λ is external to any QCD-based parametrization of decay amplitudes, one can, theoretically, dial any value for it. In particular, setting $\lambda = 0$ would only leave CF decays as experimental data for a fit. It is interesting to note that in this case, in the $SU(3)_F$ limit, we would be left with *three* irreducible $SU(3)_F$ amplitudes and *four* topological flavor-flow amplitudes. In this paper we explore the equivalency of the phenomenological descriptions of CF charmed-meson decays in light of this discrepancy.

This paper is organized as follows. In Section 3.1 we review both the flavor $SU(3)_F$ and topological flavor-flow approaches to CF charm decays. We extend the discussion by including CF decays with the real η and η' states and present associated fits. In Section 3.2, we discuss the connections between those two approaches. We conclude in Section 3.3.

3.1 Cabibbo-favored decays in light of flavor-$SU(3)$ symmetry

$SU(3)_F$ symmetry plays a prominent role in both the $SU(3)_F$ matrix-elements and topological flavor-flow approaches. Both methods use the fact that the initial and final states transform under some product representations of the $SU(3)_F$ group. In particular, the initial state D-mesons, $|D^0\rangle, |D^+\rangle, |D_s^+\rangle$, form a triplet of $SU(3)_F$, while the nine pseudoscalar mesons $(\pi^\pm, \pi^0, K^\pm, K^0, \overline{K}^0, \eta, \eta')$ contain both an octet and a singlet. The two approaches differ by the choice of the "basis" parameters, which we discuss below.

In what follows, we employ physical η and η' states that are constructed from

the $SU(3)$ octet η_8 and the singlet η_1 states using octet-singlet mixing,

$$\begin{aligned} \eta &= -\cos\theta\,\eta_8 - \sin\theta\,\eta_1, \\ \eta' &= -\sin\theta\,\eta_8 + \cos\theta\,\eta_1, \end{aligned} \tag{1}$$

where the octet η_8 and the singlet η_1 states are defined as

$$\begin{aligned} \eta_8 &= (u\bar{u} + d\bar{d} - 2\,s\bar{s})/\sqrt{6}, \\ \eta_1 &= (u\bar{u} + d\bar{d} + s\bar{s})/\sqrt{3}, \end{aligned} \tag{2}$$

and θ is the $\eta - \eta'$ mixing angle. This mixing angle has nothing to do with weak decays of heavy flavors and can be fixed externally, for example from B-meson decays [24] or radiative decays of J/ψ [25] into η and η' final states. Thus, we do not consider it a fit parameter. Oftentimes, we will use $\theta = \arcsin(1/3)$.

3.1.1 $SU(3)_F$ matrix-elements approach

The $SU(3)_F$ matrix-elements approach uses the fact that the Hamiltonian governing D decays into the light mesons also transforms as a product representations of $SU(3)_F$. The quark-level Hamiltonian for CF D-meson decays can be written as

$$\mathcal{H}_{\rm CF} = \frac{G_F}{\sqrt{2}} V_{ud} V_{cs}^* (\bar{u}d)(\bar{s}c) + \text{h.c.} \tag{3}$$

We begin by considering the Wigner-Eckart decompositions of the CF $D \to PP$ amplitudes using $SU(3)_F$ symmetry. An element of $SU(3)$ can be represented using the state $|\boldsymbol{r} Y I I_3\rangle$ where $\boldsymbol{r}$ is the irreducible representation (irrep) of the state, Y is its hypercharge, while I and I_3 stand for the isospin and its third component, respectively. Under $SU(3)_F$ symmetry, the light quarks u, d, and s (and the respective antiquarks)

transform as the fundamental triplet (anti-triplet) represented by,

$$|u\rangle = \left|\mathbf{3}, \frac{1}{3}, \frac{1}{2}, \frac{1}{2}\right\rangle , \quad |d\rangle = \left|\mathbf{3}, \frac{1}{3}, \frac{1}{2}, -\frac{1}{2}\right\rangle , \quad |s\rangle = \left|\mathbf{3}, -\frac{2}{3}, 0, 0\right\rangle , \tag{4}$$

$$|\overline{u}\rangle = -\left|\overline{\mathbf{3}}, -\frac{1}{3}, \frac{1}{2}, -\frac{1}{2}\right\rangle , \quad |\overline{d}\rangle = \left|\overline{\mathbf{3}}, \frac{1}{3}, \frac{1}{2}, \frac{1}{2}\right\rangle , \quad |\overline{s}\rangle = \left|\overline{\mathbf{3}}, \frac{2}{3}, 0, 0\right\rangle . \tag{5}$$

The charm quark (and anti-quark) is heavy and transforms as an $SU(3)_F$ singlet represented by $|\mathbf{1}, 0, 0, 0\rangle$. Using this notation one can show that the CF Hamiltonian in Eq. (3) contains the irreps $\overline{\mathbf{15}}$ and $\mathbf{6}$ [6, 8, 7] and can be represented by,

$$\mathcal{H}_{\rm CF} = -\frac{G_F}{\sqrt{2}} V_{ud} V_{cs}^* \left(A\, \mathcal{O}^{(\overline{\mathbf{15}})}_{\frac{2}{3},1,-1} + C\, \mathcal{O}^{(\mathbf{6})}_{\frac{2}{3},1,-1} \right) + \text{h.c.} , \tag{6}$$

where we have used the notation $O^{(\boldsymbol{r})}_{Y,I,I_3}$ to denote the $SU(3)$ operators, whereas A and C represent their respective coefficients.

As mentioned previously, the final states transform under a product representation of $SU(3)_F$. Since the octet-octet final states must respect Bose symmetry, we only consider the following products of $SU(3)_F$ irreps,

$$\begin{aligned} [(\mathbf{8}+\mathbf{1}) \times (\mathbf{8}+\mathbf{1})]_{PP} &= (\mathbf{8}\times\mathbf{8})_{\rm sym} + (\mathbf{8}\times\mathbf{1}) + \mathbf{1} , \\ &= \mathbf{27} + \mathbf{8}_{\mathbf{8}\times\mathbf{8}} + \mathbf{8}_{\mathbf{8}\times\mathbf{1}} + \mathbf{1}_{\mathbf{8}\times\mathbf{8}} + \mathbf{1} . \end{aligned} \tag{7}$$

Note that there are two octets in Eq. (7): one from the octet-octet final state and the other from the octet-singlet one.

Now, of the above irreps only the $\mathbf{27}$ and $\mathbf{8}$ appear in the products $\overline{\mathbf{15}} \times \mathbf{3}$ and $\mathbf{6} \times \mathbf{3}$ needed to construct the states $|\mathcal{H}|D\rangle$. Furthermore, $\overline{\mathbf{15}} \times \mathbf{3}$ contains both a $\mathbf{27}$ and an $\mathbf{8}$, while $\mathbf{6} \times \mathbf{3}$ contains only an $\mathbf{8}$. Therefore, it appears that $D \to PP$ amplitudes can be represented using the following three independent reduced matrix

elements.

$$A_{27} \;=\; \left\langle \mathbf{27}|\mathcal{O}^{\overline{\mathbf{15}}}|\mathbf{3}\right\rangle , \quad A_8 \;=\; \left\langle \mathbf{8}|\mathcal{O}^{\overline{\mathbf{15}}}|\mathbf{3}\right\rangle , \quad C_8 \;=\; \langle \mathbf{8}|\mathcal{O}^{\mathbf{6}}|\mathbf{3}\rangle \, . \tag{8}$$

These reduced matrix elements depend on five real parameters – three magnitudes and two relative strong phases (one overall phase can be ignored). The amplitudes for the CF $D \to PP$ processes can be constructed using these reduced matrix elements. As there are two different octets in Eq. (7), in general this would imply two additional reduced matrix elements for the $\mathcal{O}^{\overline{\mathbf{15}}}$ and $\mathcal{O}^{\mathbf{6}}$ operators, $A_8^{(1)}$ and $C_8^{(1)}$ respectively. In Section 3.2 we will show that indeed in order to get a complete description of these decays one must include these additional matrix elements that correspond to the $SU(3)_F$-singlet final state.

Assuming them to be the same, $A_8^{(1)} = A_8$ and $C_8^{(1)} = C_8$, which can be motivated by a nonet symmetry, the final states containing physical η and η' contain an admixture of singlet and octet $SU(3)_F$ amplitudes. The decay amplitudes into those final states can be written as shown in Table 1. Assuming, for simplicity,

Decay	Representation
$D^0 \to \overline{K}^0\eta$	$\frac{1}{10\sqrt{3}}\left[(3A_{27} - 2A_8 + \sqrt{10}C_8)\cos\theta + 2(\sqrt{10}A_8 - 5C_8)\sin\theta\right]$
$D^0 \to \overline{K}^0\eta'$	$\frac{1}{10\sqrt{3}}\left[(3A_{27} - 2A_8 + \sqrt{10}C_8)\sin\theta - 2(\sqrt{10}A_8 - 5C_8)\cos\theta\right]$
$D_s^+ \to \pi^+\eta$	$\frac{1}{5\sqrt{3}}\left[(3A_{27} - 2A_8 - \sqrt{10}C_8)\cos\theta - (\sqrt{10}A_8 + 5C_8)\sin\theta\right]$
$D_s^+ \to \pi^+\eta'$	$\frac{1}{5\sqrt{3}}\left[(3A_{27} - 2A_8 - \sqrt{10}C_8)\sin\theta + (\sqrt{10}A_8 + 5C_8)\cos\theta\right]$

Table 1: $\eta - \eta'$ decay-amplitude representations with $A_8^{(1)} = A_8$ and $C_8^{(1)} = C_8$ in the $SU(3)_F$ matrix-elements approach.

$\theta = \arcsin(1/3)$, all CF decay amplitudes can be written in terms of only three complex parameters of Eq. (8). We provide a representation of the decay amplitudes in terms of those parameters in Table 2. These matrix elements can be fit to experimentally-measured branching ratios.

The measured branching ratios, $\mathcal{B}$, for the CF $D \to PP$ decays are given in Table 3. The absolute value of each decay amplitude can be determined from the

Decay	$SU(3)_F$ Amplitude
$D^0 \to K^-\pi^+$	$\frac{G_F}{\sqrt{2}} V_{ud}V_{cs}^* \ \frac{1}{5}\left(\sqrt{2}A_{27} + \sqrt{2}A_8 - \sqrt{5}C_8\right)$
$D^0 \to \overline{K}^0\pi^0$	$\frac{G_F}{\sqrt{2}} V_{ud}V_{cs}^* \ \frac{1}{10}\left(3A_{27} - 2A_8 + \sqrt{10}C_8\right)$
$D^0 \to \overline{K}^0\eta$	$\frac{G_F}{\sqrt{2}} V_{ud}V_{cs}^* \ \frac{1}{15\sqrt{3}}\left(3\sqrt{2}A_{27} + \sqrt{2}(\sqrt{5}-2)A_8 - \sqrt{5}(\sqrt{5}-2)C_8\right)$
$D^0 \to \overline{K}^0\eta'$	$\frac{G_F}{\sqrt{2}} V_{ud}V_{cs}^* \ \frac{1}{30\sqrt{3}}\left(3A_{27} - 2(1+4\sqrt{5})A_8 + \sqrt{10}(1+4\sqrt{5})C_8\right)$
$D^+ \to \overline{K}^0\pi^+$	$\frac{G_F}{\sqrt{2}} V_{ud}V_{cs}^* \ \frac{1}{\sqrt{2}}A_{27}$
$D_s^+ \to \overline{K}^0K^+$	$\frac{G_F}{\sqrt{2}} V_{ud}V_{cs}^* \ \frac{1}{5}\left(\sqrt{2}A_{27} + \sqrt{2}A_8 + \sqrt{5}C_8\right)$
$D_s^+ \to \pi^+\eta$	$\frac{G_F}{\sqrt{2}} V_{ud}V_{cs}^* \ \frac{1}{15\sqrt{3}}\left(6\sqrt{2}A_{27} - \sqrt{2}(4+\sqrt{5})A_8 - \sqrt{5}(4+\sqrt{5})C_8\right)$
$D_s^+ \to \pi^+\eta'$	$\frac{G_F}{\sqrt{2}} V_{ud}V_{cs}^* \ \frac{1}{15\sqrt{3}}\left(3A_{27} + 2(2\sqrt{5}-1)A_8 + \sqrt{10}(2\sqrt{5}-1)C_8\right)$

Table 2: $SU(3)_F$ matrix-elements representation of Cabibbo-Favored Decays in the Standard Model. Note that the $\eta - \eta'$ angle $\theta = \arcsin(1/3)$.

measured branching ratios using,

$$|\mathcal{A}_{D\to PP}| \ = \ \sqrt{\frac{8\pi\hbar\, m_D^2\, \mathcal{B}_{D\to PP}}{\tau_D\, p^*}}, \tag{9}$$

where p^* refers to the magnitude of the three-momentum of each final-state pseudoscalar in the D-meson rest frame. Since there are eight measured $D \to PP$ branch-

Meson	Decay	Branching Ratio (%)
D^0	$K^-\pi^+$	3.950 ± 0.031
	$\overline{K}^0\pi^0$	2.480 ± 0.044
	$\overline{K}^0\eta$	1.018 ± 0.012
	$\overline{K}^0\eta'$	1.898 ± 0.064
D^+	$\overline{K}^0\pi^+$	3.124 ± 0.062
D_s^+	$\overline{K}^0K^+$	2.95 ± 0.14
	$\pi^+\eta$	1.70 ± 0.09
	$\pi^+\eta'$	3.94 ± 0.25

Table 3: Experimental branching ratios for CF D decays taken from [26].

ing ratios that depend on five real parameters (three magnitudes and two relative phases of three reduced matrix elements), a χ^2-minimization fit can be employed to determine the parameters. Such a fit has three degrees of freedom. We perform a fit by constraining the A_{27} amplitude to be purely real and find,

$$
\begin{aligned}
\chi^2_{\rm min}/{\rm dof} &= 7477/3, \\
A_{27} &= (0.279 \pm 0.002)\ {\rm GeV}^3, \\
A_8 &= (0.840 \pm 0.008)\ e^{(59\pm1)^\circ i}\,{\rm GeV}^3, \\
C_8 &= (0.17 \pm 0.02)\ e^{(-58\pm2)^\circ i}\,{\rm GeV}^3. \qquad (10)
\end{aligned}
$$

Clearly, the fit is very poor. This leads us to believe that the above description of CF $D \to PP$ decays in terms of the minimum number of $SU(3)_F$ reduced matrix elements is incomplete and needs to be modified.

In the next section we discuss another parametrization of the same matrix elements, in terms of the topological flavor-flow amplitudes. We again identify the minimal set of basis amplitudes to describe the CF decays in the flavor-$SU(3)$ limit. This minimal set appears to work better, seemingly providing an adequate description of CF decays, including those with the η and η' mesons in the final state.

3.1.2 Topological flavor-flow approach

The eight CF $D \to PP$ decays can also be described in terms of topological flavor-flow diagrams using $SU(3)_F$ symmetry, as discussed in Ref. [27]. Based on the Hamiltonian in Eq. (3), the amplitudes for the CF $D \to PP$ decays can be represented using four flavor topologies shown in Fig. 3. The basis of the topological amplitudes is obtained by identifying the color-favored tree (T), color-suppressed tree (C), exchange (E), and annihilation (A) amplitudes. These four topological amplitudes depend on seven real parameters, four magnitudes and three relative phases (once again one overall phase is ignored).

The amplitudes for CF decays with at least one η or η' meson in the final state have explicit dependence on the $\eta - \eta'$ mixing angle. The topological flavor-flow representation for these decays are given in Table 4.

Once again employing $\theta = \arcsin(1/3)$, in Table 5, we express all CF $D \to PP$

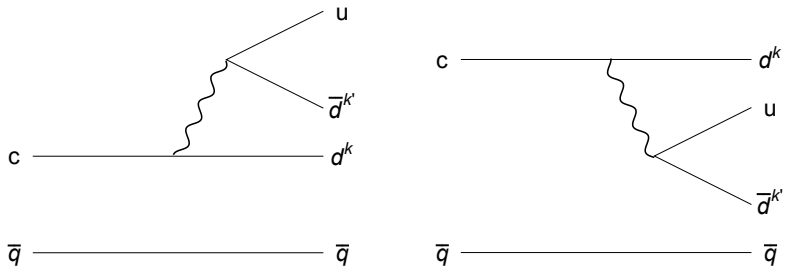

(a) Color-favored tree (T)

(b) Color-suppressed tree (C)

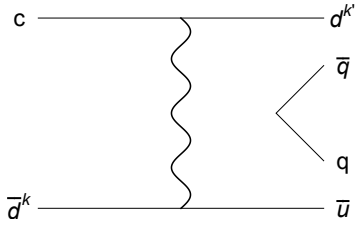

(c) Exchange (E)

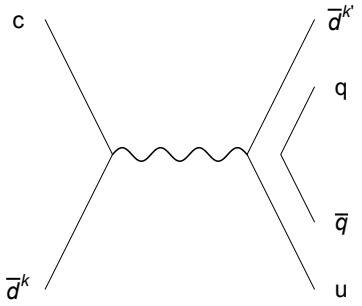

(d) Annihilation (A)

Figure 3: Topological flavor-flow diagrams used to describe CF $D \to PP$ decays.

Decay	Representation
$D^0 \to \overline{K}^0\eta$	$\frac{G_F}{\sqrt{2}}V_{ud}V_{cs}^*\left(\frac{\cos\theta}{\sqrt{6}}(C-E)+\frac{\sin\theta}{\sqrt{3}}(C+2E)\right)$
$D^0 \to \overline{K}^0\eta'$	$\frac{G_F}{\sqrt{2}}V_{ud}V_{cs}^*\left(\frac{\sin\theta}{\sqrt{6}}(C-E)-\frac{\cos\theta}{\sqrt{3}}(C+2E)\right)$
$D_s^+ \to \pi^+\eta$	$\frac{G_F}{\sqrt{2}}V_{ud}V_{cs}^*\left(\frac{2\cos\theta}{\sqrt{6}}(T-A)-\frac{\sin\theta}{\sqrt{3}}(T+2A)\right)$
$D_s^+ \to \pi^+\eta$	$\frac{G_F}{\sqrt{2}}V_{ud}V_{cs}^*\left(\frac{2\sin\theta}{\sqrt{6}}(T-A)+\frac{\cos\theta}{\sqrt{3}}(T+2A)\right)$

Table 4: Amplitudes for $\eta - \eta'$ CF decays in the topological-diagram representation with the assumption that the octet and singlet diagrams are equal.

decays in terms of flavor-topological diagrams.

The above diagrammatic description of the CF $D \to PP$ processes leads to a parametrization of the eight decay modes in terms of seven real parameters. This time, with one remaining degree of freedom, a χ^2-minimization fit can once again be performed. We perform such a fit by constraining T to be purely real and find,

Decay	Diagrammatic Amplitude
$D^0 \to K^- \pi^+$	$\frac{G_F}{\sqrt{2}} V_{ud} V_{cs}^* \ (T + E)$
$D^0 \to \overline{K}^0 \pi^0$	$\frac{G_F}{\sqrt{2}} V_{ud} V_{cs}^* \ \frac{1}{\sqrt{2}} (C - E)$
$D^0 \to \overline{K}^0 \eta$	$\frac{G_F}{\sqrt{2}} V_{ud} V_{cs}^* \ \frac{1}{\sqrt{3}} C$
$D^0 \to \overline{K}^0 \eta'$	$\frac{G_F}{\sqrt{2}} V_{ud} V_{cs}^* \ \left(-\frac{1}{\sqrt{6}}\right) (C + 3E)$
$D^+ \to \overline{K}^0 \pi^+$	$\frac{G_F}{\sqrt{2}} V_{ud} V_{cs}^* \ (C + T)$
$D_s^+ \to \overline{K}^0 K^+$	$\frac{G_F}{\sqrt{2}} V_{ud} V_{cs}^* \ (C + A)$
$D_s^+ \to \pi^+ \eta$	$\frac{G_F}{\sqrt{2}} V_{ud} V_{cs}^* \ \frac{1}{\sqrt{3}} (T - 2A)$
$D_s^+ \to \pi^+ \eta'$	$\frac{G_F}{\sqrt{2}} V_{ud} V_{cs}^* \ \frac{2}{\sqrt{6}} (T + A)$

Table 5: Amplitudes for CF D decays expressed in terms of $SU(3)_F$ flavor-topological diagrams.

$$
\begin{aligned}
\chi^2_{\text{min}}/\text{dof} &= 1.36/1 \ , \\
T &= (0.366 \pm 0.003)\, \text{GeV}^3 \ , \\
C &= (0.298 \pm 0.002)\, e^{i(-151.0 \pm 0.4)^\circ} \ \text{GeV}^3 \ , \\
E &= (0.201 \pm 0.004)\, e^{i(119.3 \pm 0.8)^\circ} \ \text{GeV}^3 \ , \\
A &= (0.04 \pm 0.01)\, e^{i(63 \pm 9)^\circ} \ \text{GeV}^3 \ . \qquad (11)
\end{aligned}
$$

This fit appears to be excellent, suggesting that the diagrammatic representation of CF $D \to PP$ decays aligns well with experimental measurements. Note that the diagrammatic approach has one additional complex-valued amplitude (i.e. two additional real-valued parameters) compared to the $SU(3)_F$ matrix-elements approach. We observe a significant decrease in the minimum value of χ^2 even though the diagrammatic description is still overdetermined, i.e. there are more observables than parameters.

In the following section we investigate the differences between the two approaches and present an argument for greater consistency between the two parametrizations.

3.2 Connections between flavor-flow and matrix elements in $SU(3)_F$

An obvious difference between the two approaches presented in the previous section is that, even in the limit of exact $SU(3)_F$ symmetry, the minimal bases contain different numbers of complex independent parameters: three in the matrix-elements approach and four in the flavor-flow approach. Yet, we expect an equivalence between the two approaches [9, 14]. The implication is either that the $SU(3)_F$ matrix-elements approach described above is incomplete or that the diagrammatic approach has too many parameters. A key observation that follows is that the one-to-one correspondence between group theory and diagrams is possible to achieve by treating the decays involving only octets separately from those also involving singlets. In order to demonstrate these separate correspondences, in Table 6, we have listed the $SU(3)_F$ matrix-elements and flavor-flow representations side-by-side.

Decay	Matrix Elements	Diagrams
$SU(3)_F$ octet-octet final states		
$D^0 \to K^-\pi^+$	$\frac{1}{5}\left(\sqrt{2}A_{27} + \sqrt{2}A_8 - \sqrt{5}C_8\right)$	$T + E$
$D^0 \to \overline{K}^0\pi^0$	$\frac{1}{10}\left(3A_{27} - 2A_8 + \sqrt{10}C_8\right)$	$(C - E)/\sqrt{2}$
$D^0 \to \overline{K}^0\eta_8$	$-\frac{1}{10\sqrt{3}}\left(3A_{27} - 2A_8 + \sqrt{10}C_8\right)$	$-(C - E)/\sqrt{6}$
$D^+ \to \overline{K}^0\pi^+$	$\frac{1}{\sqrt{2}}A_{27}$	$T + C$
$D_s^+ \to \overline{K}^0K^+$	$\frac{1}{5}\left(\sqrt{2}A_{27} + \sqrt{2}A_8 + \sqrt{5}C_8\right)$	$C + A$
$D_s^+ \to \pi^+\eta_8$	$\frac{1}{5\sqrt{3}}\left(-3A_{27} + 2A_8 + \sqrt{10}C_8\right)$	$-2(T - A)/\sqrt{6}$
$SU(3)_F$ octet-singlet final states		
$D^0 \to \overline{K}^0\eta_1$	$-\frac{1}{\sqrt{15}}\left(\sqrt{2}A_8 - \sqrt{5}C_8\right)$	$-(C + 2E)/\sqrt{3}$
$D_s^+ \to \pi^+\eta_1$	$\frac{1}{\sqrt{15}}\left(\sqrt{2}A_8 + \sqrt{5}C_8\right)$	$(T + 2A)/\sqrt{3}$

Table 6: Amplitudes for CF $D \to PP$ processes using the $SU(3)_F$ matrix-elements and flavor-flow representations. We have separated decays to final states involving octets only and those also involving singlets. Overall factors containing G_F and $V_{\rm CKM}$, that are identical in both representations, have been left out for brevity.

Focusing our attention, first, on the octet-octet final-state amplitudes in Table 6, we see that there are six decay amplitudes that depend on three $SU(3)_F$ reduced matrix elements. Therefore, there must be three relationships between these amplitudes.

They are,

$$\mathcal{A}(D^0 \to K^-\pi^+) + \sqrt{2}\mathcal{A}(D^0 \to \overline{K}^0\pi^0) = \mathcal{A}(D^+ \to \overline{K}^0\pi^+), \quad (12)$$

$$\mathcal{A}(D^0 \to \overline{K}^0\pi^0) + \sqrt{3}\mathcal{A}(D^0 \to \overline{K}^0\eta_8) = 0, \quad (13)$$

$$\sqrt{2}\,\mathcal{A}(D^+ \to \overline{K}^0\pi^+) + \sqrt{3}\,\mathcal{A}(D_s^+ \to \pi^+\eta_8) = \sqrt{2}\,\mathcal{A}(D_s^+ \to \overline{K}^0K^+). \quad (14)$$

These relationships match with sum rules previously demonstrated in Ref. [28]. Of these relationships, the first is a consequence of isospin symmetry, while the other two originate from the full $SU(3)_F$ symmetry. Note that these relationships are satisfied by both matrix elements and diagrams. Although there are still four diagrams in play, every amplitude can be written in terms of three distinct linear combinations of them. One can establish a one-to-one correspondence between the combinations of these diagrams and matrix elements as follows. The $SU(3)_F$ reduced matrix elements can be expressed in terms of the flavor-flow diagrams using

$$\begin{bmatrix} A_{27} \\ A_8 \\ C_8 \end{bmatrix} = \begin{bmatrix} 0 & \sqrt{2} & 0 \\ \frac{5\sqrt{2}}{4} & -\sqrt{2} & \frac{5\sqrt{2}}{4} \\ -\frac{\sqrt{5}}{2} & 0 & \frac{\sqrt{5}}{2} \end{bmatrix} \begin{bmatrix} T+E \\ T+C \\ C+A \end{bmatrix}. \quad (15)$$

Since the transformation matrix has a non-zero determinant it is invertible thus establishing a one-to-one correspondence. Next, we turn our attention to the octet-singlet final state amplitudes in Table 6. Here, there are two decay amplitudes that depend on two $SU(3)_F$ reduced matrix elements and two combinations of flavor-flow diagrams. Once again, the reduced matrix elements can be expressed in terms of diagrammatic amplitudes using

$$\begin{bmatrix} A_8 \\ C_8 \end{bmatrix} = \begin{bmatrix} \frac{\sqrt{10}}{4} & \frac{\sqrt{10}}{4} \\ -\frac{1}{2} & \frac{1}{2} \end{bmatrix} \begin{bmatrix} C+2E \\ T+2A \end{bmatrix}. \quad (16)$$

Here too, we see that the transformation matrix is invertible and a one-to-one correspondence exists.

Although Eqs. (15) and (16) establish a one-to-one correspondence between matrix elements and sets of flavor-flow amplitudes, it is easy to see that the correspondences are not the same. On the $SU(3)_F$ matrix-elements side this can be traced back to the definitions: while the **27** appears only in the $\mathbf{8}\times\mathbf{8}$ final states, the **8** appears in both $\mathbf{8}\times\mathbf{8}$ and $\mathbf{8}\times\mathbf{1}$. In principle, these final state octets are different and the corresponding amplitudes should be treated as such. On the side of topological flavor-flow amplitudes, similarly, this implies distinct diagrams for octet-octet and octet-singlet final states. In order to make these distinctions clear for the matrix elements, we use the following (re)definitions.

$$A_{27} \;=\; \left\langle \mathbf{27}|\mathcal{O}^{\overline{\mathbf{15}}}|\mathbf{3}\right\rangle , \quad A_8 \;=\; \left\langle \mathbf{8_{8\times 8}}|\mathcal{O}^{\overline{\mathbf{15}}}|\mathbf{3}\right\rangle , \quad C_8 \;=\; \left\langle \mathbf{8_{8\times 8}}|\mathcal{O}^{\mathbf{6}}|\mathbf{3}\right\rangle , \tag{17}$$

$$A_8^{(1)} \;=\; \left\langle \mathbf{8_{8\times 1}}|\mathcal{O}^{\overline{\mathbf{15}}}|\mathbf{3}\right\rangle , \quad C_8^{(1)} \;=\; \left\langle \mathbf{8_{8\times 1}}|\mathcal{O}^{\mathbf{6}}|\mathbf{3}\right\rangle . \tag{18}$$

For diagrams, we simply add the subscript 1 to represent the octet-singlet final states. Since these changes affect only the octet-singlet final states part of Table 6, we have listed the changes in Table 7.

Decay	Matrix Elements	Diagrams
$SU(3)_F$ octet-singlet final states		
$D^0 \to \overline{K}^0\eta_1$	$-\frac{1}{\sqrt{15}}\left(\sqrt{2}A_8^{(1)} - \sqrt{5}C_8^{(1)}\right)$	$-(C_1+2E_1)/\sqrt{3}$
$D_s^+ \to \pi^+\eta_1$	$\frac{1}{\sqrt{15}}\left(\sqrt{2}A_8^{(1)} + \sqrt{5}C_8^{(1)}\right)$	$(T_1+2A_1)/\sqrt{3}$

Table 7: Amplitudes for CF $D \to PP$ with octet-singlet final states using $SU(3)_F$ matrix-elements and diagrams. Overall factors containing G_F and $V_{\rm CKM}$, that are identical in both representations, have been left out for brevity.

Let us, now, reconsider the χ^2 minimization fits presented in Section 3.1 in light of the newly-defined amplitudes. The $SU(3)_F$ matrix-elements approach for the fits involved three complex-valued amplitudes (A_{27}, A_8, and C_8), rather than the five defined here ($A_{27}, A_8, C_8, A_8^{(1)}$, and $C_8^{(1)}$). The implicit assumptions in the fit were,

$$A_8^{(1)} \;=\; A_8 \;, \quad \text{and} \quad C_8^{(1)} \;=\; C_8 \;. \tag{19}$$

The results of the fit were poor showing that matrix elements for the octet-octet and octet-singlet final states may not be identical. On the other hand, the diagrammatic approach involved four complex-valued amplitudes (T, C, E, and A), as opposed to eight ($T, C, E, A, T_1, C_1, E_1$, and A_1). The diagrammatic fits, therefore, assumed $X = X_1$ where $X = T, C, E$, and A.

In either scenario, matrix elements or diagrams, the parametrizations established in this section are insufficient by themselves to produce a reasonable fit. Both parametrizations are equivalent as established above, and as such there are five complex-valued amplitudes which correspond to nine real-valued parameters (five magnitudes and four relative phases). With only eight branching ratios to fit, lack of additional input will lead to overfitting. Clearly, additional input is necessary to perform a fit.

On the $SU(3)_F$ matrix-elements side a fit was made possible by the assumption that the reduced matrix elements for octet-octet and octet-singlet final states were the same. These assumptions put two complex constraints reducing the number of fit parameters to five. The resulting fit was rather poor. On the other hand, the flavor-flow side assumption that individual diagrams corresponding to octet-octet and octet-singlet final states are the same led to four complex constraints reducing the number of fit parameters to seven. The resulting fit was good.

Due to the established equivalence between the $SU(3)_F$ matrix-elements and topological flavor-flow approaches, one naturally inquires about the consequence of either set of assumptions on the alternate parametrization. The $SU(3)_F$ matrix-elements side assumptions, $A_8^{(1)} = A_8$ and $C_8^{(1)} = C_8$, lead to the following relationships on the topological flavor-flow side,

$$[(T + C) + 5(E + A)] - \sqrt{5}\,[(T_1 + C_1) + 2(E_1 + A_1)] = 0\,, \tag{20}$$

$$\sqrt{5}\,[(T - C) + (E - A)] + [(T_1 - C_1) - 2(E_1 - A_1)] = 0\,. \tag{21}$$

Similarly, the flavor-flow side assumptions that $X = X_1$ where $X = T, C, E$, and A, lead to the number of reduced matrix elements being greater than that of the

flavor-flow amplitudes. Then, the relations of Eqs. (15) and (16) lead to the following phenomenological relationship on the $SU(3)_F$ matrix-elements side,

$$3\,A_{27} + 8\,A_8 - 4\sqrt{5}\,A_8^{(1)} \;=\; 0\;. \tag{22}$$

A fit performed with $A_{27}, C_8, A_8^{(1)}$, and $C_8^{(1)}$ as the available matrix elements, but with A_8 constrained through the relationship in Eq. (22), yields identical results as the diagrammatic fit assuming an equivalence between octet-octet and octet-singlet final states. We find,

$$\begin{aligned}
\chi^2_{\rm min}/{\rm dof} &= 1.36/1\;, \\
A_{27} &= (0.256 \pm 0.003)\,{\rm GeV}^3\;, \\
C_8 &= (0.357 \pm 0.010)\,e^{i(44\pm1)^\circ}\;{\rm GeV}^3\;, \\
A_8^{(1)} &= (0.71 \pm 0.02)\,e^{i(-67\pm1)^\circ}\;{\rm GeV}^3\;, \\
C_8^{(1)} &= (0.348 \pm 0.005)\,e^{i(-143\pm2)^\circ}\;{\rm GeV}^3\;.
\end{aligned} \tag{23}$$

Note that neither Eqs. (20) and (21), nor Eq. (22) automatically imply underlying relationships between the related parameters at a fundamental level. However, the fact that the fit on the diagrammatic side is far better than on the matrix-elements side, indicates a phenomenological preference for Eq. (22).

For the sake of completeness, we performed additional seven-parameter χ^2-minimization fits to the data, each time changing the input relationship between the $SU(3)_F$ matrix elements. The minimum values of χ^2 obtained in these fits are listed in Table 8. We see that all but one of the fits appear worse than the fit with octet-octet and octet-singlet diagrams set equal to each other. The fit that has a smaller minimum χ^2 is one where we imposed the relationship $C_8^{(1)} = C_8$. For this fit, we find,

Input relationship	$\chi^2_{\rm min}$
$A_{27} = 0$	2660
$\arg(\mathrm{A}_8^{(1)}) = \arg(\mathrm{A}_8)$ and $\arg(\mathrm{C}_8^{(1)}) = \arg(\mathrm{C}_8)$	175
$\arg(\mathrm{A}_8^{(1)}) = \arg(\mathrm{C}_8^{(1)})$ and $\arg(\mathrm{A}_8) = \arg(\mathrm{C}_8)$	162
$A_8 = 0$	160
$C_8 = 0$	88.2
$A_8^{(1)} = 0$	9.31
$A_8^{(1)} = A_8$	8.32
$C_8^{(1)} = 0$	7.80
$\lvert A_8^{(1)}\rvert = \lvert A_8\rvert$ and $\lvert C_8^{(1)}\rvert = \lvert C_8\rvert$	3.05
$3\,A_{27} + 8\,A_8 - 4\sqrt{5}\,A_8^{(1)} = 0$	1.36
$\lvert A_8^{(1)}\rvert = \lvert C_8^{(1)}\rvert$ and $\lvert A_8\rvert = \lvert C_8\rvert$	0.937
$C_8^{(1)} = C_8$	0.801

Table 8: Input relationships between $SU(3)_F$ matrix elements used to perform χ^2 minimization fits, listed in descending order of minimum χ^2 value obtained in a fit. Each input relationship adds two real-valued constraints. The corresponding fits each have one degree of freedom. arg(X) refers to the phase of the matrix element X.

$$
\begin{aligned}
\chi^2_{\rm min}/{\rm dof} &= 0.801/1, \\
A_{27} &= (0.253 \pm 0.003)\mathrm{GeV}^3, \\
A_8 &= (1.021 \pm 0.009)\, e^{i(96\pm1)^\circ}\ \mathrm{GeV}^3, \\
C_8 &= (0.089 \pm 0.005)\, e^{i(-55\pm5)^\circ}\ \mathrm{GeV}^3, \\
A_8^{(1)} &= (0.79 \pm 0.02)\, e^{i(-140\pm1)^\circ}\ \mathrm{GeV}^3.
\end{aligned}
\tag{24}
$$

Diagrammatically, this input relationship is equivalent to Eq. (20) on the flavor-flow side.

We conclude this section with the following observation. Since in the most general case the number of basis decay parameters exceeds the number of experimentally-measured CF decay modes, additional assumptions must be employed to extract individual reduced matrix elements or flavor-flow amplitudes presented above. Yet, the relations such as Eqs. (15) and (16) are rather general. This allows us to make a comment regarding hadronic final state interactions (FSI) in charm. In the $SU(3)_F$ limit

FSI cannot change the values of the reduced matrix elements. In other words, action of the strong interaction S-matrix on the basis of the $SU(3)_F$ reduced matrix elements leaves this basis invariant. This is not necessarily so for the individual flavor-flow amplitudes. Yet, the *combinations* of these amplitudes are preserved under strong FSI. Extraction of the magnitudes and phases of the individual amplitudes is only possible with additional assumptions.

3.3 Conclusions

Nonleptonic decays of charmed mesons provide plethora of interesting information about QCD dynamics in its nonperturbative regime. In this paper we discussed two phenomenological parametrizations of those decay amplitudes based on $SU(3)_F$ symmetry, which have been proven equivalent in the decays of B-mesons.

We argue that application of such parametrizations to charm decays require care due to insufficient number of experimentally-measured decay models and the presence of final state interactions. Noting that the Wolfenstein parameter λ is external to any QCD-based parametrization of decay amplitudes, the equivalency of the flavor $SU(3)_F$ and the topological flavor-flow approaches must be separately realized for the Cabibbo-favored decays of charmed mesons. Including decays to the physical η and η' mesons in our description, we find relationships between the basis parameters of the flavor-flow amplitudes. This can be interpreted from the point of view that quark rescatterings imply that only certain linear combinations of flow diagrams can contribute to the decay amplitudes. We presented extractions of the basis amplitudes in two approaches under various assumptions.

4 R-parity Violating Supersymmetry

Weak decays of charmed mesons, D^0, D^+, and D_s^+, are dominated by tree-level contributions in the Standard Model (SM). Since the tree-level decays of the charm quark involve transitions between the first and second generation quarks, the CKM matrix elements that come into play (the upper-left 2×2 block of the CKM matrix) are either unsuppressed, or suppressed at most by one power of the Wolfenstein parameter ($\lambda \sim 0.2$) [16]. Depending on the power of λ in the decay amplitude, weak hadronic decays of charm are therefore categorized into Cabibbo favored (CF) decays, proportional to the product $V_{cs}^* V_{ud} \sim \mathcal{O}(1)$; singly-Cabibbo suppressed (SCS) decays, proportional to $V_{cq}^* V_{uq} \sim \mathcal{O}(\lambda)$ where $q = d, s$; and doubly-Cabibbo suppressed (DCS) decays proportional to $V_{cd}^* V_{us} \sim \mathcal{O}(\lambda^2)$.

The CF, and DCS modes involve only distinct quark flavors, and as such receive no SM penguin contributions [2]. The SCS modes receive SM penguin contributions, however, the associated direct CP violation appears to be CKM suppressed by $\mathcal{O}(\lambda^4)$. Since large direct-CP asymmetries require two amplitudes that are comparable in size, but have different weak and strong phases, the above anatomy of charm decays leads to very tiny predictions for direct-CP asymmetries within the SM [29].

The LHCb Collaboration has observed a difference between direct CP asymmetries in $D^0 \to K^+K^-$ and $D^0 \to \pi^+\pi^-$ decays using 5.9 fb^{-1} of data at 13 TeV [30]. A combination of measurements (new and old, as well as $\pi-$ and $\mu-$tagged D^0 decay data) leads to the result,

$$\Delta A_{\rm CP} = (-15.4 \pm 2.9) \times 10^{-4}. \tag{25}$$

This result establishes that the direct CP asymmetry in charm decays is more than

[2] These modes can receive contributions from highly-suppressed SM box diagrams

five standard deviations away from a null hypothesis. Moreover, since the measured central value of this $\Delta A_{\rm CP}$ is several times larger than its prediction within SM theory [29], it presents an opportunity for intrigue. An earlier LHCb measurement on $\Delta A_{\rm CP}$ in these same channels [31] had pegged the central value of this observable at several times the current measurement,

$$\Delta A_{\rm CP} = [-0.82 \pm 0.21(\text{stat}) \pm 0.11(\text{syst})]\,\%, \tag{26}$$

and led to several theory papers on how to explain the discrepancy between the measurements and the predicted value, including suggestions of dynamical enhancement of the SM penguin contributions [32, 33, 34, 35, 36, 37, 38], as well as models of new physics [39, 40, 41, 42, 43]. Some of us had emphasized the role of flavor-SU(3) symmetry in the decay of charm quarks [44, 45, 12, 46].

In the present paper we first explore the phenomenology of charmed meson decays in light of SU(3) symmetry. We treat the CF decays separately from the SCS decays to determine a baseline for the amplitudes of the contributing diagrams and show they are insufficient to account for $SU(3)_F$ breaking. We then consider R-parity violating (RPV) supersymmetry (SUSY) as an example model for understanding the difference between SM predictions and the LHCb measurement. The paper is organized as follows. In Section II we describe the flavor SU(3) approach to charm decays and present associated fits. In Section III, we introduce RVP SUSY as a potential model for lifting the discrepancies between theory and experiment. In Section IV we determine constraints on these couplings from other processes. In Section V we perform fits to determine the couplings. In Section VI we analyse these contributions to the generation of neutrino mass.

4.1 Flavor-SU(3) symmetry in charmed meson decays

We begin by characterizing CF decays of D^0, D^+, D_s^+ mesons using four distinct flavor topologies, "color-favored tree" (T), "color-suppressed tree" (C), "exchange" (E), and

"annihilation" (A), as described in Refs. [47, 48, 49, 50]. As such, the decay amplitude corresponding to each topology is a parametric representation of the flow of light-quark flavor (u, d, s) in the corresponding process. The topological amplitudes then include not only the short-distance contributions arising from weak interactions, but also any contribution from final-state interactions that typically occur at long distances. This is represented by the observation that, although in theory four topological amplitudes represent the CF decays, a fit to experimental data reveals that they cannot all be real. In fact, when the four topological amplitudes are represented by four magnitudes and three complex relative phases, one finds that all three relative phases are very different from zero, indicating large final-state interactions.

To determine the structure of these diagrams we first determine the effective Hamitonian for the transition $c \to d^k u \overline{d}^{k'}$ within the Standard Model. The basic vertex is shown in Fig. 4, with the vertex factor given by

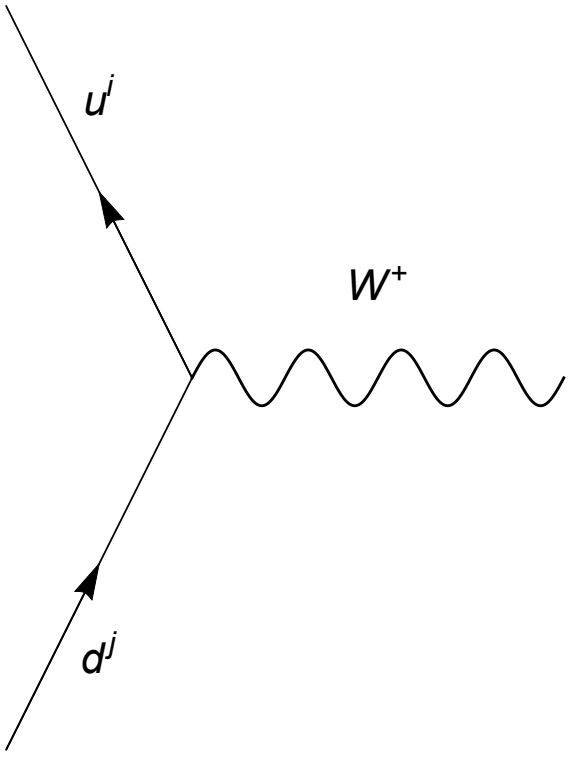

Figure 4: The basic SM vertex

$$-\frac{\imath g}{\sqrt{2}}V_{ij}\gamma^{\mu}\frac{(1-\gamma^5)}{2} \tag{27}$$

where V_{ij} is the CKM matrix element. The amplitude of the $c \to d^k u\overline{d}^{k'}$ transitions is then given by

$$\mathcal{M} = \imath\frac{g^2}{2m_W^2}V_{ck}^*V_{uk'}\ \overline{d}_{\alpha}^{k}\gamma^{\mu}c_{L\alpha}\ \overline{u}_{\beta}\gamma_{\mu}d_{L\beta}^{k'} \tag{28}$$

after integrating out the W boson, and now we have the effective Hamiltonian. The effective process is represented by the Feynman diagram shown in Fig. 5

$$\mathcal{H}_{\text{eff}}^{\text{SM}} = \frac{4G_F}{\sqrt{2}}V_{ck}^*V_{uk'}\ \overline{d}_{\alpha}^{k}\gamma^{\mu}c_{L\alpha}\ \overline{u}_{\beta}\gamma_{\mu}d_{L\beta}^{k'} = \frac{G_F}{\sqrt{2}}V_{ck}^*V_{uk'}\ \left(\overline{d}_{\alpha}^{k}\ c_{\alpha}\right)_{V-A}\left(\overline{u}_{\beta}\ d_{\beta}^{k'}\right)_{V-A} \tag{29}$$

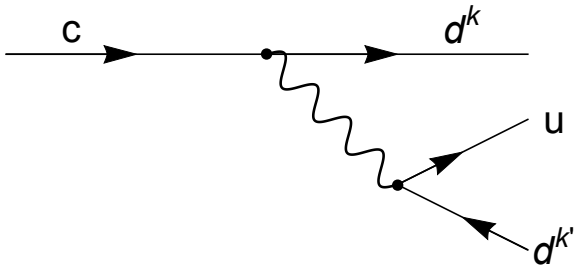

Figure 5: The Standard Model interaction

The diagrams $T, C, E,$ and A are then obtained by taking the appropriate contractions for the process of interest. For example, if we consider the process $D^0 \to K^-\pi^+$ we have

$$\left\langle K^-\pi^+|\mathcal{H}_{\text{eff}}^{\text{SM}}|D^0\right\rangle = \frac{G_F}{\sqrt{2}}V_{ck}^*V_{uk'}\left\langle s\bar{u}\ u\bar{d}|\left(\overline{d}_{\alpha}^{k}\ c_{\alpha}\right)_{V-A}\left(\overline{u}_{\beta}\ d_{\beta}^{k'}\right)_{V-A}|c\bar{u}\right\rangle \tag{30}$$

This matrix element can be contracted by contracting the quarks in the operator with the quarks in the initial and final states, keeping in mind that the color structure must also be maintained. The quarks/antiquarks that comprise the mother and daughter mesons must be the same color/anticolor, this is accomplished through

color Fierz transformations. This procedure is explained more fully in Sec. 4.3. Looking at all of the possible ways that these contractions can be accomplished results in 4 distinct tree-level topological classes [51]. These classes can be represented by diagrams. The diagrams are shown in Fig. 6 and will be used throughout the rest of this paper.

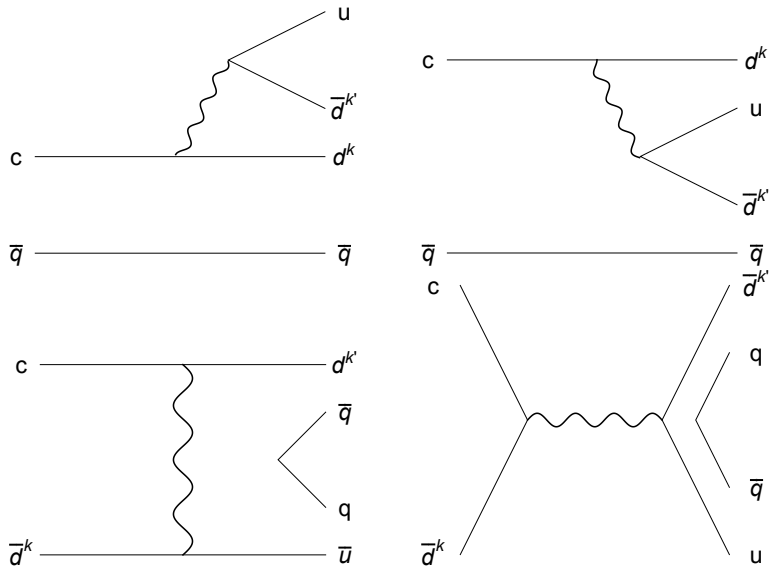

Figure 6: The T, C, E, and A topological diagrams in the Standard Model.

Meson	Decay	Representation	Branching Ratio (%)
D^0	$K^-\pi^+$	$\frac{G_F}{\sqrt{2}}V_{cs}^*V_{ud}(T+E)$	3.950 ± 0.031
	$\overline{K}^0\pi^0$	$\frac{G_F}{\sqrt{2}}V_{cs}^*V_{ud}\frac{1}{\sqrt{2}}(C-E)$	2.48 ± 0.044
	$\overline{K}^0\eta$	$-\frac{G_F}{\sqrt{2}}V_{cs}^*V_{ud}\frac{1}{\sqrt{3}}C$	1.018 ± 0.012
	$\overline{K}^0\eta'$	$\frac{G_F}{\sqrt{2}}V_{cs}^*V_{ud}\frac{1}{\sqrt{6}}(C+3E)$	1.898 ± 0.064
D^+	$\overline{K}^0\pi^+$	$\frac{G_F}{\sqrt{2}}V_{cs}^*V_{ud}(C+T)$	3.124 ± 0.062
D_s^+	$\overline{K}^0K^+$	$\frac{G_F}{\sqrt{2}}V_{cs}^*V_{ud}(C+A)$	2.95 ± 0.14
	$\pi^+\eta$	$\frac{G_F}{\sqrt{2}}V_{cs}^*V_{ud}\frac{1}{\sqrt{3}}(T-2A)$	1.70 ± 0.09
	$\pi^+\eta'$	$\frac{G_F}{\sqrt{2}}V_{cs}^*V_{ud}\frac{2}{\sqrt{6}}(T+A)$	3.94 ± 0.25

Table 9: Flavor-topological representations and experimental branching ratios for Cabibbo-Favored D decays. The branching ratios were taken from the Particle Data Group (PDG) [52], and uses data from BESIII ([53]), and CLEO([54]) Collaborations.

Flavor-SU(3) symmetry dictates that the exchange and annihilation diagrams contribute to the decays in which they participate equally, without regard to whether

they couple the charm quark to a down or strange quark. The reason for assuming this symmetry is that when the W boson is integrated out of the amplitude, we obtain a single 4-quark vertex and the amplitude should just depend on the topology of the contraction and not on the flavors involved in said contraction. Now we turn to analyzing the Cabibbo-favored decays to see how well this effective theory agrees with data obtained through experiments.

The branching ratio for a two-body D-meson decay can be expressed in terms of the decay amplitude $\mathcal{A}$ as,

$$\mathcal{B}(D \to PP) \;=\; \frac{|\vec{p}_P|}{8\pi m_D^2 \Gamma_D} |\mathcal{A}|^2 \;, \tag{31}$$

where $\vec{p}_P$ represents the three momentum of the daughter pseudoscalars in the D-meson rest frame, while m_D and Γ_D respectively represent the mass and width of the decaying D meson. The experimental branching ratios for the eight CF D-meson decays to a pair of pseudoscalars are given in Table 9, alongside the flavor-topological representation for each decay assuming flavor-SU(3) symmetry. The eight data entries in Table 9 depend on a total of seven parameters – four magnitudes and three relative phases. We perform a fit to extract these parameters, and present our results in Table 10.

Diagram	Magnitude ((GeV)^3)	Phase (Degrees)
T	0.352 ± 0.003	0
C	0.286 ± 0.002	-151.0 ± 0.4
E	0.193 ± 0.003	119.3 ± 0.8
A	0.04 ± 0.01	63 ± 9

Table 10: Magnitude and relative strong phases of flavor-topology amplitudes T, C, E, and A, describing CF $D \to PP$ decays under flavor-SU(3) symmetry. These parameters were extracted using a χ^2-minimization fit to the Table 9 data. The minimum χ^2 for this fit was 1.37 (one degree of freedom) indicating an absence of flavor-SU(3) breaking in CF D decays. This fit also leaves little room for new physics in CF D decays.

Working entirely within the SM, we find that the data and the theory work

very well if we limit our observations to just the Cabibbo-Favored decays. Considering just the CF decays (Table 9) and we obtain a χ^2/d.o.f = 1.37/1, which indicates a very good fit. The results of this fit are given in Table 10. From this fit it is clear that there is little room for andy new physics in the CF decays of D mesons. However, when we take these fitted values and apply them to the SCS decays involving just the kaons and pions we get very poor agreement between theory and experiment. This is shown in Table 11, and we see that the poorness of the fit arises mainly from the SCS decays that involve an exchange diagram (E).

Meson	Decay	SM Diagrams	Exp. BR ($\times 10^{-3}$)	Pred. BR ($\times 10^{-3}$)	χ^2
D^0	$\pi^+\pi^-$	$\frac{G_F}{\sqrt{2}} V_{cd}^* V_{ud}(T+E)$	1.455 ± 0.024	2.254	1108
	$\pi^0\pi^0$	$\frac{G_F}{\sqrt{2}} V_{cd}^* V_{ud} \frac{1}{\sqrt{2}}(C-E)$	0.826 ± 0.025	1.409	544
	K^+K^-	$\frac{G_F}{\sqrt{2}} V_{cs}^* V_{us}(T+E)$	4.08 ± 0.06	1.93	1284
	$\overline{K}^0 K^0$	$\frac{G_F}{\sqrt{2}} \left(V_{cd}^* V_{ud} + V_{cs}^* V_{us}\right) E$	0.282 ± 0.010	0	795
D^+	$\pi^+\pi^0$	$-\frac{G_F}{\sqrt{2}} V_{cd}^* V_{ud} \frac{1}{\sqrt{2}}(T+C)$	1.247 ± 0.033	0.893	115
	$K^+\overline{K}^0$	$\frac{G_F}{\sqrt{2}} \left(V_{cs}^* V_{us} T + V_{cd}^* V_{ud} A\right)$	6.08 ± 0.18	5.815	2.2
D_s^+	$\pi^+ K^0$	$\frac{G_F}{\sqrt{2}} (V_{cd}^* V_{ud} T + V_{cs}^* V_{us} A)$	2.44 ± 0.12	2.94	17
	$\pi^0 K^+$	$\frac{G_F}{\sqrt{2}} \frac{1}{\sqrt{2}} (-V_{cd}^* V_{ud} C + V_{cs}^* V us A)$	0.63 ± 0.21	0.84	1

Table 11: The Singly Cabibbo Suppressed Decays involving kaons and pions. The primes indicate that these amplitudes are proportional to $\lambda = \tan\theta_{\text{Cabbibo}} = .2307$. The predicted Branching Ratios are obtained using the parameters found in Table 10.

Upon inspection of the D^0 SCS decays it is immediately obvious that there is some SU(3) breaking since the $D^0 \to \overline{K}^0 K^0$ decay has a measured non-zero amplitude. The diagrammatic amplitude is zero because of cancelation between $c \to d$ and $c \to s$ exchange topologies. We assume here that these exchange diagrams involving the d and s quarks do not cancel. To accomdate this we distinguish the two diagrams E^d and E^s, indicating the transition of the charm quark in the decay. This choice is motivated in part by the non-zero measured branching ratio of the $D^0 \to \bar{K}^0 K^0$ decay and also because the main source of discrepency between theory and experiment is in processes that involve the exchange diagram. We introduce the SU(3) symmetry breaking by splitting this diagram into two separate diagrams. This allows us to perform another

fit using the CF data and the SCS decays of the D^0 meson. We make the definition

$$E = \frac{E^d + E^s}{2} \tag{32}$$

for the CF decays and distinguish E^d and E^s in the SCS decays. This gives us the decay amplitudes listed in Table 12.

Meson	Decay	SM Diagrams
D^0	$\pi^+\pi^-$	$\frac{G_F}{\sqrt{2}} V_{cd}^* V_{ud}(T + E^d)$
	$\pi^0\pi^0$	$\frac{G_F}{\sqrt{2}} V_{cd}^* V_{ud} \frac{1}{\sqrt{2}}(C - E^d)$
	K^+K^-	$\frac{G_F}{\sqrt{2}} V_{cs}^* V_{us}(T - E^s)$
	$\overline{K}^0 K^0$	$\frac{G_F}{\sqrt{2}}(V_{cs}^* V_{us} E^s + V_{cd}^* V_{ud} E^d)$

Table 12: The Singly Cabibbo Suppressed Decays involving only D^0 for a fit assuming SU(3) Flavor symmetry breaking in the exchange diagram. E^d indicates $c \to d$ and E^s indicates $c \to s$.

Using this parameterization we find a much better fit to the data with a $\chi^2/\text{dof} = 30.5/3$. Which is much better than simply using the CF results to predict the SCS decays. The results of this fit are as follows (in units of $(\text{GeV})^3$):

$$T = 0.354 \pm 0.003 \tag{33}$$

$$C = (0.286 \pm 0.003) e^{\imath(-151.5 \pm 0.4)^\circ} \tag{34}$$

$$A = (0.03 \pm 0.01) e^{\imath(61 \pm 7)^\circ} \tag{35}$$

$$E^d = (0.180 \pm 0.006) e^{\imath(139.0 \pm 0.8)^\circ} \tag{36}$$

$$E^s = (0.2007 \pm 0.005) e^{\imath(103.6 \pm 0.5)^\circ} \tag{37}$$

Another method of introducing SU(3) symmetry breaking is through the use of a penguin amplitude, P, for $c \to u$ transitions [13]. This is normally thought to be very small because the contributions from the d and s quarks cancel each other in the intermediate state. If we assume this cancellation is inexact we can use the penguin as a proxy for SU(3) violation. We also introduce a penguin annihilation amplitude

(PA) that contributes only to the D^0 decays. We also account for any SU(3) breaking in the SCS T amplitude by considering the following expressions

$$T_{D^0\to\pi^+\pi^-} \;=\; T_{D^+\to\pi^+\pi^0} \;=\; T_{D_s^+\to\pi^+K^0} \;=\; T_\pi \;, \tag{38}$$

$$T_{D^0\to K^+K^-} \;=\; T_{D^+\to K^+\overline{K}^0} \;=\; T_K \tag{39}$$

This gives us a relationship between the CF T amplitude and the SCS T amplitudes and we find that they are related through form factors as follows:

$$T_\pi = T\cdot\left|\frac{f_{+(D^0\to\pi^-)}(m_\pi^2)}{f_{+(D^0\to K^-)}(m_\pi^2)}\right|\cdot\frac{m_D^2-m_\pi^2}{m_D^2-m_K^2} \tag{40}$$

$$T_K = T\cdot\left|\frac{f_{+(D^0\to K^-)}(m_K^2)}{f_{+(D^0\to K^-)}(m_\pi^2)}\right|\cdot\frac{f_K}{f_\pi} \tag{41}$$

Where we have neglected the contribution from $f_-(q^2)$ at $q = m_{\pi,K}$. We are also able to introduce SU(3) breaking through the SCS A amplitudes:

$$A_{D^+\to K^+\overline{K}^0} \;=\; A\cdot\frac{f_{D^+}}{f_{D_s^+}} \;=\; A_{D^+} \tag{42}$$

$$A_{D_s^+\to\pi^+K^0} \;\simeq\; A_{D_s^+\to K^+\pi^0} \;=\; A \tag{43}$$

The decay constants [55] and meson masses [52] (in GeV) are:

$$f_\pi = 0.13041; \quad f_K = 0.1544; \quad f_{D^+} = 0.2074; \quad f_{D_s^+} = 0.2472; \tag{44}$$

$$m_{D^0} = 1.8648; \quad m_\pi = 0.13957018; \quad m_K = 0.493677. \tag{45}$$

and the approximate values for the form factors [56, 57] are obtained from semileptonic decays:

$$|f_{+(D^0\to\pi^-)}(m_\pi^2)| \simeq 0.616, \quad |f_{+(D^0\to K^-)}(m_\pi^2)| \simeq 0.768, \tag{46}$$

$$|f_{+(D^0\to K^-)}(m_K^2)| \simeq 0.810 \tag{47}$$

With these definitions we now have that the SCS decays are parameterized in Table 13.

Decay Mode	Amplitude Representation	Meas. Amp. ($\times 10^{-7}$ GeV)	Pred. Amp. ($\times 10^{-7}$ GeV)	χ^2
$D^0 \to \pi^+\pi^-$	$\frac{G_F}{\sqrt{2}}\left[V_{cd}^* V_{ud}(T_\pi + E) + (P + PA)\right]$	4.71 ± 0.04	4.72	.08
$D^0 \to K^+K^-$	$\frac{G_F}{\sqrt{2}}\left[V_{cs}^* V_{us}(T_K + E) + (P + PA)\right]$	8.51 ± 0.06	8.43	1.5
$D^0 \to \pi^0\pi^0$	$\frac{G_F}{\sqrt{2}}\frac{1}{\sqrt{2}}\left[V_{cd}^* V_{ud}(E - C) - (P + PA)\right]$	3.54 ± 0.05	3.38	8.7
$D^+ \to \pi^+\pi^0$	$-\frac{G_F}{\sqrt{2}}\frac{V_{cd}^* V_{ud}}{\sqrt{2}}(T_\pi + C)$	2.74 ± 0.04	1.99	396
$D^0 \to K^0\overline{K}^0$	$\frac{G_F}{\sqrt{2}}\left[(V_{cd}^* V_{ud} + V_{cs}^* V_{us})E - (P + PA) + P\right]$	2.24 ± 0.04	2.26	.21
$D^+ \to K^+\overline{K}^0$	$\frac{G_F}{\sqrt{2}}\left[(V_{cs}^* V_{us} T_K + V_{cd}^* V_{ud} A_{D^+}) + P\right]$	6.53 ± 0.05	6.70	10.6
$D^+ \to \pi^+K^0$	$\frac{G_F}{\sqrt{2}}\left[(V_{cd}^* V_{ud} T_\pi + V_{cs}^* V_{us} A) + P\right]$	5.8 ± 0.1	6.98	64
$D_s^+ \to \pi^0K^+$	$\frac{G_F}{\sqrt{2}}\frac{1}{\sqrt{2}}\left[(-V_{cd}^* V_{ud} C + V_{cs}^* V_{us} A) - P\right]$	3.0 ± 0.5	4.24	6.8

Table 13: The SCS decays involving the penguin (P) and penguin annihilation (PA) amplitudes.

We run a χ^2-minimaztion fit on just the first three amplitudes to obtain a value for $P + PA$, which leads to

$$P + PA = (2.8 \pm 0.1)e^{\imath(105.1 \pm 0.7)^\circ} \times 10^{-7} \text{ GeV}; \qquad \chi^2/\text{dof} = 9.7/1 \tag{48}$$

Using this result and the final four amplitudes in Table 13, we obtain a value for P by itself

$$P = (1.60 \pm 0.05)e^{\imath(155 \pm 1)^\circ} \times 10^{-7} \text{ GeV}; \qquad \chi^2/\text{dof} = 81.3/2 \tag{49}$$

which leads to

$$PA = (2.15 \pm 0.11)e^{\imath(70 \pm 3)^\circ} \times 10^{-7} \text{ GeV} \tag{50}$$

We see that this fit is not very good. The main sources of discrepency are the $D^+ \to \pi^+\pi^0$ and $D_s^+ \to \pi^+K^0$ amplitudes.

One other thing that can be done with the CF and SCS decays within the SM is to consider the mixing angle θ_η as a free parameter. We adopt the definition

$$\eta = -\eta_8 \cos\theta_\eta - \eta_1 \sin\theta_\eta, \quad \eta' = -\eta_8 \sin\theta_\eta + \eta_1 \cos\theta_\eta, \quad \text{where} \tag{51}$$

$$\eta_8 \equiv (u\overline{u} + d\overline{d} - 2s\overline{s})/\sqrt{6}, \qquad \eta_1 \equiv (u\overline{u} + d\overline{d} + s\overline{s})/\sqrt{3} \tag{52}$$

This leads to expressions for the CF decays involving η and η' which are given in Table 14

Decay	Representation
$D^0 \to \overline{K}^0\eta$	$\frac{G_F}{\sqrt{2}}V_{cs}^*V_{ud}\left[C\left(-\frac{1}{\sqrt{6}}\cos\theta_n - \frac{1}{\sqrt{3}}\sin\theta_n\right) + E\left(\frac{1}{\sqrt{6}}\cos\theta_n - \frac{2}{\sqrt{3}}\sin\theta_n\right)\right]$
$D^0 \to \overline{K}^0\eta'$	$\frac{G_F}{\sqrt{2}}V_{cs}^*V_{ud}\left[C\left(\frac{1}{\sqrt{3}}\cos\theta_n - \frac{1}{\sqrt{6}}\sin\theta_n\right) + E\left(\frac{2}{\sqrt{3}}\cos\theta_n + \frac{1}{\sqrt{6}}\sin\theta_n\right)\right]$
$D_s^+ \to \pi^+\eta$	$\frac{G_F}{\sqrt{2}}V_{cs}^*V_{ud}\left[T\left(\frac{2}{\sqrt{6}}\cos\theta_n - \frac{1}{\sqrt{3}}\sin\theta_n\right) + A\left(-\frac{2}{\sqrt{6}}\cos\theta_n - \frac{2}{\sqrt{3}}\sin\theta_n\right)\right]$
$D_s^+ \to \pi^+\eta'$	$\frac{G_F}{\sqrt{2}}V_{cs}^*V_{ud}\left[T\left(\frac{1}{\sqrt{3}}\cos\theta_n + \frac{2}{\sqrt{6}}\sin\theta_n\right) + A\left(\frac{2}{\sqrt{3}}\cos\theta_n - \frac{2}{\sqrt{6}}\sin\theta_n\right)\right]$

Table 14: Ampitude representation for the CF decays involving η and η'

Including θ_η as a free parameter in a fit on the CF decays leaves us with zero degrees of freedom, but we obtain a $\chi^2 \approx 10^{-5}$. The results of this fit are given here in units of $(\text{GeV})^3$.

$$T = 0.360 \pm 0.006 \tag{53}$$

$$C = (0.30 \pm 0.01)e^{\imath(-151.5\pm0.5)^\circ} \tag{54}$$

$$E = (0.18 \pm 0.01)e^{\imath(121\pm2)^\circ} \tag{55}$$

$$A = (0.05 \pm 0.01)e^{\imath(32\pm20)^\circ} \tag{56}$$

$$\theta = (15 \pm 3)^\circ \tag{57}$$

These results are in very good agreement with the fit done without using θ_η as a free parameter. The value of θ_η is close to the accepted value of $\sim 19.5^\circ$.

The purpose of doing these fits has been to test the SM. We have found that the SM is sufficient in describing the Cabibbo-favored decays but is lacking when we consider the Singly-Cabibbo-Suppressed decays. We have attempted to account for the deficiencies in the SM by introducing flavor-SU(3) symmetry breaking in various ways and have seen that the disagreement between experiment and theory is somewhat explained but there is still much room for improvement. Something more drastic that merely introducing the symmetry breaking must be considered.

4.2 R-parity Violating SUSY

In supersymmetric models, R-parity invariance is often imposed on the Lagrangian in order to maintain the separate conservation of baryon number and lepton number. The R-parity of a field with spin S, baryon number B and lepton number L is defined to be

$$R = (-1)^{2S+3B+L} \ . \tag{58}$$

R is $+1$ for all the SM particles and -1 for all the supersymmetric particles.

The presence of R-parity conservation implies that super particles must be produced in pairs in collider experiments and the lightest super particle (LSP) must be absolutely stable. The LSP therefore provides a good candidate for cold dark matter. There is, however, no compelling theoretical motivation, such as gauge invariance, to impose R-parity conservation.

The most general superpotential of the MSSM, consistent with $SU(3)\times SU(2)\times U(1)$ gauge symmetry and supersymmetry, can be written as

$$\mathcal{W} = \mathcal{W}_R + \mathcal{W}_{\not R} \ , \tag{59}$$

where $\mathcal{W}_R$ is the R-parity conserving piece, and $\mathcal{W}_{\not R}$ breaks R-parity. They are given by

$$\mathcal{W}_R = h_{ij} L_i H_2 E^c_j + h'_{ij} Q_i H_2 D^c_j + h''_{ij} Q_i H_1 U^c_j \ , \tag{60}$$

$$\mathcal{W}_{\not R} = \frac{1}{2}\lambda_{[ij]k} L_i L_j E^c_k + \lambda'_{ijk} L_i Q_j D^c_k + \frac{1}{2}\lambda''_{i[jk]} U^c_i D^c_j D^c_k + \mu_i L_i H_2 \ . \tag{61}$$

Here $L_i(Q_i)$ and $E_i(U_i, D_i)$ are the left-handed lepton (quark) doublet and lepton (quark) singlet chiral superfields, where i, j, k are generation indices and c denotes a charge conjugate field. $H_{1,2}$ are the chiral superfields representing the two Higgs doublets.

The λ and λ' couplings in [Eq. (61)], violate lepton number conservation, while

the λ'' couplings violate baryon number conservation. There are 27 λ'-type couplings and 9 each of the λ and λ'' couplings as $\lambda_{[ij]k}$ is antisymmetric in the first two indices and $\lambda''_{i[jk]}$ is antisymmetric in the last two indices. The non-observation of proton decay imposes very stringent conditions on the simultaneous presence of both the baryon-number and lepton-number violating terms in the Lagrangian [58]. It is therefore customary to assume the existence of either L-violating couplings or B-violating couplings, but not both. The terms proportional to λ are not relevant to our present discussion and will not be considered further.

We now turn to the L-violating couplings. In terms of four-component Dirac spinors, these are given by [59, 60]

$$\begin{aligned}\mathcal{L}_{\lambda'} &= -\lambda'_{ijk}\Big[\tilde{\nu}^i_L \bar{d}^k_R d^j_L + \tilde{d}^j_L \bar{d}^k_R \nu^i_L + (\tilde{d}^k_R)^*(\bar{\nu}^i_L)^c d^j_L \\ &\qquad -\tilde{e}^i_L \bar{d}^k_R u^j_L - \tilde{u}^j_L \bar{d}^k_R e^i_L - (\tilde{d}^k_R)^*(\bar{e}^i_L)^c u^j_L\Big] + h.c. \end{aligned} \tag{62}$$

As we are considering only non-leptonic decays we will be interested in 4-quark operators which are generated by the following subset of operators in Eq. 62. Since all of these quantities have been determined in the flavor basis, we must rotate to the mass basis. To accomplish this we can assume that the down-type quarks are in the mass basis and the rotation of the up-type quarks consists of just multiplying the up quark spinors by the CKM matrix. This constitues replacing the weak term, u^j_L, with the mass mixing term, $\left(V^\dagger_{CKM}\ \hat{u}_L\right)^j$. The sleptons can be taken to be in the mass basis as well [61].

$$\mathcal{L}_{\rm int} = \lambda'_{ijk}\left[\tilde{\nu}^i_L\, \overline{d}^k_{R\alpha}\, d^j_{L\alpha} - \tilde{e}^i_L\, \overline{d}^k_{R\beta}\, u^j_{L\beta}\right] + h.c. \tag{63}$$

These interactions are depicted in Fig.7.

Working with just the first term we construct the amplitude

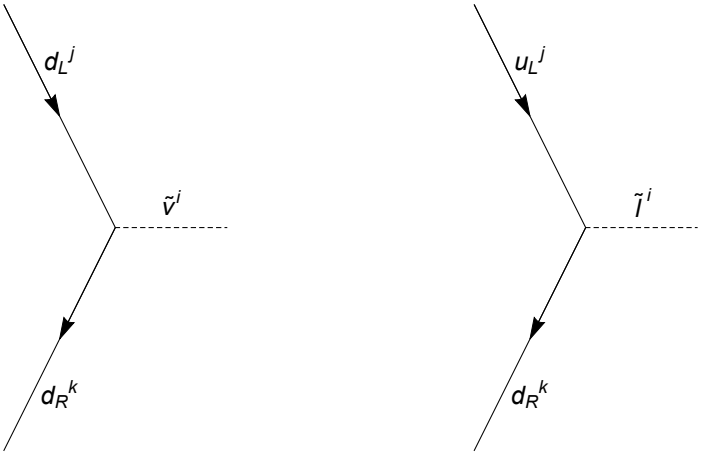

Figure 7: The basic quark-quark vertices in R-Parity Violation SUSY.

$$\mathcal{M} = \lambda'_{ijk}\left[\tilde{\nu}^i_L\,\overline{d}^k_{R\alpha}\,d^j_{L\alpha}\right]\left\{\lambda'_{ij'k'}\left[\tilde{\nu}^i_L\,\overline{d}^{k'}_{R\beta}\,d^{j'}_{L\beta}\right]\right\}^\dagger = \lambda'_{ijk}\lambda'^*_{ij'k'}\left[\tilde{\nu}^i_L\,\overline{d}^k_{R\alpha}\,d^j_{L\alpha}\,d^{j'\dagger}_{L\beta}\,\overline{d}^{k'\dagger}_{R\beta}\tilde{\nu}^{i\dagger}_L\right] \quad (64)$$

contracting the sparticles we obtain the propagator for the sparticle. This gives us

$$\mathcal{M} = J_{jk}J_{j'k'}\Delta_F \quad \text{with} \quad \Delta_F = \frac{1}{k^2 - m^2_{\tilde{\nu}^i} + \imath\epsilon} \quad (65)$$

Evaluating $\mathcal{M}$ we have

$$\mathcal{M} = \lambda'_{ijk}\lambda'^*_{ij'k'}\left[\overline{d}^k_{R\alpha}\,d^j_{L\alpha}\right]\left[\overline{d}^{j'}_{L\beta}\gamma^0\,\gamma^0 d^{k'}_{R\beta}\right]\frac{1}{k^2 - m^2_{\tilde{\nu}^i} + \imath\epsilon} \quad (66)$$

Integrating out the sparticle, we have that

$$\mathcal{M} = -\frac{\lambda'_{ijk}\lambda'^*_{ij'k'}}{m^2_{\tilde{\nu}^i_L}}\left(\overline{d}^k_{R\alpha}\,d^j_{L\alpha}\right)\left(\overline{d}^{j'}_{L\beta}\,d^{k'}_{R\beta}\right) \quad (67)$$

Now perform a Fierz transformation[62] to obtain a vector current.

$$\frac{1}{2}\left(\overline{d}^k_{R\alpha}(1-\gamma^5)d^j_\alpha\right)\frac{1}{2}\left(\overline{d}^{j'}_{L\beta}(1+\gamma^5)d^{k'}_\beta\right) = \frac{1}{2}\left(\overline{d}^k_{R\alpha}\gamma^\mu\frac{1+\gamma^5}{2}d^{k'}_\beta\right)\left(\overline{d}^{j'}_L\gamma_\mu\frac{1-\gamma^5}{2}d^j_\alpha\right)$$

$$= \frac{1}{2}\left(\overline{d}^k_{R\alpha}\gamma^\mu d^{k'}_{R\beta}\right)\left(\overline{d}^{j'}_{L\beta}\gamma_\mu d^j_{L\alpha}\right) \quad (68)$$

An exact working of this with the other term in the interaction Lagrangian yields the full four-fermion operators:

$$\mathcal{M} = -\frac{\lambda'_{ijk}\lambda'^{*}_{ij'k'}}{2m^2_{\tilde{\nu}^i_L}}\ \overline{d}^k_{R\alpha}\,\gamma^\mu\,d^{k'}_{R\beta}\ \overline{d}^{j'}_{L\beta}\,\gamma_\mu\,d^j_{L\alpha} - \frac{\lambda'_{ijk}\lambda'^{*}_{ij'k'}}{2m^2_{\tilde{l}^i_L}}\ \overline{d}^k_{R\alpha}\,\gamma^\mu\,d^{k'}_{R\beta}\ \left(\hat{\overline{u}}^m_{L\beta}V_{mj'}\right)\ \gamma_\mu\ \left(V^*_{jn}\,\hat{u}^n_{L\alpha}\right) \tag{69}$$

This gives us that the operators will contain a linear combination of the up-type quarks. We will consider only the first two generations of up quarks due to the large suppression of the third generation arising from the CKM matrix elements associated with these components. For non-leptonic D decays these couplings allow for tree level processes and penguins through the diagrams in Fig. 8. These correspond to the second term in the amplitude given in Eq. 69. The first term also arises in K meson decays and $K^0 - \bar{K}^0$ mixing.

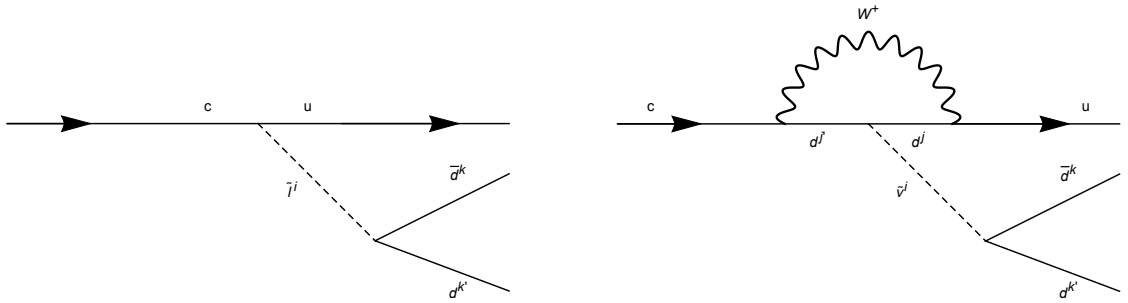

Figure 8: The effective transitions $c \to ud^k\overline{d}^{k'}$. Tree level on the left, penguin on the right.

We will restrict our analysis of D decays to the tree level diagrams, so only the second term will be utilized in what follows. This gives us the effective Hamiltonian for $c \to ud^{k'}\bar{d}^k$:

$$\mathcal{H}^{\rm NP}_{\rm eff} = -\left[\frac{\lambda'_{i2k}\lambda'^{*}_{i1k'}}{2m^2_{\tilde{l}^i_L}}V_{ud}V^*_{cs} + \frac{\lambda'_{i1k}\lambda'^{*}_{i1k'}}{2m^2_{\tilde{l}^i_L}}V_{ud}V^*_{us} + \frac{\lambda'_{i2k}\lambda'^{*}_{i2k'}}{2m^2_{\tilde{l}^i_L}}V_{cd}V^*_{cs} + \frac{\lambda'_{i1k}\lambda'^{*}_{i2k'}}{2m^2_{\tilde{l}^i_L}}V_{us}V^*_{cd}\right]$$

$$\times\ \overline{d}^k_{R\alpha}\,\gamma^\mu\,d^{k'}_{R\beta}\ \hat{\overline{u}}_{L\beta}\,\gamma_\mu\ \hat{c}_{L\alpha} \tag{70}$$

$$\mathcal{H}_{\rm eff}^{\rm NP} = -\frac{\lambda'_{i2k}\lambda'^{*}_{i1k'}}{8m^2_{\tilde{l}^i_L}}\ V_{ud}V^*_{cs}\ \left(\overline{d}^k_\alpha d^{k'}_\beta\right)_{V+A}\left(\overline{u}_\beta\ c_\alpha\right)_{V-A} \tag{71}$$

4.3 New Physics Diagrams

Now we can determine the various diagrams under this effective theory. All amplitudes are given by

$$\mathcal{A} = \left\langle M_1 M_2|\mathcal{H}_{\rm eff}^{\rm SM} + \mathcal{H}_{\rm eff}^{\rm SM,F} + \mathcal{H}_{\rm eff}^{\rm NP} + \mathcal{H}_{\rm eff}^{\rm NP,F}|M_0\right\rangle$$

Where M_0 is the parent meson, and $M_{1,2}$ are the daughter mesons involved in the decay. The diagrams (T, C, E, A) that contribute to the amplitudes can all be written in terms of contractions which determine the topology of the diagram.

We now construct the amplitudes in terms of these diagrams. The effective New Physics Hamiltonian for the four fermion vertex has the form

$$\mathcal{H}_{\rm eff}^{\rm NP} = -\frac{\lambda'_{i2k}\lambda'^{*}_{i1k'}}{8m^2_{\tilde{l}^i}}\ C\ (\overline{d}^k_\alpha\ d^{k'}_\beta)_{V+A}\ (\overline{u}_\beta\ c_\alpha)_{V-A} \tag{72}$$

Looking at the decay $D^0 \to K^-\pi^+$ we have

$$\mathcal{A} = -\frac{\lambda'_{i2k}\lambda'^{*}_{i1k'}}{8m^2_{\tilde{l}^i}} C\left\langle K^-\pi^+|\mathcal{H}_{\rm eff}^{\rm NP}|D^0\right\rangle$$

4.3.1 A_s Diagram

$$\mathcal{A} = -\frac{\lambda'_{i2k}\lambda'^{*}_{i1k'}}{8m^2_{\tilde{l}^i}}\left[\left\langle s\overline{u}\ u\overline{d}|(\overline{d}^k_\alpha\ d^{k'}_\beta)_{V+A}\ (\overline{u}_\beta\ c_\alpha)_{V-A}|c\overline{u}\right\rangle\right] \tag{73}$$

This expression is color-suppressed upon factorization (which we will require in all amplitudes) and we can perform a color Fierz to obtain a color-favored structure, remembering that the octet currents obtained in the color Fierz vanish upon factorization.

$$\mathcal{A} = -\frac{\lambda'_{i2k}\lambda'^{*}_{i1k'}}{8m^2_{\tilde{l}^i}}\left\langle s\overline{u}\ u\overline{d}|\frac{1}{N_c}(\overline{d}^k_\alpha\ d^{k'}_\alpha)_{V+A}\ (\overline{u}_\beta\ c_\beta)_{V-A}|c\overline{u}\right\rangle \tag{74}$$

The $V+A$ term in the operator contracts with the $K^-\pi^+$ and the $V-A$ term contracts with the D^0 and the resulting diagram is what we will call A_s.

4.3.2 C_s Diagram

We can also Fierz the NP Hamiltonian and we obtain

$$\mathcal{H}_{\text{eff}}^{\text{NP,F}} = \frac{\lambda'_{i2k}\lambda'^{*}_{i1k'}}{4m^2_{\tilde{l}^i}} \left(\overline{d}^k_\alpha\, c_\alpha\right)_{S-P} \left(\overline{u}_\beta\, d^{k'}_\beta\right)_{S+P} \tag{75}$$

The amplitude obtained with this operator is

$$\mathcal{A}^F = \left\langle K^-\pi^+|\mathcal{H}_{\text{eff}}^{\text{NP,F}}|D^0\right\rangle$$

$$= \frac{\lambda'_{i2k}\lambda'^{*}_{i1k'}}{4m^2_{\tilde{l}^i}} \left\langle s\overline{u}\; u\overline{d}|(\overline{d}^k_\alpha\, c_\alpha)_{S-P}\; (\overline{u}_\beta\, d^{k'}_\beta)_{S+P}|c\overline{u}\right\rangle \tag{76}$$

This expression is already color favored for factorization. This gives us

$$\mathcal{A}^F = \frac{\lambda'_{i2k}\lambda'^{*}_{i1k'}}{4m^2_{\tilde{l}^i}} \left\langle s\overline{u}\; u\overline{d}| \left(\overline{d}^k_\alpha\, c_\alpha\right)_{S-P} \left(\overline{u}_\beta\, d^{k'}_\beta\right)_{S+P} |c\overline{u}\right\rangle \tag{77}$$

This amplitude is factorized by contracting the $S-P$ term with the K^- and D^0 mesons and the $S+P$ term with the π^+. This gives us the C_s diagram. Notice that this diagram may be enhanced due to it being a scalar operator.

4.3.3 T_s Diagram

We can also obtain the T_s and E_s diagrams in a similar fashion. Consider the $D_s^+ \to \overline{K}^0 K^+$ decay. This amplitude is given by

$$\mathcal{A} = -\frac{\lambda'_{i2k}\lambda'^{*}_{i1k'}}{8m^2_{\tilde{l}^i}} \left\langle s\overline{d}\; u\overline{s}|(\overline{d}^k_\alpha\, d^{k'}_\beta)_{V+A}\; (\overline{u}_\beta\, c_\alpha)_{V-A}|c\overline{s}\right\rangle$$

After a color Fierz on this expression to obtain the proper color structure for factorizaiton, we obtain

$$\mathcal{A} = -\frac{\lambda'_{i2k}\lambda'^{*}_{i1k'}}{8m^2_{\tilde{l}^i}} \left\langle s\overline{d}\ u\overline{s}|\frac{1}{N_c}(\overline{d}^k_\alpha\ d^{k'}_\alpha)_{V+A}\ (\overline{u}_\beta\ c_\beta)_{V-A}|c\overline{s}\right\rangle \tag{78}$$

And the amplitude is contracted by taking the $V+A$ term with the $\overline{K}^0$ and the $V-A$ term with the K^+ and D_s^+. This is the T_s diagram.

4.3.4 E_s Diagram

A Fierz on the Hamiltonian gives

$$\mathcal{A}^F = \frac{\lambda'_{i2k}\lambda'^{*}_{i1k'}}{4m^2_{\tilde{l}^i}} \left\langle s\overline{d}\ u\overline{s}|(\overline{d}^k_\alpha\ c_\alpha)_{S-P}\ (\overline{u}_\beta\ d^{k'}_\beta)_{S+P}|c\overline{s}\right\rangle \tag{79}$$

This expression is already in the color favored structure for factorization and we have

$$\mathcal{A}^F = \frac{\lambda'_{i2k}\lambda'^{*}_{i1k'}}{4m^2_{\tilde{l}^i}} \left\langle s\overline{d}\ u\overline{s}|(\overline{d}^k_\alpha\ c_\alpha)_{S-P}\ (\overline{u}_\beta\ d^{k'}_\beta)_{S+P}|c\overline{s}\right\rangle \tag{80}$$

and contracting the $S-P$ term with D_s^+ and the $S+P$ term with the $\overline{K}^0$ and K^+ gives us the E_s diagram.

We expect the SM matrix elements and the NP matrix elements to be of the same order, so we will encourage that in the fits to be performed. To accomodate this we first acknowlege that the SM parameters of our fit (T, C, E, A) are essentially just the matrix elements of a four-fermion operator .To ensure that the NP parameters to be fit will be of the same order, they too will be just the matrix elements of the four-fermion operators found in the previous section. Now, we have that the NP amplitudes are given by

$$\mathcal{A}^{\rm NP} = \frac{\lambda'_{i2k}\lambda'^{*}_{i1k'}}{8m^2_{\tilde{l}^i}} \left\{-T^{\rm NP}, 2C^{\rm NP}, 2E^{\rm NP}, -A^{\rm NP}\right\} \tag{81}$$

This will ensure that the the SM parameters T, C, E, A will be of the same order as the NP parameters we will call $T^{\rm NP}, C^{\rm NP}, E^{\rm NP}, A^{\rm NP}$. We do this so that we can see clearly

where the suppression of the NP diagrams arises. For a slepton mass of 1 TeV, which is the lower bound on this mass obtained from collider data, we have a suppression of $\mathcal{O}(10^{-1})$. An additional suppression arises from the product of the λ''s.

4.4 Constraints from other processes

In this section we will discuss constraints on the RPV couplings in Eq. 71. The couplings that we will be interested in are

$$\lambda'_{i21}\lambda'^{*}_{i11} \quad \lambda'_{i21}\lambda'^{*}_{i12} \quad \lambda'_{i22}\lambda'^{*}_{i11} \quad \lambda'_{i22}\lambda'^{*}_{i12} \tag{82}$$

There are numerous sources [63, 58, 64, 65, 66, 67, 68] that give bounds on all of the RPV couplings. Starting from Eq. 71, one can see that $D^0 - \bar{D}^0$ mixing can arise at loop level but the contribution is highly suppressed [69] andthe resulting constraint on the coupling is weak. We now turn to see if we can obtain bounds on any of these couplings from other processes. We therefore must look at the other processes that these vertices can contribute to. Looking at each of the terms in Eq. 62 we see that the operators with a mediating squark result in the following four fermion operators [63]

$$\frac{\lambda'_{ijk}\lambda'^{*}_{i'j'k}}{2m^2_{\tilde{d}^k_R}}(\bar{\nu}^{i'}\gamma^\mu\nu^i)_{V-A}(\bar{d}^{j'}\gamma_\mu d^j)_{V-A}, \quad \frac{\lambda'_{ijk}\lambda'^{*}_{i'jk'}}{2m^2_{\tilde{d}^j_L}}(\bar{\nu}^{i'}\gamma^\mu\nu^i)_{V-A}(\bar{d}^{k}\gamma_\mu d^{k'})_{V+A} \tag{83}$$

$$\frac{\lambda'_{ijk}\lambda'^{*}_{i'j'k}}{2m^2_{\tilde{d}^k_R}}(\bar{e}^{i'}\gamma^\mu e^i)_{V-A}(\bar{u}^{j'}\gamma_\mu u^j)_{V-A}, \quad \frac{\lambda'_{ijk}\lambda'^{*}_{i'jk'}}{2m^2_{\tilde{u}^j_L}}(\bar{e}^{i'}\gamma^\mu e^i)_{V-A}(\bar{d}^{k}\gamma_\mu d^{k'})_{V+A} \tag{84}$$

To be relevant to our couplings in Eq. 82 we set $i' = i$. It is also clear that j, j', k, k' can take values 1 and 2 for the couplings of our interest. The processes that can be generated are decays of light unflavored mesons, like π^0, η, η', ϕ e.t.c., to invisible states. An analysis by the NA62 experiment, sets a limit on the invisible decays of the neutral pions from $K^+ \to \pi^+\pi^0$: $BR[\pi^0 \to \text{invisible}] < 4.4 \times 10^{-9}$ [70]. The limits on the other decays are typically $\sim 10^{-4}$ [55] The other processes the operators gives rise

to are the $K_L \to \pi^0 \nu\bar{\nu}$ and $K^+ \to \pi^+ \nu\bar{\nu}$ decays. The branching ratios for K_S decays are not considered as they are suppressed because of the K_S short lifetime. The rare kaon decays, $K_L \to \pi^0 \nu\bar{\nu}$ and $K^+ \to \pi^+ \nu\bar{\nu}$, are being probed by the KOTO experiment at J-PARC and the NA62 experiment at CERN. Recent reports from KOTO [71, 72] indicate that $K_L \to \pi^0 \nu\bar{\nu}$ decays occur at a rate much larger than predicted by the SM.

$$BR(K_L \to \pi^0 \nu\bar{\nu})_{\rm KOTO} = 2.1^{+2.0(+4.1)}_{-1.1(-1.7)} \times 10^{-9} \,. \tag{85}$$

This result is two orders of magnitude larger than the SM prediction, $BR(K_L \to \pi^0 \nu\bar{\nu})_{\rm SM} = (3.4 \pm 0.6) \times 10^{-11}$ [73]. On the other hand NA62 obtains a bound for $K^+ \to \pi^+ \nu\bar{\nu}$ [74],

$$BR(K^+ \to \pi^+ \nu\bar{\nu})_{\rm NA62} < 2.44 \times 10^{-10}. \tag{86}$$

The E787 and E949 experiments at BNL have also measured $BR(K^+ \to \pi^+ \nu\bar{\nu})$ [75, 76] assuming the pion spectrum predicted by the SM. According to Ref. [76],

$$BR(K^+ \to \pi^+ \nu\bar{\nu}) = (1.73^{+1.15}_{-1.05}) \times 10^{-10}. \tag{87}$$

To constrain the couplings of the operators in Eq. 83 involving the neutrinos we will use the $K_L \to \pi^0 \nu\bar{\nu}$ and $K^+ \to \pi^+ \nu\bar{\nu}$ decays we use the ratio of the experimental measurements [52] to the SM predictions [77]

$$R_{K\to\pi\nu\bar{\nu}} = \frac{\Gamma_{RPV}}{\Gamma_{SM}} = \sum_{i=e,\mu,\tau} \frac{1}{3} \left| 1 + \frac{\Delta^{RPV}_{\nu_i,\bar{\nu}_i}}{X_0(x_t) V_{ts} V^*_{td}} \right|^2 + \sum_{i\neq i'} \frac{1}{3} \left| \frac{\Delta^{RPV}_{\nu_i,\bar{\nu}'_i}}{X_0(x_t) V_{ts} V^*_{td}} \right|^2$$

$$\Delta^{RPV}_{\nu_i,\bar{\nu}'_i} = \frac{\pi s^2_W}{\sqrt{2} G_F \alpha} \left| - \frac{\lambda'_{i2k} \lambda_{i'1k}}{2 m^2_{\tilde{d}^k_R}} \right|^2 \quad , \qquad X_0(x_t) = \frac{x(x+2)}{8(x-1)} + \frac{3x(x-2)}{8(x-1)^2} \ln x \tag{88}$$

where $x_t = m_t^2/m_W^2$. The second sum in the expression involves couplings with $i \neq i'$ and we will neglect those and consider only the couplings in the first term. The SM

predictions for the $K_L \to \pi^0 \nu\bar{\nu}$ and $K^+ \to \pi^+ \nu\bar{\nu}$ are given as [74]

$$\mathcal{B}(K_L \to \pi^0 \nu\bar{\nu})_{SM} = .34 \times 10^{-10} \qquad \text{and} \qquad \mathcal{B}(K^+ \to \pi^+ \nu\bar{\nu}) = .84 \times 10^{-10} \tag{89}$$

This gives us bounds on the couplings and the results are in Table. 15. As we will see later, from the fits to the D decays, taking the squark masses of the first two generations larger than the slepton masses by factor of 10 will satisfy the bounds from the rare Kaon decays.

Turning to the operators in Eq. 84, we the first operator generates the decays $D^0 \to \ell^+\ell^-, D^0 \to \pi^0\ell^+\ell^-$ where $\ell = \mu, e$. The strongest constraint comes from $D^0 \to \mu^+\mu^-$ [55] and we use this as a representative decay in Table. 15. These operators also contribute to the decay of unflavored mesons containing the upquark to $\ell^+\ell^-$ final states. One notices that these bounds can be avoided if we choose the squark masses of the first two generations large enough. The bounds to say e^+e^- states can be also be avoided by choosing non zero couplings for $i = 2, 3$ only. Moving on to the second operator in Eq. 84 we will generate the decays $K_{L,S} \to \ell^+\ell^-, K_{L,S} \to \pi^0\ell^+\ell^-$. Again choosing $K_L \to \mu^+\mu^-$ as a representative process we show the bounds on the coupling in Table. 15. The leptonic decays are 2 body decays and for the $D^0 \to e^i\bar{e}^{i\prime}$ the decay width [77] is given by

$$\Gamma(D^0 \to \mu\bar{\mu}) = \frac{1}{128\pi}\left|\frac{\lambda'_{21k}\lambda'^{*}_{22k}}{m^2_{\tilde{d}^k_R}}\right|^2 f_D^2 m_D m_\mu^2 \sqrt{1 - \frac{4m_\mu^2}{m_D^2}} \tag{90}$$

where $f_D = 207$ MeV, and $f_K = 156.1$ MeV. A similar formula can be used for $K_L \to \mu^+\mu^-$.

These processes are extremely rare so we should be able to establish fairly strong bounds on the couplings. The relevane branching ratios are presented in Table 15. We will ignore the B meson decays since the couplings that contribute to those decays result in $j(') = 3$ or $k(') = 3$ indices and these couplings will not concern our analysis.

RPV Coupling	Process	Branching Ratio	Constraint
$\frac{\lambda'_{21k}\lambda'^*_{22k}}{m^2_{\tilde{d}^k_R}}$ $(1\text{ TeV})^2$	$D^0 \to \mu\bar{\mu}$	$< 6.2 \times 10^{-9}$ [52]	$< 6.7 \times 10^{-2}$
$\frac{\lambda'_{2j1}\lambda'^*_{2j2}}{m^2_{\tilde{u}^j_R}}$ $(1\text{ TeV})^2$	$K_L \to \mu\bar{\mu}$	6.84×10^{-9} [52]	$< 5.4 \times 10^{-4}$
$\frac{\lambda'_{i2k}\lambda'^*_{i1k}}{m^2_{\tilde{d}^k_R}}$ $(1\text{ TeV})^2$	$K^0_L \to \pi^0\nu\bar{\nu}$ $K^+ \to \pi^+\nu\bar{\nu}$	$< 2.1 \times 10^{-9}$[52] 1.73×10^{-10}[74]	$< 2.2 \times 10^{-3}$ 1.4×10^{-3}
$\frac{\lambda'_{ij2}\lambda'^*_{ij1}}{m^2_{\tilde{d}^j_L}}$ $(1\text{ TeV})^2$	$K^0_L \to \pi^0\nu\bar{\nu}$ $K^+ \to \pi^+\nu\bar{\nu}$	$< 2.1 \times 10^{-9}$[52] 1.73×10^{-10}[74]	$< 2.2 \times 10^{-3}$ 1.4×10^{-3}

Table 15: The constraints obtained on the RPV couplings from the various processes. The semi-leptonic decays retain the index over the neutinos since there isn't an experimental determination of the neutrino flavor.

This accounts for all of the terms in the Lagrangian 62 that involve a mediating squark. We now look to the decays with a mediating sneutrino.

4.4.1 $K^0 \to \pi\pi$ and $K^0 - \bar{K}^0$ mixing

The operators that we have developed from the R-parity violating Lagrangian will contribute to the decays of K mesons as well as to the mixing of K^0 and $\bar{K}^0$. These will lead to constraints on the sums of interest. The relevant terms from the effective Hamiltonian are

$$\frac{\lambda'_{i21}\lambda'^*_{i11}}{2m^2_{\tilde{\nu}^i_L}}(\bar{d}s)_{V-A}(\bar{d}d)_{V+A} \qquad (K \to \pi\pi) \tag{91}$$

and

$$\frac{\lambda'_{i21}\lambda'^*_{i12}}{2m^2_{\tilde{\nu}^i_L}}(\bar{d}s)_{V-A}(\bar{d}s)_{V+A} \qquad (K^0 - \bar{K}^0 \text{ mixing}) \tag{92}$$

Constraints on these couplings come from the branching ratios for the decays and the mass difference in the mixing. The constraint from the mixing of K^0 and $\bar{K}^0$ comes from the mass difference $\Delta m = |K^0_S - K^0_L|$. Since the mass difference is very small, this will yield a very strong constraint on the coupling constant. The mass difference is given by

$$\Delta m^{NP}_K = 2Re(M_{12}) = 2\text{Re}\left\langle \bar{K}^0 | \frac{\lambda'_{i21}\lambda'^*_{i12}}{2m^2_{\tilde{\nu}^i_L}}(\bar{d}s)_{V-A}(\bar{d}s)_{V+A} | K^0 \right\rangle, \tag{93}$$

where M_{12} represents the mixing in the K^0 and $\bar{K}^0$ system. In the vacuum insertion approximation we have [64]

$$\Delta m_K^{NP} = \frac{\lambda'_{i21}\lambda'^*_{i12}}{m^2_{\tilde{\nu}^i_L}} m_K f_K^2 \left[\frac{1}{12} + \frac{1}{2}\left(\frac{m_K}{m_s + m_d}\right)^2\right], \tag{94}$$

where f_K is the kaon decay constant and $m_{s,d}$ are the strange and down quark masses. We have taken the coupling $\lambda'_{i21}\lambda'^*_{i12}$ to be real and so this coupling does not contribute to the CP violating parameter $\epsilon \sim Im(M_{12})$. This leads us to obtaining the constraint on the coupling

$$\left|\frac{\lambda'_{i21}\lambda'^*_{i12}}{m^2_{\tilde{\nu}^i_L}}\right| (1 \text{ TeV})^2 < 2.2 \times 10^{-8} \tag{95}$$

From this constraint we have that $\lambda'_{i21}\lambda'^*_{i12}$ is effectively equal to zero. This could be due to the incoherent sum over i allowing for cancelation, or it could be due to each term in the sum vanishing. We know that the sum vanishes, so we will work with that assumption. These constraints give us the ability to limit the parameters that will be used in the fit to our model.

The decay widths $K_L \to \pi\pi$ and $K^+ \to \pi\pi$ can put constraints on $\frac{|\lambda'_{i21}\lambda'^*_{i11}|}{2m^2_{\tilde{\nu}^i_L}}$. In the SM these go via tree level charged current single Cabibbo suppressed transitions and so assuming the RPV contribution is the same size as the SM contribution we get

$$|\lambda'_{i21}\lambda'^*_{i11}| \sim \lambda \frac{G_F}{\sqrt{2}} 2m^2_{\tilde{\nu}^i_L} \sim 4\left(\frac{m_{\tilde{\nu}^i_L}}{1TeV}\right)^2. \tag{96}$$

The phase of $\lambda'_{i21}\lambda'^*_{i11}$ will be severely constrained from the CPV violating parameter $\frac{\varepsilon'}{\varepsilon}$ [64, 69] and so we will take the coupling to be real to avoid this constraint. The same argument can be applied to loop level contribution to $\frac{\varepsilon'}{\varepsilon}$ generated from Eq. 71 as the contribution is proportional to $Im(\lambda'_{i21}\lambda'^*_{i11})$.

4.5 Fits

We now look to determine the new physics parameters that best fit the data available at this point. The branching ratios [52] are listed in Tables 19,20,21, and 22, along with

their predicted values from the fit performed. From the two body decay kinematics we have that

$$B_i = \frac{\Gamma_i}{\Gamma} = \tau_0 \Gamma_i = \tau_0 \left[\frac{p}{8\pi\hbar M_0^2} |\mathcal{A}_i|^2 \right]$$

$$\Rightarrow \qquad |\mathcal{A}_i| = \sqrt{\frac{8\pi\hbar M_0^2 B_i}{p\tau_0}} \tag{97}$$

where p is the magnitude of the 3-momentum of the product mesons in the center of mass frame of the parent meson of mass M_0 and lifetime τ_0. Using this we determine the experimental amplitude of each decay. This gives us 28 amplitudes to constrain our system.

In Table 16 we list the SM amplitudes [13] in the first column and the new diagram contributions in the second column. In Table 17 we list the Singly-Cabibbo-Suppressed decays involving only kaons and pions.The Doubly-Cabibbo-Suppressed decays are listed in Table 18. To alleviate some notation we introduce the following definition:

$$X^i_{kk'} = \frac{\lambda_{i2k}\lambda_{i1k'}}{8m^2_{\tilde{l}^i}} \tag{98}$$

and we will take $m_{\tilde{l}^i} = 2$ TeV. Furthermore, we impliment the constraints that we derived above and we can further limit the parameter space by making the assumption that $X^i_{12} = 0$.

Meson	Decay	Standard Model Diagrams	New Physics Diagrams
D^0	$K^-\pi^+$	$\frac{G_F}{\sqrt{2}} V^*_{cs}V_{ud}(T+E)$	$X^i_{21}\left(C^{\rm NP}+A^{\rm NP}\right)$
	$\overline{K}^0\pi^0$	$\frac{G_F}{\sqrt{2}} \frac{V^*_{cs}V_{ud}}{\sqrt{2}}(C-E)$	$\frac{1}{\sqrt{2}}X^i_{21}(T^{\rm NP}-A^{\rm NP})$
	$\overline{K}^0\eta$	$-\frac{G_F}{\sqrt{2}} \frac{V^*_{cs}V_{ud}}{\sqrt{3}}C$	$-\frac{1}{\sqrt{3}}X^i_{21}T^{\rm NP}$
	$\overline{K}^0\eta'$	$\frac{G_F}{\sqrt{2}} \frac{V^*_{cs}V_{ud}}{\sqrt{6}}(C+3E)$	$\frac{1}{\sqrt{6}}X^i_{21}(T^{\rm NP}+3A^{\rm NP})$
D^+	$\overline{K}^0\pi^+$	$\frac{G_F}{\sqrt{2}} V^*_{cs}V_{ud}(C+T)$	$X^i_{21}(T^{\rm NP}+C^{\rm NP})$
D^+_s	$\overline{K}^0K^+$	$\frac{G_F}{\sqrt{2}} V^*_{cs}V_{ud}(C+A)$	$X^i_{21}(T^{\rm NP}+E^{\rm NP})$
	$\pi^+\eta$	$\frac{G_F}{\sqrt{2}} \frac{V^*_{cs}V_{ud}}{\sqrt{3}}(T-2A)$	$\frac{1}{\sqrt{3}}X^i_{21}(C^{\rm NP}-2E^{\rm NP})$
	$\pi^+\eta'$	$\frac{G_F}{\sqrt{2}} \frac{2V^*_{cs}V_{ud}}{\sqrt{6}}(T+A)$	$\frac{2}{\sqrt{6}}X^i_{21}(C^{\rm NP}+E^{\rm NP})$

Table 16: The Cabibbo-Favored decays

Meson	Decay	Standard Model Diagrams	New Physics Diagrams
D^0	$\pi^+\pi^-$	$\frac{G_F}{\sqrt{2}}V_{cd}^*V_{ud}(T+E)$	$X_{11}^i(C^{\rm NP}+A^{\rm NP})$
	$\pi^0\pi^0$	$\frac{G_F}{\sqrt{2}}\frac{V_{cd}^*V_{ud}}{\sqrt{2}}(-C+E)$	$-\frac{1}{\sqrt{2}}X_{11}^i(T^{\rm NP}-A^{\rm NP})$
	K^+K^-	$\frac{G_F}{\sqrt{2}}V_{cs}^*V_{us}(T+E)$	$X_{22}^i(C^{\rm NP}+A^{\rm NP})$
	$\overline{K}^0K^0$	$\frac{G_F}{\sqrt{2}}(V_{cd}^*V_{ud}+V_{cs}^*V_{us})E$	$(X_{11}^i+X_{22}^i)A^{\rm NP}$
D^+	$\pi^+\pi^0$	$-\frac{G_F}{\sqrt{2}}\frac{V_{cd}^*V_{ud}}{\sqrt{2}}(T+C)$	$-\frac{1}{\sqrt{2}}X_{11}^i(T^{\rm NP}+C^{\rm NP})$
	$K^+\overline{K}^0$	$\frac{G_F}{\sqrt{2}}V_{cs}^*V_{us}T+V_{cd}^*V_{ud}A$	$X_{22}^iC^{\rm NP}+X_{11}^iE^{\rm NP}$
D_s^+	π^+K^0	$\frac{G_F}{\sqrt{2}}V_{cd}^*V_{ud}T+V_{cs}^*V_{us}A$	$X_{11}^iC^{\rm NP}+X_{22}^iE^{\rm NP}$
	π^0K^+	$\frac{G_F}{\sqrt{2}}\frac{1}{\sqrt{2}}(-V_{cd}^*V_{ud}C+V_{cs}^*V_{us}A)$	$-\frac{1}{\sqrt{2}}(X_{11}^iT^{\rm NP}-X_{22}^iE^{\rm NP})$

Table 17: The Singly Cabibbo Suppressed Decays involving kaons and pions.

Meson	Decay	Standard Model Diagrams	New Physics Diagrams
D^0	$K^+\pi^-$	$\frac{G_F}{\sqrt{2}}V_{cd}^*V_{us}(T+E)$	$X_{12}^i(C^{\rm NP}+A^{\rm NP})$
	$K^0\pi^0$	$\frac{G_F}{\sqrt{2}}\frac{V_{cd}^*V_{us}}{\sqrt{2}}(C-E)$	$\frac{1}{\sqrt{2}}X_{12}^i(T^{\rm NP}-A^{\rm NP})$
	$K^0\eta$	$-\frac{G_F}{\sqrt{2}}\frac{V_{cd}^*V_{us}}{\sqrt{3}}C$	$-\frac{1}{\sqrt{3}}X_{12}^iT^{\rm NP}$
	$K^0\eta'$	$\frac{G_F}{\sqrt{2}}\frac{V_{cd}^*V_{us}}{\sqrt{6}}(C+3E)$	$\frac{1}{\sqrt{6}}X_{12}^i(T^{\rm NP}+3A^{\rm NP})$
D^+	$K^0\pi^+$	$\frac{G_F}{\sqrt{2}}V_{cd}^*V_{us}(C+A)$	$X_{12}^i(T^{\rm NP}+E^{\rm NP})$
	$K^+\pi^0$	$-\frac{G_F}{\sqrt{2}}\frac{V_{cd}^*V_{us}}{\sqrt{2}}(T-A)$	$-\frac{1}{\sqrt{2}}X_{12}^i(C^{\rm NP}-E^{\rm NP})$
	$K^+\eta$	$-\frac{G_F}{\sqrt{2}}\frac{V_{cd}^*V_{us}}{\sqrt{3}}T$	$-\frac{1}{\sqrt{3}}X_{12}^iC^{\rm NP}$
	$K^+\eta'$	$\frac{G_F}{\sqrt{2}}\frac{V_{cd}^*V_{us}}{\sqrt{6}}(T+3A)$	$\frac{1}{\sqrt{6}}X_{12}^i(C^{\rm NP}+3E^{\rm NP})$
D_s^+	K^0K^+	$\frac{G_F}{\sqrt{2}}V_{cd}^*V_{us}(T+C)$	$X_{12}^i(T^{\rm NP}+C^{\rm NP})$

Table 18: The Doubly Cabibbo Suppressed amplitudes.

We can further constrain our system by including the measurements [52]

$$A_{CP}(D^0\to K^+K^-) = -0.07\pm 0.11\ \% \tag{99}$$

$$A_{CP}(D^0\to \pi^+\pi^-) = 0.13\pm 0.14\ \% \tag{100}$$

$$\Delta A_{CP} = -0.161\pm 0.029\ \% \tag{101}$$

where

$$A_{CP}(D^0\to f) = \frac{\Gamma(D^0\to f)-\Gamma(\overline{D}^0\to \overline{f})}{\Gamma(D^0\to f)+\Gamma(\overline{D}^0\to \overline{f})}$$

and

$$\Delta A_{CP} = A_{CP}(D^0\to K^+K^-) - A_{CP}(D^0\to \pi^+\pi^-)$$

The partial widths are proportional to the amplitude squared. If we write the

amplitude as

$$\mathcal{A}(f) = |S|e^{\imath\phi_S} + |N|e^{\imath\phi_N}$$

where $|S|, |N|$ are the magnitudes of the SM contributions and NP contributions, respectively, then ϕ_S, ϕ_N are their associated phases. The SM phase arises entirely from the diagrams, if we neglect the tiny phase contributions from the CKM matrix elements, and thus are strong phases and unaffected when we take the CP conjugate amplitude. The overall NP phase has a contribution from the $X^i_{kk'}$ which is affected in the CP conjugate amplitude. So, $\phi_N = \phi_X + \phi_D$, where ϕ_X denotes the phase due to the coupling constants, and ϕ_D represents the strong phase coming from the new physics diagrams. This gives us that

$$\mathcal{A}(\overline{f}) = |S|e^{\imath\phi_S} + |N|e^{\imath(-\phi_X+\phi_D)} \tag{102}$$

From this we calculate the CP-asymmetry as

$$A_{CP}(f) = \frac{2|S||N|\sin\phi_X \sin(\phi_S - \phi_D)}{|S|^2 + |N|^2 + 2|S||N|\cos\phi_X \cos(\phi_S - \phi_D)} \tag{103}$$

Using this we can include the individual measurements of $A_{CP}(K^+K^-)$ and $A_{CP}(\pi^+\pi^-)$ as constraints, as well as ΔA_{CP}. Naively we would assume that this asymmetry is dominated by $|N|/|S| \approx A_{CP} \approx 10^{-3}$, with the caveat that the weak phase of the coupling constant can also play a significant role in suppressing this quantity.

Two additional constraints come from the definition of the coupling constants themselves

$$X^i_{kk'} = \frac{\lambda'_{i2k}\lambda'^*_{i1k'}}{8m^2_{\tilde{l}^i}} \qquad \Rightarrow \qquad X^i_{11}X^i_{22} = X^i_{12}X^i_{21} \tag{104}$$

The real and imaginary parts must be the same, thus giving us two more constraints, for a total of 31 constraints on our system.

The fits are performed using the MINUIT[78] package for Python[79]. We have already determined the extent to which new physics is necessary by performing fits on

just the Standard Model amplitudes.

For the fit involving the new physics parameters we have a system of 27 unknown parameters. We will set the X_{12}^i parameter to zero as a result of the discussion of $K^0 - \bar{K}^0$ mixing, and we are down to 25 parameters. We further assume that the X_{11}^i is real so we are down to 24 parameters. We are determining all strong phases relative to the SM T diagram. We also have 33 constraints on these parameters. If we ignore the SCS decays involving η and η' we are down to 25 constraints, but we no longer need to fit the SE and SA amplitudes, so the number of parameters is now 20 and a χ^2 function minimization is thus possible. We find a value of $\chi^2/\text{d.o.f} = 8.31/5$ with the values of parameters given in Tables 23 and 24, for the diagrams and couplings, respectively.

With this fit we obtain the values

$$\frac{|N_{K^+K^-}|}{|S|} = \frac{|X_{22}(C^{\rm NP} + A^{\rm NP})|}{|\lambda(T+E)|} = 0.010 \quad \text{and} \quad \frac{|N_{\pi^+\pi^-}|}{|S|} = \frac{|X_{11}(C^{\rm NP} + A^{\rm NP})|}{|\lambda(T+E)|} = 0.024 \tag{105}$$

in fairly good agreement with our naive assumption.

We now impose the color constraints on the NP diagrams. Within the factorization scheme outlined in Sec.4.3, we see that the NP amplitudes $T_s, A_s \propto 1/N_c$ and $C_s, E_s \propto 1$. We impose the following constraints

$$\frac{T_s}{A_s} \approx 1 \qquad \frac{C_s}{E_s} \approx 1 \qquad \frac{T_s}{C_s} \approx \frac{1}{3} \qquad \frac{A_s}{E_s} \approx \frac{1}{3} \tag{106}$$

and perform a fit which yields a $\chi^2/\text{d.o.f} = 47/8$, which is a fairly poor fit. We also find that $|N|/|S|$ is slightly larger than for the unconstrained fit. For $D^0 \to K^+K^-$ it is 0.05, and for $D^0 \to \pi^+\pi^-$ it is 0.06. A possible explanation for this is that the matrix elements for the scalar and vector operators could be much different and imposing this naive assumption may not be warranted.

Meson	Decay Mode	Experimental Branching Ratio (%)	Predicted (%)	χ^2
D^0	$K^-\pi^+$	3.950 ± 0.031	3.95	0
	$\overline{K}^0\pi^0$	2.48 ± 0.044	2.47	0.1
	$\overline{K}^0\eta$	1.018 ± 0.012	1.022	0.1
	$\overline{K}^0\eta'$	1.898 ± 0.064	1.909	0.03
D^+	$\overline{K}^0\pi^+$	3.124 ± 0.062	3.130	0.01
D_s^+	$\overline{K}^0K^+$	2.95 ± 0.14	2.89	0.2
	$\pi^+\eta$	1.70 ± 0.09	1.70	0
	$\pi^+\eta'$	3.94 ± 0.25	3.69	1.0

Table 19: The branching ratios of the Cabbibo-Favored decays. Experimental data is taken from PDG, the predicted values are obtained from the fitted parameters.

Meson	Decay Mode	Branching Ratio ($\times 10^{-3}$)	Predicted ($\times 10^{-3}$)	χ^2
D^0	$\pi^+\pi^-$	1.455 ± 0.024	1.454	0.001
	$\pi^0\pi^0$	0.826 ± 0.025	0.825	0.0007
	K^+K^-	4.08 ± 0.06	4.06	0.06
	$K^0\overline{K}^0$	0.282 ± 0.010	0.283	0.008
D^+	$\pi^+\pi^-$	1.247 ± 0.033	1.247	0
	$K^+\overline{K}^0$	6.08 ± 0.18	6.12	0.06
D_s^+	π^+K^0	2.44 ± 0.12	2.47	0.06
	π^0K^+	0.63 ± 0.21	0.59	0.03

Table 20: The branching ratios of the Singly-Cabbibo-Suppressed decays involving only pions and kaons. Experimental data is taken from PDG, the predicted values are obtained from the fitted parameters.

4.6 Neutrino Mass

We now have sufficient information to determine the effects these interactions will contribute to the masses of the neutrinos. Refering back to Eq.62, we see that we can construct a loop using the second and third terms that involve a quark-squark-neutrino vertex. This will yield the one-loop diagram shown in Fig.9.

The mass matrix is given by [80]

$$m_{\nu^i} \sim \frac{3}{8\pi^2} \frac{\lambda'_{ijk}\lambda'_{ikj}}{2m_{\tilde{d}^j_L}} M_{\text{SUSY}} m_{d^j} m_{d^k} \tag{107}$$

Looking at just the indexed terms in the expression we see that the ii' element

Meson	Decay Mode	Branching Ratio ($\times 10^{-3}$)
D^0	$\pi^0\eta$	0.63 ± 0.06
	$\pi^0\eta'$	0.92 ± 0.010
	$\eta\eta$	2.11 ± 0.19
	$\eta\eta'$	1.01 ± 0.19
D^+	$\pi^+\eta$	3.77 ± 0.09
	$\pi^+\eta'$	4.97 ± 0.19
D_s^+	$K^+\eta$	1.77 ± 0.35
	$K^+\eta'$	1.8 ± 0.6

Table 21: The branching ratios of the Singly-Cabbibo-Suppressed decays involving η and η'. These were not included in the fit.

Meson	Decay Mode	Branching Ratio ($\times 10^{-4}$)	Predicted ($\times 10^{-4}$)	χ^2
D^0	$K^+\pi^-$	1.364 ± 0.026	1.379	0.3
	$K^0\pi^0$	–	–	–
	$K^0\eta$	–	–	–
	$K^0\eta'$	–	–	–
D^+	$K^0\pi^+$	–	–	–
	$K^+\pi^0$	2.08 ± 0.21	1.66	4.0
	$K^+\eta$	1.25 ± 0.16	1.32	0.2
	$K^+\eta'$	1.85 ± 0.20	1.74	0.8
D_s^+	K^0K^+	–	–	–

Table 22: The branching ratios of the Doubly-Cabbibo-Suppressed decays. Experimental data is taken from PDG, the predicted values are obtained from the fitted parameters. Many of these ratios are unavailable. They have been excluded from the fit.

Diagram	Magnitude $(\text{GeV})^3$	Phase (degrees)
T	0.383 ± 0.002	0
C	0.263 ± 0.004	-155 ± 1
E	0.168 ± 0.001	117.1 ± 0.9
A	0.151 ± 0.010	60 ± 2
T^{NP}	0.93 ± 0.10	-22 ± 3
C^{NP}	0.432 ± 0.009	7.9 ± 0.4
E^{NP}	0.86 ± 0.05	115 ± 3
A^{NP}	0.60 ± 0.01	-128.0 ± 0.6

Table 23: The Standard Model diagram amplitudes, T, C, E, A and the New Physics amplitudes, T_s, C_s, E_s, A_s.

Coupling	Magnitude	Phase (degrees)
$\lambda'_{i21}\lambda'^*_{i11}$	0.131 ± 0.005	0
$\lambda'_{i22}\lambda'^*_{i11}$	0.52 ± 0.04	120 ± 2
$\lambda'_{i22}\lambda'^*_{i12}$	0.32 ± 0.01	-79 ± 3

Table 24: The coupling constants determined from the fit.

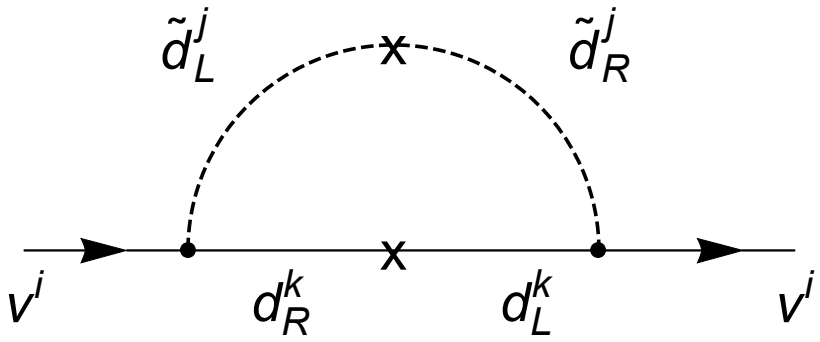

Figure 9: The one-loop contribution to neutrino mass involving a quark-squark loop.

of the matrix is proportional to

$$\begin{aligned}&\lambda'_{i11}\lambda'_{i'11}m_d^2 + \lambda'_{i22}\lambda'_{i'22}m_s^2 + \lambda'_{i33}\lambda'_{i'33}m_b^2 \\ &2\lambda'_{i12}\lambda'_{i'21}m_d m_s + 2\lambda'_{i13}\lambda'_{i'31}m_d m_b + 2\lambda'_{i23}\lambda'_{i'32}m_s m_b \end{aligned} \tag{108}$$

and we see that the largest contribution to each element comes from $\lambda'_{i33}\lambda'_{i'33}$ term, due to the large mass of the the b quark. The terms that we've determined using the D decays (the first two terms from the first line and the first term from the second line) will be suppressed by factors of $m_d^2/m_b^2 \approx 10^{-6}$, $m_s^2/m_b^2 \approx 10^{-3}$, and $m_d m_s/m_b^2 \approx 10^{-5}$, respectively compared with this term.

5 Unified explanation of $b \to s\mu^+\mu^-$, neutrino masses, and $B \to \pi K$ puzzle

Searching for beyond the SM (BSM) physics has been the primary focus of the high energy community. Rare B decays have been widely studied to look for BSM effects. Because these decays get small SM contributions, new physics (NP) can compete with the SM and produce deviations from SM predictions. Over the last few years measurement in certain B decays have shown deviations from the SM. These deviations are observed in two groups- in charged current (CC) processes mediated by the $b \to c\tau^-\bar{\nu}$ tansitions and in the neutral current (NC) processes mediated by $b \to s\ell^+\ell^-$ transition with $\ell = \mu, e$. We will focus here on the NC anomalies although it is possible that the CC and the NC anomalies are related [81] but we will not explore that possibility here.

Let us start with the $b \to s\ell^+\ell^-$ decays which are fertile grounds to look for new physics effects [82, 83]. In $b \to s\mu^+\mu^-$ transitions there are discrepancies with the SM in a number of observables in $B \to K^*\mu^+\mu^-$ [84, 85, 86, 87, 88] and $B_s^0 \to \phi\mu^+\mu^-$ [89, 90].

There are also measurements that are different from the SM expectations that involve ratios of $b \to s\mu^+\mu^-$ and $b \to se^+e^-$ transitions. These measured quantities are tests of Lepton Universality (LUV) and are defined as $R_K \equiv \mathcal{B}(B^+ \to K^+\mu^+\mu^-)/\mathcal{B}(B^+ \to K^+e^+e^-)$ [91, 92] and $R_{K^*} \equiv \mathcal{B}(B^0 \to K^{*0}\mu^+\mu^-)/\mathcal{B}(B^0 \to K^{*0}e^+e^-)$ [93, 94].

While the discrepancies in $b \to s\mu^+\mu^-$ can be understood with lepton universal new physics[95], hints of LUV in R_K and R_K^* require NP that couple differently to the lepton generations. A well studied scenarios is to assume NP coupling dominantly to the muons though NP coupling to electrons is not ruled out [96, 97]. The $b \to$

$s\mu^+\mu^-$ transitions are defined via an effective Hamiltonian with vector and axial vector operators:

$$\begin{aligned} H_{\rm eff} &= -\frac{\alpha G_F}{\sqrt{2}\pi} V_{tb}V_{ts*} \sum_{a=9,10} \left(C_a O_a + C'_a O'_a\right) , \\ O_{9(10)} &= [\bar{s}\gamma_\mu P_L b][\bar{\mu}\gamma^\mu(\gamma_5)\mu] , \end{aligned} \tag{109}$$

where the V_{ij} are elements of the Cabibbo-Kobayashi-Maskawa (CKM) matrix and the primed operators are obtained by replacing L with R. It is assumed Wilson coefficients (WCs) include both the SM and NP contributions: $C_X = C_{X,\rm SM} + C_{X,\rm NP}$. One now fits to the data to extract $C_{X,\rm NP}$. There are several scenarios that give a good fit to the data and results of recent fits can be found Ref. [98, 99, 100, 101, 97]. One of the popular scenario is $C^{\mu\mu}_{9,\rm NP} = -C^{\mu\mu}_{10,\rm NP}$ which can arise from the tree level exchange of leptoquarks (LQ) or a Z' which may be heavy [102, 103, 104] or light [105, 96, 106, 107, 108, 109]. Here we will focus on the LQ solution and there are three types of LQ that can generate this scenario. They are a $SU(2)_L$-triplet scalar (S_3), a $SU(2)_L$-singlet vector (U_1), and a $SU(2)_L$-triplet vector (U_3) and we will focus on the S_3 which along with diquarks can be used to generate neutrino masses at loop level [110, 111]. To generate the neutrino masses, one can fix the S_3 couplings by a fit to the $b \to s\ell^+\ell^-$ data and then the diquark couplings are constrained from the neutrino parameters. In this paper we point out that the diquark couplings can be fixed from nonleptonic B decays and now one can check whether the correct neutrino masses and mixings are reproduced. In other words we are looking for a consistent framework with leptoquarks and diquarks that can explain the semileptonic and nonleptonic B measurements and neutrino masses and mixing.

The observations that we will use for the nonleptonic decays are the set of $B \to \pi K$ decays. These are penguin dominated nonleptonic b decays and been studied extensively. The decays in the set include $B^+ \to \pi^+ K^0$ (designated as $+0$), $B^+ \to \pi^0 K^+$ $(0+)$, $B^0 \to \pi^- K^+$ $(-+)$ and $B^0 \to \pi^0 K^0$ (00). Their amplitudes are not

independent, but obey a quadrilateral isospin relation:

$$\sqrt{2}A^{00} + A^{-+} = \sqrt{2}A^{0+} + A^{+0} \ . \tag{110}$$

Using these decays, nine observables have been measured: the four branching ratios, the four direct CP asymmetries A_{CP}, and the mixing-induced indirect CP asymmetry S_{CP} in $B^0 \to \pi^0 K^0$. Shortly after these measurements were first made (in the early 2000s), it was noted that there was an inconsistency among them. This was referred to as the "$B \to \pi K$ puzzle" [112, 113, 114, 115].

Recently the fits were updated [116, 117, 118]. In Ref. [116] it was observed that the key input to understanding the data was the ratio of the color suppressed tree amplitude (C') to the color allowed (T') amplitude. Theoretically, this ratio is predicted to be $0.15 \lesssim |C'/T'| \lesssim 0.5$ with a default value of around 0.2. It was found that for a large $|C'/T'| = 0.5$, the SM can explain the data satisfactorily. However, with a small, $|C'/T'| = 0.2$, the fit to the data has a p-value of 4%, which is poor. Hence, if $|C'/T'|$ is small, the SM cannot explain the $B \to \pi K$ puzzle – NP is needed. The precise statement of the situation is then, the measurements of $B \to \pi K$ decays *allow* for NP and so in this paper we will assume there is NP in these decays. There are two types of NP mediators that one can consider for the $B \to \pi K$ decays. One is a Z' boson that has a flavor-changing coupling to $\bar{s}b$ and also couples to $\bar{u}u$ and/or $\bar{d}d$. The second option is a diquark that has db and ds couplings or ub and us couplings. We will focus on the diquark explanation as the diquarks can contribute to neutrio masses

The paper is organized in the following manner. In section. 2 we describe the setup with leptoquarks and diquarks that leads to neutrino masses and mixing at the loop level. In that section we also discuss the low energy constraints for the leptoquark Yukawa couplings including the $b \to s\ell^+\ell^-$ data. In section. 3 we explore the $B \to \pi K$ decays mediated by the exchange of diquarks and we consider the constraints on the diquark Yukawa couplings from the $B \to \pi K$ decays and meson oscillations. Finally

in section. 4 consider the collider constraints on the diquark and leptoquarks coupling and masses and we give a scan of all their couplings that satisfy all the constraints and generate the correct neutrino masses and couplings. For a few benchmark cases we present explicit expressions for the diquark and the leptoquark Yukawa couplings and predict the branching ratios for the rare decays $B \to \phi\pi$ and $B \to \phi\phi$. Finally in section.4 we present our conclusions.

5.1 Colored Zee Babu Model

Set Up

We briefly summarise here the main features of the colored Zee Babu Model [119, 110] that are central to our idea. The model includes a scalar leptoquark S_L(with lepton number 1) of mass m_L and a scalar diquark S_D of mass m_S transforming as $(3, 3, -1/3)$ [3] and $(6, 1, -2/3)$[4] respectively under SM gauge group $SU(3)_c \times SU(2) \times U(1)_Y$ with $Q = T_3 + Y$. The baryon number of S_L is taken to be 1/3 whereas S_D is assigned 2/3. With this assignment of baryon number, the baryon conservation is immediate and thus the proton decay is forbidden. The soft-breaking term of the lepton number is introduced so as to generate the Majorana neutrino mass.

With the particle content discussed above, the most general interaction lagrangian is given as

$$\mathcal{L}_{int} = -Y_l^{ij}\,\overline{L_i^c}\,i\,\sigma_2\,Q_j^{\alpha}\,S_L^{\alpha *} - Y_d^{ij}\,\overline{d_{iR}^{\alpha c}}\,d_{jR}^{\beta}\,S_D^{\alpha\beta *} + \mu\,S_L^{\alpha *}\,S_L^{\beta *}\,S_D^{\alpha\beta} + (H.c.), \qquad (111)$$

where $\alpha, \beta = r, b, g$ are $SU(3)_c$ indices and $i, j = 1, 2, 3$ are generation indices, the diquark coupling matrix, Y_d^{ij}, is symmetric whereas the leptoquark coupling matrix, Y_l^{ij}, is general complex matrix. The leptoquark couples lepton and quark as $\sqrt{2}\nu_{iL}\,u_{jL} - \sqrt{2}e_{iL}\,d_{jL} + \nu_{iL}\,d_{jL} + e_{iL}\,u_{jl}$. Note that, in Eqn 111, we can also have additional scalar in-

[3] The choice $(3, 1, -1/3)$ is also possible as it couples neutrinos to down type quarks but will not explain R_K and R_K^* anomaly as this scalar couples up-type quarks to charged leptons.

[4] Note that if we had chosen diquark to be $(3, 1, -2/3)$, Y_d and, hence, neutrino mass matrix would be antisymmetric.

teraction terms(not relevant to our analysis), such as $\left[\lambda_1 \Phi^\dagger \Phi \mathrm{Tr}(S_L^\dagger S_L) + \lambda_2 \mathrm{Tr}(\Phi^\dagger S_L S_L^\dagger \Phi)\right]$ where Φ is Higgs doublet. These terms would give rise to splitting in the mass of S particles, comprising three states of electric charges $-4/3$, $-1/3$ & $2/3$, and would contribute to the oblique corrections[120]. To avoid that, we take $\lambda_{1,2} = 0$ such that all S_L particles/states have same mass, m_L. Along with this, there are quartic and quadratic terms of these scalars. We assume that their coefficients are adjusted such that only the Higgs doublet gets the vev and the potential is bounded from below.

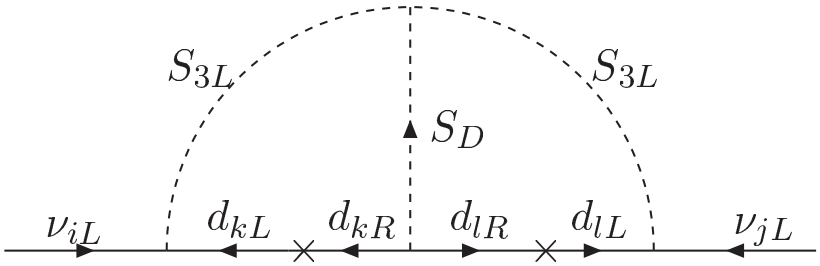

Figure 10: Generation of Neutrino masses via two leptoquarks and a diquark.

The above lagrangian would generate majorana neutrino mass at two loop as depicted in the figure. The resultant neutrino matrix is given as [121, 110],

$$M_\nu^{ij} = 24\,\mu\, Y_l^{ik} m_d^k Y_d^{kl} I^{kl} m_d^l Y_l^{lj}, \tag{112}$$

where I^{kl} is a loop integral, which in the limit of large leptoquark and diquark masses simplifies to

$$I^{kl} \simeq \frac{1}{(4\pi)^4} \frac{1}{m_L^2} \tilde{I}\left(\frac{m_S^2}{m_L^2}\right), \tag{113}$$

with

$$\tilde{I}(r) = \int_0^1 dx \int_0^{1-x} dy \frac{1}{x + y(y + r - 1)} \ln\left(\frac{x + ry}{y(1-y)}\right), \tag{114}$$

and m_d is 3×3 diagonal mass matrix for down-type quarks. Note that we have chosen diagonal bases of mass matrix for down type quarks and charged leptons. So to obtain the correct masses of neutrino, we need to diagonalise the mass matrix, M_ν by the PMNS matrix, $\mathcal{U}$ as

$$m_\nu = \mathcal{U}^\dagger M_\nu \mathcal{U}. \tag{115}$$

The standard parametrization is adopted that

$$\mathcal{U} = \begin{pmatrix} 1 & 0 & 0 \\ 0 & c_{23} & s_{23} \\ 0 & -s_{23} & c_{23} \end{pmatrix} \begin{pmatrix} c_{13} & 0 & s_{13}e^{-i\delta} \\ 0 & 1 & 0 \\ -s_{13}e^{i\delta} & 0 & c_{13} \end{pmatrix} \begin{pmatrix} c_{12} & s_{12} & 0 \\ -s_{12} & c_{12} & 0 \\ 0 & 0 & 1 \end{pmatrix} \begin{pmatrix} 1 & 0 & 0 \\ 0 & e^{i\alpha_{21}/2} & 0 \\ 0 & 0 & e^{i\alpha_{31}/2} \end{pmatrix} \tag{116}$$

where c_{ij} and s_{ij} represent $\cos\theta_{ij}$ and $\sin\theta_{ij}$, respectively. In the case of Majorana neutrinos, α_{21} and α_{31} are the extra CP phases that cannot be determined from the oscillation experiments. However, these phase could be sensitive to the upcoming neutrinoless double beta decay searches. Finally, it should be stressed that the mass dimension 1 parameter, μ, is constrained by demanding the perturbativity of the theory. The trilinear terms in Eqn. 111 would generate one-loop correction to leptoquarks and diquarks masses. These corrections(Δm_S^2) are, in general, proportional to $\frac{\mu^2}{16\pi^2}$. Requiring corrections to be smaller than the corresponding masses implies $\mu \ll 4\pi m_{S/L}$[121]. As various collider searches, discussed in section 5.4, does not allow the scalar masses smaller than 1 TeV, we would take μ from 0.1-1 TeV commensurating with the above constraint.

Having discussed the details of the model, next, we list all the possible constraints, coming from various experiments, on Leptoquarks and Diquark coupling matrix.

5.2 Leptoquarks

- **Lepton flavour violation at tree level**: Collider searches of leptoquarks indicates that they are heavy. So we can study their low energy effects by writing 4-fermi operators of two lepton-two quarks. Using Fierz rearrangement, we should get

$$\frac{Y_l^{ik}Y_l^{jn*}}{2m_L^2}(\overline{l_i}\gamma^\mu P_L l_j)(\overline{q_k}\gamma_\mu P_L q_n) + \text{h.c.} \tag{117}$$

as an effective operator where l and q denote leptons and quarks. These are organized in terms of the four-Fermi effective interactions with normalised dimensionless Wilson coefficients as

$$\mathcal{H}_{\text{eff}} = \sum_{ijkn} \frac{Y_l^{ik} Y_l^{jn*}}{2m_L^2} \mathcal{O}_{ijkn} = \frac{-4G_F}{\sqrt{2}} \sum_{ijkn} C^{ijkn} \mathcal{O}_{ijkn} \tag{118}$$

and are decided by various experiments given in [122].

In Ref.[122], constraints on such operators have been extensively studied. Keeping in mind that Y_l^{ij} should be able to explain small neutrino mass, following are the most crucial operators related to our work

- $(\overline{e_i}\gamma^\mu P_L e_j)(\overline{d}\gamma_\mu P_L d)$-The $\mu - e$ conversion in nuclei sets a bound on Wilson coefficient of this operator, i.e

$$C^{1211} = \left| \frac{Y_l^{11} Y_l^{21*}}{4\sqrt{2} G_F m_L^2} \right| < 8.5 \times 10^{-7}. \tag{119}$$

- $(\overline{\mu}\gamma^\mu P_L e)(\overline{d}\gamma_\mu P_L s)$-The bound from the decay $K^\circ \to e^+\mu^-$ sets a bound on C^{1212}

$$C^{1212} = \left| \frac{Y_l^{12} Y_l^{21*}}{4\sqrt{2} G_F \, m_L^2} \right| < 3.0 \times 10^{-7}. \tag{120}$$

- $(\overline{\nu_i}\gamma^\mu P_L \nu_j)(\overline{d_k}\gamma_\mu P_L d_l)$- The constraint on the K meson decay to pion and neutrinos($\nu_i\nu_j$) sets another bound:

$$C^{ij12} = \left| \frac{Y_l^{i1} Y_l^{j2*}}{4\sqrt{2} G_F \, m_L^2} \right| < 9.4 \times 10^{-6}, \tag{121}$$

Apart from this, we have also taken care of all the Wilson coefficients mentioned in Ref.[122].

- **Lepton flavour violation(LFV) radiative decay**: The LFV radiative decays $l_i \to l_j \gamma$ are induced at one loop by the exchange of a leptoquark S_L with the

branching ratio [120]:

$$\mathrm{BR}(\ell_i \to \ell_j \gamma) \simeq \frac{3\alpha\chi_i}{256\pi G_F^2}\frac{1}{m_L^4}\left|(Y_l Y_l^\dagger)^{ij}\right|^2. \tag{122}$$

where $\alpha = \frac{e^2}{4\pi}$, $\chi_\mu = 1$ and $\chi_\tau = 1/5$. In the case of τ lepton, there are two leptonic modes and hadronic modes can be approximated by a single partonic mode(with three colors). Hence there is a factor of 5 difference in μ and τ-lepton branching ratio. The current experimental bounds[123, 124] are

- $\mathrm{BR}(\mu \to e\gamma) < 4.2 \times 10^{-13}$,
- $\mathrm{BR}(\tau \to \mu\gamma) < 4.4 \times 10^{-8}$,
- $\mathrm{BR}(\tau \to e\gamma) < 3.3 \times 10^{-8}$.

- **$\mathbf{b \to s\ell^+\ell^-}$ anomalies**: As discussed in the introduction one can do fits to the $b \to s\ell^+\ell^-$ data and scenarios in terms of Wilson's co-efficients that give a good description of the data. In the above set up, the exchange of the S_L leptoquark at tree level contributes to the decay $b \to s\ell^+\ell^-$, and in particular generates the scenario $C^{\mu\mu}_{9,\mathrm{NP}} = -C^{\mu\mu}_{10,\mathrm{NP}}$. The effective Hamiltonian describing the decay is parameterized as,

$$\mathcal{H}_{\text{eff}} = -\frac{4G_F}{\sqrt{2}}\frac{\alpha}{4\pi}V_{tb}V_{ts*}\sum_i C_i(\mu)\mathcal{O}_i(\mu) + \text{h.c.}, \tag{123}$$

where $\mathcal{O}_i(\mu)$ are effective operators with Wilson coefficients $C_i(\mu)$ renormalized at the scale μ. For the model under consideration, only the operators $\mathcal{O}_9^{\ell_i} = (\bar{s}\gamma^\mu P_L b)(\bar{\ell}_i\gamma^\mu\ell_i)$ and $\mathcal{O}_{10}^{\ell_i} = (\bar{s}\gamma^\mu P_L b)(\bar{\ell}_i\gamma^\mu\gamma_5\ell_i)$ are induced. Using Fierz identity, we obtain the following Wilson coefficients

$$C_9^{\ell_i} = -C_{10}^{\ell_i} = -\frac{\sqrt{2}\pi}{4\alpha G_F m_L^2}\frac{(Y_l^{i3})(Y_l^{i2*})}{V_{tb}V_{ts*}}, \tag{124}$$

A model independent analysis on the above operators [97] from the R_K, R_K^* and

P_5' suggests that

$$C_9^{\mu\mu}(\mathrm{NP}) = -0.53 \pm 0.08. \tag{125}$$

5.3 Diquark

5.3.1 Nonleptonic Decays and the $B \to \pi K$ Puzzle

In the Standard Model (SM) the amplitudes for hadronic B decays of the type $b \to q\bar{f}f$ are generated by the following effective Hamiltonian

$$H_{eff}^q = \frac{G_F}{\sqrt{2}} \left[V_{fb}V_{fq}^*(c_1 O_{1f}^q + c_2 O_{2f}^q) - \sum_{i=3}^{10} V_{tb}V_{tq}^* c_i^t O_i^q \right] + H.C. , \tag{126}$$

where the superscript t indicates the internal quark, f can be u or c quark. q can be either a d or a s quark depending on whether the decay is a $\Delta S = 0$ or $\Delta S = -1$ process. The operators O_i^q are defined as

$$\begin{aligned}
O_{f1}^q &= \bar{q}_\alpha \gamma_\mu L f_\beta \bar{f}_\beta \gamma^\mu L b_\alpha , \qquad O_{2f}^q = \bar{q}\gamma_\mu L f \bar{f}\gamma^\mu L b , \\
O_{3,5}^q &= \bar{q}\gamma_\mu L b \bar{q}'\gamma^\mu L(R) q' , \qquad O_{4,6}^q = \bar{q}_\alpha \gamma_\mu L b_\beta \bar{q}'_\beta \gamma^\mu L(R) q'_\alpha , \\
O_{7,9}^q &= \frac{3}{2}\bar{q}\gamma_\mu L b e_{q'} \bar{q}'\gamma^\mu R(L) q' , \; O_{8,10}^q = \frac{3}{2}\bar{q}_\alpha \gamma_\mu L b_\beta e_{q'} \bar{q}'_\beta \gamma^\mu R(L) q'_\alpha ,
\end{aligned} \tag{127}$$

where $R(L) = 1 \pm \gamma_5$, and q' is summed over u, d, s, c and b. O_2 and O_1 are the tree level and QCD corrected operators, respectively. O_{3-6} are the strong gluon induced penguin operators, and operators O_{7-10} are due to γ and Z exchange (electroweak penguins), and "box" diagrams at loop level. The Wilson coefficients c_i^f are defined at the scale $\mu \approx m_b$ and have been evaluated to next-to-leading order in QCD. The c_i^t are the regularization scheme independent values and can be found in Ref. [125].

The diquarks discussed in section 2 in the context of neutrino mass generation can contribute to the $B \to \pi K$ decays and we can write down the new physics operators that will be generated by a 6 or $\overline{3}$ diquark [126]. In the general case we get the effective

Hamiltonian for b quark decays $b \to \bar{d}_i d_j d_k$ as,

$$\mathcal{H}^d_{NP} = X^d \, \bar{d}_{\alpha,k} \gamma_\mu (1+\gamma^5) b_\alpha \, \bar{d}_{\beta,j} \gamma^\mu (1+\gamma^5) d_{\beta,i}, \tag{128}$$

where the superscript d in X^d equals 6 or $\overline{3}$ corresponding to the color sextet or the anti-triplet diquark. The greek subscripts represent color and the latin subscripts the flavor. We have

$$X^d = -\frac{Y^d_{i3} Y^{*d}_{jk}}{4m_S^2}, \tag{129}$$

where the Yukawa Y are symmetric for the sextet diquark and antisymmetric for the ant-triplet diquark and we have assumed the same masses for the diquarks.

For b decays of the type $b \to \bar{s}ss$ the diquark contribution is tiny as the effective Hamiltonian is proportional to Y^d_{22} which vanishes for the $\overline{3}$ diquark and is highly suppressed from K and B mixing for the sextet diquark. Similarly the $b \to \bar{d}dd$ transition is proportional to Y^d_{11} is also small.

For $b \to s\bar{d}d$($b \to \bar{d}sd$ and $b \to \bar{d}ds$) transitions we have the following Hamiltonian

$$\begin{aligned} \mathcal{H}^d_{NP} &= X^d \, \bar{s}_\alpha \gamma_\mu (1+\gamma^5) b_\alpha \, \bar{d}_\beta \gamma^\mu (1+\gamma^5) d_\beta \\ &+ X^d_C \, \bar{s}_\alpha \gamma_\mu (1+\gamma^5) b_\beta \, \bar{d}_\beta \gamma^\mu (1+\gamma^5) d_\alpha, \end{aligned} \tag{130}$$

with

$$\begin{aligned} X^d &= -\frac{Y^d_{13} Y^{*d}_{12}}{4m_S^2}, \\ X^d_C &= -\frac{Y^d_{13} Y^{*d}_{21}}{4m_S^2}, \end{aligned} \tag{131}$$

and

$$\begin{aligned} X^{\overline{3}} &= -X_C^{\overline{3}}, \\ X^6 &= X_C^6. \end{aligned} \tag{132}$$

We can rewrite the effective Hamiltonian after a color Fierz transformation as

$$\begin{aligned} \mathcal{H}^d_{NPF} &= X^i\, \bar{d}_\beta \gamma_\mu (1+\gamma^5) b_\alpha\, \bar{s}_\alpha \gamma^\mu (1+\gamma^5) d_\beta \\ &+ X^i_C\, \bar{d}_\beta \gamma_\mu (1+\gamma^5) b_\beta\, \bar{s}_\alpha \gamma^\mu (1-\gamma^5) d_\alpha. \end{aligned} \tag{133}$$

The only other unsuppressed transitions is $b \to s\bar{s}d($ $b \to \bar{s}sd$ and $b \to \bar{s}ds$) which has the effective Hamiltonian,

$$\begin{aligned} \mathcal{H}^d_{NP} &= X^d\, \bar{s}_\alpha \gamma_\mu (1+\gamma^5) b_\alpha\, \bar{d}_\beta \gamma^\mu (1+\gamma^5) s_\beta \\ &+ X^d_C\, \bar{s}_\alpha \gamma_\mu (1+\gamma^5) b_\beta\, \bar{d}_\beta \gamma^\mu (1+\gamma^5) s_\alpha, \end{aligned} \tag{134}$$

with

$$\begin{aligned} X^d &= -\frac{Y^d_{23} Y^{*d}_{12}}{4m_S^2}, \\ X^d_C &= -\frac{Y^d_{23} Y^{*d}_{21}}{4m_S^2}, \end{aligned} \tag{135}$$

In this case at the meson level we can have the decays $B \to \phi\pi$ and the annhilation decays $B \to \phi\phi$. These decays are highly suppressed in the SM and the observance of these decays could signal the presence of diquarks

5.3.2 Naive $B \to \pi K$ Puzzle

We begin by reviewing the $B \to \pi K$ puzzle. As in Ref. [116] we can analyze the $B \to \pi K$ decays in terms of topological amplitudes. Including only the leading diagrams

the $B \to \pi K$ amplitudes become

$$\begin{aligned} A^{+0} &= -P'_{tc} \ , \\ \sqrt{2}A^{0+} &= -T'e^{i\gamma} + P'_{tc} - P'_{EW} \ , \\ A^{-+} &= -T'e^{i\gamma} + P'_{tc} \ , \\ \sqrt{2}A^{00} &= -P'_{tc} - P'_{EW} \ . \end{aligned} \tag{136}$$

Here, T' is the color allowed tree amplitude, P'_{tc} is gluonic penguin amplitudes and P'_{EW} is the color allowed electroweak penguin amplitude. Furthermore in the SU(3) limit the T' and P'_{EW} are proportional to each other and so have the same strong phases. Now consider the direct CP asymmetries of $B^+ \to \pi^0 K^+$ and $B^0 \to \pi^- K^+$. Such CP asymmetries are generated by the interference of two amplitudes with nonzero relative weak and strong phases. In both A^{0+} and A^{-+}, T'-P'_{tc} interference leads to a direct CP asymmetry. On the other hand, in A^{0+}, P'_{EW} and T' have the same strong phase ($P'_{EW} \propto T'$, while P'_{EW} and P'_{tc} have the same weak phase ($= 0$), so that P'_{EW} does not contribute to the direct CP asymmetry. This means that we expect $A_{CP}(B^+ \to \pi^0 K^+) = A_{CP}(B^0 \to \pi^- K^+)$.

The latest $B \to \pi K$ measurements are shown in Table 25. Not only are $A_{CP}(B^+ \to \pi^0 K^+)$ and $A_{CP}(B^0 \to \pi^- K^+)$ not equal, they are of opposite sign! Experimentally, we have $(\Delta A_{CP})_{\rm exp} = (12.2 \pm 2.2)\%$. This differs from 0 by 5.5σ. This is the naive $B \to \pi K$ puzzle.

Mode	$BR[10^{-6}]$	A_{CP}	S_{CP}
$B^+ \to \pi^+ K^0$	23.79 ± 0.75	-0.017 ± 0.016	
$B^+ \to \pi^0 K^+$	12.94 ± 0.52	0.040 ± 0.021	
$B^0 \to \pi^- K^+$	19.57 ± 0.53	-0.082 ± 0.006	
$B^0 \to \pi^0 K^0$	9.93 ± 0.49	-0.01 ± 0.10	0.57 ± 0.17

Table 25: Branching ratios, direct CP asymmetries A_{CP}, and mixing-induced CP asymmetry S_{CP} (if applicable) for the four $B \to \pi K$ decay modes. The data are taken from Ref. [52].

5.3.3 Model-independent new physics formalism

In the general approach of Ref. [127, 128], the NP operators that contribute to the $B \to \pi K$ amplitudes take the form $\mathcal{O}_{NP}^{ij,q} \sim \bar{s}\Gamma_i b\, \bar{q}\Gamma_j q$ $(q = u, d)$, where $\Gamma_{i,j}$ represent Lorentz structures, and color indices are suppressed. The NP contributions to $B \to \pi K$ are encoded in the matrix elements $\langle \pi K | \, \mathcal{O}_{NP}^{ij,q} \, | B \rangle$. In general, each matrix element has its own NP weak and strong phases.

Note that the strong phases are basically generated by QCD rescattering from diagrams with the same CKM matrix elements. One can argue that the strong phase of T' is expected to be very small since it is due to self-rescattering. For the same reason, all NP strong phases are also small, and can be neglected. In this case, many NP matrix elements can be combined into a single NP amplitude, with a single weak phase:

$$\sum \langle \pi K | \, \mathcal{O}_{NP}^{ij,q} \, | B \rangle = \mathcal{A}^q e^{i\Phi_q} \ . \tag{137}$$

Here the strong phase is zero. There are two classes of such NP amplitudes, differing only in their color structure: $\bar{s}_\alpha \Gamma_i b_\alpha \, \bar{q}_\beta \Gamma_j q_\beta$ and $\bar{s}_\alpha \Gamma_i b_\beta \, \bar{q}_\beta \Gamma_j q_\alpha$ $(q = u, d)$. They are denoted $\mathcal{A}'^q e^{i\Phi'_q}$ and $\mathcal{A}'^{C,q} e^{i\Phi'^C_q}$, respectively [128]. Here, Φ'_q and Φ'^C_q are the NP weak phases. In general, $\mathcal{A}'^q \neq \mathcal{A}'^{C,q}$ and $\Phi'_q \neq \Phi'^C_q$. Note that, despite the "color-suppressed" index C, the matrix elements $\mathcal{A}'^{C,q} e^{i\Phi'^C_q}$ are not necessarily smaller than $\mathcal{A}'^q e^{i\Phi'_q}$.

There are therefore four NP matrix elements that contribute to $B \to \pi K$ decays. However, only three combinations appear in the amplitudes: $\mathcal{A}'^{comb} e^{i\Phi'} \equiv -\mathcal{A}'^u e^{i\Phi'_u} + \mathcal{A}'^d e^{i\Phi'_d}$, $\mathcal{A}'^{C,u} e^{i\Phi'^C_u}$, and $\mathcal{A}'^{C,d} e^{i\Phi'^C_d}$ [128]. The $B \to \pi K$ amplitudes can now be written in terms of the SM diagrams and these NP matrix elements. Here we

neglect the small SM diagram P'_{uc} but include the color suppressed amplitudes:

$$\begin{aligned}
A^{+0} &= -P'_{tc} - \frac{1}{3}P'^{C}_{EW} + \mathcal{A}'^{C,d}e^{i\Phi'^{C}_{d}} \ , \\
\sqrt{2}A^{0+} &= P'_{tc} - T'\,e^{i\gamma} - P'_{EW} - C'\,e^{i\gamma} - \frac{2}{3}P'^{C}_{EW} + \mathcal{A}'^{,comb}e^{i\Phi'} - \mathcal{A}'^{C,u}e^{i\Phi'^{C}_{u}} \ , \\
A^{-+} &= P'_{tc} - T'\,e^{i\gamma} - \frac{2}{3}P'^{C}_{EW} - \mathcal{A}'^{C,u}e^{i\Phi'^{C}_{u}} \ , \\
\sqrt{2}A^{00} &= -P'_{tc} - P'_{EW} - C'\,e^{i\gamma} - \frac{1}{3}P'^{C}_{EW} + \mathcal{A}'^{,comb}e^{i\Phi'} + \mathcal{A}'^{C,d}e^{i\Phi'^{C}_{d}} \ . \qquad (138)
\end{aligned}$$

Here we can define the various matrix elements as

$$\begin{aligned}
\mathcal{A}'^{C,d}e^{i\Phi'^{C}_{d}} &= \sqrt{2}\left\langle\pi^0K^0\right|\mathcal{H}^{d}_{NPF}\left|B^0\right\rangle = \left\langle\pi^+K^0\right|\mathcal{H}^{d}_{NPF}\left|B^+\right\rangle \\
\mathcal{A}'^{C,u}e^{i\Phi'^{C}_{u}} &= -\sqrt{2}\left\langle\pi^0K^+\right|\mathcal{H}^{u}_{NPF}\left|B^+\right\rangle = \left\langle\pi^-K^+\right|\mathcal{H}^{u}_{NPF}\left|B^0\right\rangle \\
\mathcal{A}'^{,comb}e^{i\Phi'} &= \sqrt{2}\left\langle\pi^0K^+\right|\left[\mathcal{H}^{u}_{NP}+\mathcal{H}^{d}_{NP}\right]\left|B^+\right\rangle = \sqrt{2}\left\langle\pi^0K^0\right|\left[\mathcal{H}^{u}_{NP}+\mathcal{H}^{d}_{NP}\right]\left|B^0\right\rangle \qquad (139)
\end{aligned}$$

In our model $\mathcal{H}^{u}_{NP}$ and $\mathcal{H}^{u}_{NPF}$ are absent while $\mathcal{H}^{d}_{NP}$ and $\mathcal{H}^{d}_{NPF}$ are defined in Eq. 130 and Eq. 133. In the factorization assumption and using Eq. 130 and Eq. 133 we get the following results for the non-zero amplitudes,

$$\begin{aligned}
\mathcal{A}'^{C,d}e^{i\Phi'^{C}_{d}} &= \left[X^6 - X^{\bar{3}} + \frac{X^6 + X^{\bar{3}}}{N_c}\right] \\
&\quad \times \left\langle\pi^+\right|\bar{d}_\beta\gamma_\mu(1+\gamma^5)b_\beta\left|B^+\right\rangle\left\langle K^0\right|\bar{s}_\alpha\gamma^\mu(1+\gamma^5)d_\alpha\left|0\right\rangle
\end{aligned}$$

$$\begin{aligned}
\mathcal{A}'^{,d}e^{i\Phi'_{d}} &= \sqrt{2}\left[X^6 + X^{\bar{3}} + \frac{X^6 - X^{\bar{3}}}{N_c}\right] \\
&\quad \times \left\langle K^+\right|\bar{s}_\beta\gamma_\mu(1+\gamma^5)b_\beta\left|B^+\right\rangle\left\langle\pi^0\right|\bar{d}_\alpha\gamma^\mu(1+\gamma^5)d_\alpha\left|0\right\rangle \qquad (140)
\end{aligned}$$

In Ref. [129], a different set of NP operators is defined:

$$\begin{aligned}
P'_{EW,NP}\,e^{i\Phi'_{EW}} &\equiv \mathcal{A}'^{,u}e^{i\Phi'_{u}} - \mathcal{A}'^{,d}e^{i\Phi'_{d}} \ , \\
P'_{NP}\,e^{i\Phi'_{P}} &\equiv \frac{1}{3}\mathcal{A}'^{C,u}e^{i\Phi'^{C}_{u}} + \frac{2}{3}\mathcal{A}'^{C,d}e^{i\Phi'^{C}_{d}} \ , \\
P'^{C}_{EW,NP}\,e^{i\Phi'^{C}_{EW}} &\equiv \mathcal{A}'^{C,u}e^{i\Phi'^{C}_{u}} - \mathcal{A}'^{C,d}e^{i\Phi'^{C}_{d}} \ . \qquad (141)
\end{aligned}$$

In this case we have

$$\begin{aligned} P'_{EW,NP}\, e^{i\Phi'_{EW}} &\equiv -\mathcal{A}'^{,d} e^{i\Phi'_d}\ , \\ P'_{NP}\, e^{i\Phi'_P} &\equiv \frac{2}{3}\mathcal{A}'^{C,d} e^{i\Phi'^C_d} = -(2/3) P'^C_{EW,NP} \\ P'^C_{EW,NP}\, e^{i\Phi'^C_{EW}} &\equiv -\mathcal{A}'^{C,d} e^{i\Phi'^C_d}\ . \end{aligned} \tag{142}$$

NP fit (1): χ^2/d.o.f. $= 3.75/4$, p-value $= 0.44$	
Parameter	Best-fit value
γ	$(67.5 \pm 3.4)^\circ$
β	$(21.80 \pm 0.68)^\circ$
Φ'	$(37.0 \pm 12.6)^\circ$
$\lvert T'\rvert$	19.1 ± 2.8
$\lvert P'_{tc}\rvert$	48.7 ± 1.2
$P'_{EW,NP}$	8.6 ± 2.5
$P'^C_{EW,NP}$	2.7 ± 1.1
$\delta_{P'_{tc}}$	$(-4.0 \pm 1.1)^\circ$
$\delta_{C'}$	$(-60.0 \pm 115.6)^\circ$

NP fit (2): χ^2/d.o.f. $= 3.82/4$, p-value $= 0.43$	
Parameter	Best-fit value
γ	$(74.7 \pm 5.2)^\circ$
β	$(21.80 \pm 0.68)^\circ$
Φ'	$(18.7 \pm 33.9)^\circ$
$\lvert T'\rvert$	19.7 ± 7.1
$\lvert P'_{tc}\rvert$	45.5 ± 3.9
$P'_{EW,NP}$	6.7 ± 3.9
$P'^C_{EW,NP}$	6.5 ± 3.7
$\delta_{P'_{tc}}$	$(-4.0 \pm 2.0)^\circ$
$\delta_{C'}$	$(-48.9 \pm 23.5)^\circ$

Table 26: $\chi^2_{\rm min}$/d.o.f. and best-fit values of unknown parameters for the Diquark model where the Fit 1 has $X^6 = X^{\overline{3}}$, and Fit 2 has $X^{\overline{3}} = 0$. Constraints: $B \to \pi K$ data, measurements of β and γ, $|C'/T'| = 0.2$, $|P'^C_{EW,NP}/P'_{EW,NP}| = 0.3$ (Fit 1), and $|P'^C_{EW,NP}/P'_{EW,NP}| = 1$ (Fit 2).

We consider two models, the first with

$$X^6 = X^{\overline{3}} \tag{143}$$

This leads to $P'^C_{EW,NP}/P'_{EW,NP} = \frac{1}{3}$ with both amplitudes having the same weak phase.

$$\begin{aligned} P'_{EW,NP}\, e^{i\Phi'_{EW}} &\equiv \frac{Y^6_{d13}Y^{*6}_{d12}}{4m_S^2}\sqrt{2}\left\langle K^+\right|\, \bar{s}_\beta\gamma_\mu(1+\gamma^5)b_\beta\left|B^+\right\rangle\left\langle 0\right|\, \bar{s}_\alpha\gamma^\mu(1+\gamma^5)d_\alpha\left|K^0\right\rangle\ , \\ P'_{NP}\, e^{i\Phi'_P} &\equiv \frac{2}{3}\mathcal{A}'^{C,d}e^{i\Phi'^C_d} = -(2/3)P'^C_{EW,NP} \\ P'^C_{EW,NP}\, e^{i\Phi'^C_{EW}} &\equiv -\mathcal{A}'^{C,d}e^{i\Phi'^C_d} = P'_{EW,NP}\, e^{i\Phi'_{EW}}/3\ . \end{aligned} \tag{144}$$

The second model has

$$X^{\overline{3}} = 0 \tag{145}$$

This leads to $P'^C_{EW,NP}/P'_{EW,NP} = 1$, again with both amplitudes having the same weak phase.

A χ^2 fit for the new physics within this scenario was performed to determine the parameters of the model. The procedure for deterimining such a fit is as follows. We define the function

$$\chi^2 = \sum_{i=1}^{N}\left(\frac{\mathcal{O}_{exp}-\mathcal{O}_{th}}{\Delta\mathcal{O}_{exp}}\right)^2 \tag{146}$$

where $\mathcal{O}_{exp}$ and $\Delta\mathcal{O}_{exp}$ are the experimentally determined quantities with their associated uncertainties, respectively, as listed in Table 25. $\mathcal{O}_{th}$ are determined from the model and are thus functions of the unknown parameters. The goal from here is to find the values of the parameters that minimize χ^2. There are many programs available to accomplish this, one of the most widely used is MINUIT [78], which is used here. The goodness of the fit is determined by the value of χ^2 at the minimum and the number of degrees of freedom in the fit. The degrees of freedom are the number of constraints included in the fit minus the number of parameters that are fitted. In this case the number of constraints is 13: the $B \to \pi K$ data, the independent measurements of β and γ, and the constraints on $|C'/T'|$ and $|P'^C_{EW,NP}/P'_{EW,NP}|$. The number of parameters is nine and we have that the number of degrees of freedom are four. A "good"

fit is one where $\chi^2_{min} \approx$ d.o.f., but a better measure is the p-value which gives the probablility that the model tested adequately describes the observations.

The results of the fit for this case are shown in Table 26. Here the p-value is 44% for $X^6 = X^{\bar{3}}$, and 43% for $X^{\bar{3}} = 0$, which is not bad (and is far better than that of the SM).

The SM T' diagram involves the tree-level decay $\bar{b} \to \bar{u}W^{+*}(\to u\bar{s} = K^+)$. The NP $P'_{EW,NP}$ diagram looks very similar and is expressed relative to the T' diagram. Within factorization, the SM and NP diagrams involve $A_{\pi K} \equiv F_0^{B\to\pi}(0)f_K$ and $A_{K\pi} \equiv F_0^{B\to K}(0)f_\pi$, respectively, where $F_0^{B\to K,\pi}(0)$ are form factors and $f_{\pi,K}$ are decay constants. The hadronic factors are similar in size: $|A_{K\pi}/A_{\pi K}| = 0.9 \pm 0.1$ [125]. Taking central values for $X^6 = X^{\bar{3}}$, we have [116]

$$\begin{aligned} & \Phi' = Arg[Y^6_{d13}Y^{*6}_{d12}] \\ & \left|\frac{P'_{EW,NP}}{T'}\right| \simeq \frac{2A_{K\pi}|X^{\bar{3}}|}{A_{\pi K}(G_F/\sqrt{2})|V_{ub*}V_{us}|} = \frac{8.6}{19.1} \\ \Longrightarrow \quad & \left|\frac{Y^6_{d13}Y^{*6}_{d12}}{2m_S^2}\right| = (3.4 \pm 1.2) \times 10^{-3}\ \text{TeV}^{-2}\ . \end{aligned} \tag{147}$$

For $X^{\bar{3}} = 0$ we obtain

$$\left|\frac{Y^6_{d13}Y^{*6}_{d12}}{2m_S^2}\right| = (2.6 \pm 1.8) \times 10^{-3}\ \text{TeV}^{-2} \tag{148}$$

5.3.4 Neutral Meson Mixing

Diquarks, inspite of being charged, through their coupling to the same generation quarks can mediate the mixing between neutral mesons at tree level. Following the convention in [130], the mixing can be depicted as the six dimension operator:

$$\mathcal{O}_{mix} = \frac{Y_d^{*ij}Y_d^{kl}}{m_S^2}\bar{\psi^k}_R\gamma^\mu\psi^i{}_R\,\bar{\psi^l}_R\gamma_\mu\psi^j{}_R \tag{149}$$

The 90 % C.L bounds on the corresponding Wilson coefficients[130] is then given as:

$$\begin{aligned}
\mathbf{K^\circ - \overline{K^\circ}} \qquad & \left|\frac{Y_d^{*11}Y_d^{22}}{4\sqrt{2}G_F m_S^2}\right| < 2.9\times10^{-8} \\
\mathbf{B_d^\circ - \overline{B_d^\circ}} \qquad & \left|\frac{Y_d^{*11}Y_d^{33}}{4\sqrt{2}G_F m_S^2}\right| < 7.0\times10^{-7} \\
\mathbf{B_s^\circ - \overline{B_s^\circ}} \qquad & \left|\frac{Y_d^{*22}Y_d^{33}}{4\sqrt{2}G_F m_S^2}\right| < 3.3\times10^{-5}
\end{aligned}$$

5.4 Numerical Analysis and Discussion

Before we go ahead with the analysis, we first discuss the limits from collider experiments. The Collider experiments provide direct limits on the leptoquark states through their decay to leptons and quark in the final state. There have many studies where potential signatures are discussed [131, 132]. The leptoquarks can be pair produced from gg and $q\bar{q}$ or singly produced at hadron colliders via $g + q \to S_L +$lepton. Recent studies at ATLAS[133] and CMS[134] with 13 TeV data puts a bound on the scalar leptoquark mass, $m_L > 1, 1.2(\text{ATLAS}), 0.9(\text{CMS})\text{TeV}$ when decays to ue, $c\mu$ and $t\tau$ with 100% branching fraction, respectively at 95 % C.L. The previous results[135, 136] at 8 TeV from the search of single leptoquark production were of order 0.65 TeV for final state $c\mu$. So, for our analysis, we will be taking $m_L > 1\,\text{TeV}$.

Similar to the Leptoquarks, Diquarks can be looked at the LHC through dijets in the final state. The recent studies at CMS on dijet final states allows scalar diquark of mass greater than 6 TeV. However, these limits are derived for the E_6 diquark which couples with an up-type quark and a down-type quark[137]. These limits are very sensitive to the assumptions of decay branching fraction as well as the flavor dependant coupling strengthes. Also, the diquark in our work couples only to down-type quarks contrary to E_6 diquark. This leads to a decrease in the flux factor and hence the crossection and thereby the bounds on m_S should be lower. Hence, we would assume $m_S \in [5:20]\,\text{TeV}$, covering all the important values.

With these mass range of scalars, we first randomly generated a sample of diquark couplings satisfying the constraints discussed in section 3. For $m_S \in [5:$

20] TeV, the $B \to \pi K$ fit requires $Y_d^{12,13}$ to be greater than 0.1. So we genrated this couplings randomly in range [0.1 : 1]. We fixed Y_d^{23} of order 10^{-2} and Y_d^{33} was generated $\in [10^{-4} : 10^{-2}]$. The choice for Y_d^{33} is justified in the context of neutrino mass calculation as this coupling is multiplied to square of bottom quark mass. For the remaining Y_d^{ij}, i.e, $Y_d^{11,12}$, we scan in range $[10^{-5}, 1]$. Except Y_d^{23}, all the diquark coupling can be complex. It should be noted that the signs of the couplings are randomly assigned with equal probabilities being positive or negative in the whole calculation.

As for the leptoquark case, Y_l^{2i} couplings(real) are generated randomly in the range $[10^{-5} : 1]$. With the obtained sets of couplings, we calculated the strength of leptoquark couplings for randomly genrated LQ mass solving Eqn.112 so as to get the correct neutrino masses. The Neutrino mass matrix in Eqn.112 gives six equations corresponding to six independent parameters given in Table 27. We have kept majorana phases to be 0, and have employed the 2σ ranges for the neutrino mixing parameters for Normal Hierarchy from [138, 139]. Finally, we selected those sets of LQ couplings that satisfy all the constraints in section 5.2. The results for the LQ couplings are given in Fig.12.

The pattern in the lower limit of $Y_l^{22,23}$ coupling is mainly decided by $b \to s\ell^+\ell^-$ anomalies. The DQ couplings $Y_d^{12/13}$ always comes with product of down and strange/bottom quark masses in Eqn.112. Since down quark mass is very small, the largeness of the coupling doesn't have very strong effects.

We have compared our results obtained for leptoquark coupling with the results given in [111] and [140], and found them consistent. A few benchmark points(B.P) are given in Appendix A. For these BP, we present branching ratios for the rare decays in Table 28. Hence, this analysis shows that the B anomalies and the neutrino masses can all be accomodated in a consistent framework.

δm^2	$7.07 - 7.73 \times 10^{-5}\text{eV}^2$
$\sin^2\theta_{12}$	$0.265 - 0.334$
$\lvert\Delta m^2\rvert$	$2.454 - 2.606 \times 10^{-3}\text{eV}^2$
$\sin^2\theta_{13}$	$0.0199 - 0.0231$
$\sin^2\theta_{23}$	$0.395 - 0.470$
δ/π	$1.00 - 1.90$

Table 27: Neutrino data with 2σ deviation for Normal Hierarchy[138, 139].

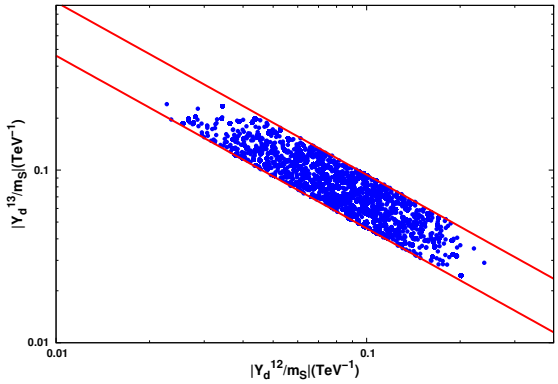

Figure 11: The correlation between $\frac{|Y_d^{12}|}{m_S}$ and $\frac{|Y_d^{13}|}{m_S}$. The shaded area correspond to mass range $m_S \in [5:20]$.

B.P	BR($\mathbf{B}^\pm \to \phi\pi^\pm$)	BR($\mathbf{B}^\pm \to \phi\pi^\circ$)	BR($\mathbf{B}^\pm \to \phi\phi$)
A	1.45×10^{-10}	7.2×10^{-11}	1.45×10^{-12}
B	6.5×10^{-14}	3.2×10^{-14}	6.5×10^{-16}
C	1.19×10^{-12}	5.95×10^{-13}	1.19×10^{-14}

Table 28: Branching ratio obtained for the couplings that can produce required neutrino mass and also satisfy the constraints coming from $B \to \pi K$ puzzle.

5.5 Conclusion

In conclusion we have discussed a unified framework to provide solutions to three problems. They are the anomalies in $b \to s\mu^+\mu_-$ measurements, nonleptonic $B \to \pi K$ decays, and the issue of generating neutrino masses and mixing. Our framework contained a scalar triplet leptoquark, a scalar color sextet diquark, and also, possibly, a color antitriplet diquark. We considered several low energy as well as collider bounds

on the leptoquark, diquark couplings and masses. For the leptoquarks these low energy observables included the $b \to s\ell^+\ell^-$ measurements. The solutions to the $B \to \pi K$ puzzle provided constraints on products of the diquark Yukawa couplings. We then checked that the correct neutrino masses and mixings were reproduced with the allowed couplings of the leptoquarks and diquarks. We also predicted the branching ratios for a few rare B decays whose observations could signal the existence of diquarks. However, we found the branching ratios of these decays to be unobservably small.

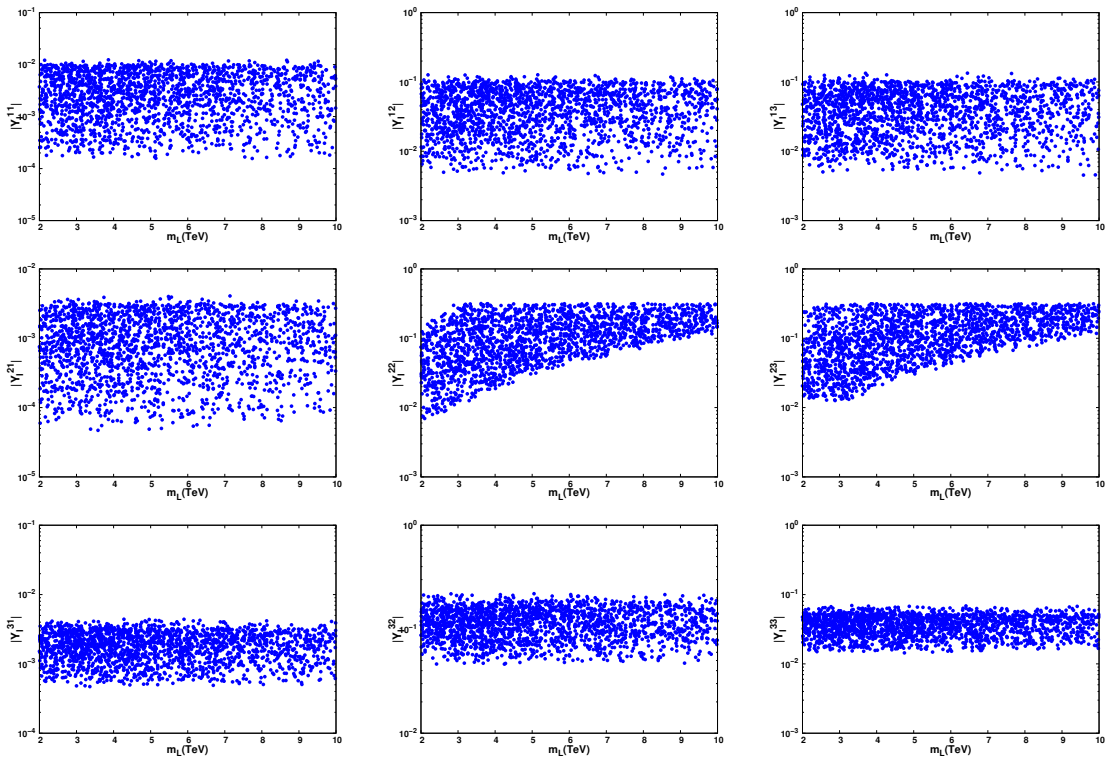

Figure 12: Parameter space scan in $Y_l^{ij} - m_L$ plane.

6 Axion-like particles resolve the $B \to \pi K$ puzzle and $g-2$ anomalies

The b-quark system is known to be an excellent place to test the Standard Model (SM) as well as models of New Physics (NP). Flavor Changing Neutral Current (FCNC) processes like $b \to s$ penguin decays are ideal places to look for NP. The FCNC decays in the B system have been studied in detail by experiments over the years. In recent times, measurements in the FCNC semileptonic $b \to s\ell^+\ell^-$ decays have revealed discrepancies with SM predictions. These discrepancies, or anomalies, have been widely studied over most of the last decade. Almost a decade before the semileptonic $b \to s\ell^+\ell^-$ anomalies arose, another anomaly in non-leptonic B-meson decays dominated by $b \to s$ penguins had attracted a great deal of interest. The anomaly was in the CP violation measurement of $B \to \pi K$ decays where an inconsistency was observed and this was called the "$B \to \pi K$ puzzle" [112, 113, 114]. The amplitudes of the four $B \to \pi K$ decays, $B^+ \to \pi^+ K^0$ (designated as $+0$ below), $B^+ \to \pi^0 K^+$ ($0+$), $B^0 \to \pi^- K^+$ ($-+$), and $B^0 \to \pi^0 K^0$ (00), are related by a single isospin relationship,

$$\sqrt{2}A^{00} + A^{-+} = \sqrt{2}A^{0+} + A^{+0}\,. \tag{150}$$

In these decays, experiments measure nine observables: the four branching ratios, the four direct CP asymmetries A_{CP}, and the mixing-induced indirect CP asymmetry S_{CP} in $B^0 \to \pi^0 K^0$. Expressing the $B \to \pi K$ decays in terms of topological amplitudes one can perform a fit to obtain the SM as well as the NP amplitudes [115]. As new experimental numbers were reported, updated fits were performed in Refs. [141, 129, 116, 117, 118]. Although the fits revealed a strong hint of NP in these decays, complicated strong dynamics made it difficult to draw a definite conclusion.

In this paper we explore the possibility that a light pseudoscalar particle close

to the pion mass can solve the $B \to \pi K$ puzzle. The key observation is that in the $B \to \pi K$ set of decays, the discrepancies from the SM predictions involve modes with a π^0 in the final state. The basic idea to solve the $B \to \pi K$ puzzle is to assume that there is a light pseudoscalar particle, a, that mixes with the π^0. In our model, an FCNC $B \to Ka$ amplitude is generated through the usual top-penguin diagram followed by the a mixing with the π^0 to produce a new contribution to the $B \to K\pi^0$ amplitudes. We then show that this new amplitude can solve the $B \to \pi K$ puzzle while being consistent with constraints from various other processes. We point out that the ALP can also solve the $(g-2)_{\mu,e}$ anomalies via its couplings to leptons and photons.

6.1 $B \to \pi K$ puzzle

We begin by explaining the $B \to \pi K$ puzzle by following the discussion in Ref. [116]. Within the diagrammatic approach [9, 142], B-decay amplitudes are expressed in terms of six diagrams. The $B \to \pi K$ decay amplitudes are

$$A^{+0} = -P'_{tc} + P'_{uc}e^{i\gamma} - \frac{1}{3}P'^{C}_{EW}\,, \tag{151}$$

$$\sqrt{2}A^{0+} = -T'e^{i\gamma} - C'e^{i\gamma} + P'_{tc} - P'_{uc}e^{i\gamma} - P'_{EW} - \frac{2}{3}P'^{C}_{EW}\,, \tag{152}$$

$$A^{-+} = -T'e^{i\gamma} + P'_{tc} - P'_{uc}e^{i\gamma} - \frac{2}{3}P'^{C}_{EW}\,, \tag{153}$$

$$\sqrt{2}A^{00} = -C'e^{i\gamma} - P'_{tc} + P'_{uc}e^{i\gamma} - P'_{EW} - \frac{1}{3}P'^{C}_{EW}\,. \tag{154}$$

The various diagrams are discussed in Ref. [115] and in the topological amplitudes above, we explicitly show the weak-phase dependence. In these decays the electroweak penguin amplitudes play an important role and it has been shown [143, 144, 145] that, to a good approximation, the electroweak penguins P'_{EW} and P'^{C}_{EW} can be related to

the tree-level diagrams T' and C' within the SM using flavor-SU(3) symmetry:

$$\begin{aligned} P'_{EW} &= \frac{3}{4}\frac{c_9+c_{10}}{c_1+c_2}R(T'+C')+\frac{3}{4}\frac{c_9-c_{10}}{c_1-c_2}R(T'-C')\,, \\ P'^{C}_{EW} &= \frac{3}{4}\frac{c_9+c_{10}}{c_1+c_2}R(T'+C')-\frac{3}{4}\frac{c_9-c_{10}}{c_1-c_2}R(T'-C')\,, \end{aligned} \tag{155}$$

where the c_i are Wilson coefficients (WC) [146] and $R \equiv |(V^*_{tb}V_{ts})/(V^*_{ub}V_{us})| = 45.8$ [52]. Following Eq. (155), P'_{EW} receives a relatively large contribution from T' but a much smaller contribution from C'. In contrast, P'^{C}_{EW} receives a relatively large contribution from C' and a much smaller T' contribution. In this sense, P'_{EW} and T' are of roughly similar size, and so are P'^{C}_{EW} and C'.

6.2 $B \to \pi K$ puzzle simplified

Keeping the leading-order diagrams in Eq. (151), the $B \to \pi K$ amplitudes become

$$\begin{aligned} A^{+0} &= -P'_{tc}\,, \\ \sqrt{2}A^{0+} &= -T'e^{i\gamma} + P'_{tc} - P'_{EW}\,, \\ A^{-+} &= -T'e^{i\gamma} + P'_{tc}\,, \\ \sqrt{2}A^{00} &= -P'_{tc} - P'_{EW}\,. \end{aligned} \tag{156}$$

Consider, now, the direct CP asymmetries of $B^+ \to \pi^0 K^+$ and $B^0 \to \pi^- K^+$. A direct CP asymmetry is generated by the interference of two amplitudes with nonzero relative weak and strong phases. In A^{-+}, T'-P'_{tc} interference leads to a direct CP asymmetry. Note that P'_{EW} and P'_{tc} have the same weak phase (= 0). As discussed earlier, $P'_{EW} \propto T'$ once we neglect C' (see Eq. 155). Therefore, if we assume that P'_{EW} and T' have a similar strong phase, the contribution to direct CP-asymmetry in A^{0+} can be assumed to be originated from the interference of T'-P'_{tc}. This means, to leading order in $|T'|/|P'_{tc}|$, we expect $A_{CP}(B^+ \to \pi^0 K^+) = A_{CP}(B^0 \to \pi^- K^+)$.

The latest $B \to \pi K$ measurements are shown in Table 29. Not only are

Decay	BR($\times 10^{-6}$) [147]	A_{CP}	S_{CP} [147]
$B^+ \to \pi^+ K^0$	23.79 ± 0.75	-0.017 ± 0.016 [52]	
$B^+ \to \pi^0 K^+$	12.94 ± 0.52	0.025 ± 0.016 [148]	
$B_d^0 \to \pi^- K^+$	19.57 ± 0.53	-0.084 ± 0.004 [149]	
$B_d^0 \to \pi^0 K^0$	9.93 ± 0.49	-0.01 ± 0.10 [147]	0.57 ± 0.17

Table 29: CP-averaged branching ratios, direct CP asymmetries $A_{CP} \equiv [\mathrm{BR}(\bar{B} \to \bar{F}) - \mathrm{BR}(B \to F)]/[\mathrm{BR}(\bar{B} \to \bar{F}) + \mathrm{BR}(B \to F)]$ (with final states $F\,, \bar{F}$), and mixing-induced CP asymmetry S_{CP} (if applicable) for the four $B \to \pi K$ decay modes.

$A_{CP}(B^+ \to \pi^0 K^+)$ and $A_{CP}(B^0 \to \pi^- K^+)$ not equal, they are of opposite sign! Experimentally, $(\Delta A_{CP})_{\rm exp} = A_{CP}^{0+} - A_{CP}^{-+} = (10.8 \pm 1.6)\%$ which differs from 0 by 6.5σ. We have performed a fit to data with the SM parameters. The fit is of poor quality, as we show below. This is a simplified version of the $B \to \pi K$ puzzle.

6.3 ALPs

Axions and axion-like particles have been extensively studied since the introduction of the axion to solve the strong-CP problem [150, 151, 152, 153]. For our purpose, we assume that there is a pseudoscalar ALP a, that is a pseudo-Nambu-Goldstone boson, emerging from the breaking of some global $U(1)$ symmetry. We write the flavor-conserving Lagrangian for a at low energy as

$$\begin{aligned} \mathcal{L}_a &= \frac{1}{2}(\partial_\mu a)^2 - \frac{1}{2} m_a^2 a^2 - i \sum_{f=d,l} \xi_f \frac{m_f}{\mathfrak{f}} \bar{f} \gamma_5 f a \\ &\quad - i \sum_{f=u} \eta_f \frac{m_f}{\mathfrak{f}} \bar{f} \gamma_5 f a - \frac{1}{4} \kappa a F_{\mu\nu} \widetilde{F}^{\mu\nu} \,, \end{aligned} \tag{157}$$

where $\mathfrak{f}$ is the ALP decay constant, and the dual electromagnetic field tensor is $\widetilde{F}^{\mu\nu} = \frac{1}{2}\epsilon^{\mu\nu\alpha\beta} F_{\alpha\beta}$. The last term of Eq. (194) reproduces the anomalous $\pi^0\gamma\gamma$ coupling if a and κ are replaced by π^0 and $g_{\pi\gamma\gamma} = \frac{\sqrt{2}\alpha}{\pi f_\pi} \sim 2.5 \times 10^{-2}$ GeV^{-1} (with the neutral pion decay constant $f_\pi = 130$ MeV), respectively.

We assume the ALP has properties that are desirable to solve the $B \to \pi K$ puzzle. We take a to have a mass close to the π^0 mass and require it to promptly decay to the $\gamma\gamma$ final state via its mixing with the π^0. The decay $a \to \gamma\gamma$ can occur

through a direct coupling to photons or through mixing with a π^0 and so its effective coupling is

$$g_{a\gamma\gamma} = \kappa + \sin\theta g_{\pi\gamma\gamma}\,, \tag{158}$$

where $\sin\theta$ is the $a-\pi^0$ mixing angle. The ALP width is then $\Gamma_a = g_{a\gamma\gamma}^2 m_a^3/(64\pi)$, which reduces to the π^0 width for $\kappa = 0$ and $\sin\theta = 1$. Assuming $\kappa \ll \sin\theta g_{\pi\gamma\gamma}$, $\Gamma_a \sim \sin^2\theta\Gamma_{\pi^0}$. Since we will be interested in $\sin\theta \sim 0.1$ for $m_a \sim m_{\pi^0}$ [154], we have $\Gamma_a \sim 10^{-2}\Gamma_{\pi^0} \ll m_a$. Constraints on the $a\gamma\gamma$ coupling with the ALP mass near the π^0 mass have been obtained from collider and astrophysical observations [155, 156, 157, 158, 159]. Our choice for the $a\gamma\gamma$ coupling is consistent with existing constraints. Note that our $g_{a\gamma\gamma}$ is unrelated to a tree-level $Za\gamma$ coupling that arises in models in which the ALP couples to the W and Z bosons. One-loop contributions to the $Za\gamma$ coupling from charged fermion loops are at least three orders of magnitude smaller than the fermion couplings [160]. For $\eta_u, \xi_d \sim 0.01$ and $\xi_{e,\mu} \sim 0.1$, our model is unconstrained by the $Z \to \pi^0\gamma$ branching fraction [160, 161].

In our model, the ALP contributes to $B \to \pi K$ decays through the $b \to s$ penguin which arises from the usual penguin loop and is divergent. We write a renormalization-group equation for the WC of the FCNC operator [162, 163, 164] and obtain the penguin amplitude at the electroweak scale,

$$\begin{aligned} \mathcal{L}_{bsa}(\mu_{EW}) &= g_{bs}(\mu_{EW})\bar{s}P_R b\; a\,, \quad \text{with} \\ g_{bs}(\mu_{EW}) &= i\frac{\eta_t(\Lambda)m_b}{\mathfrak{f}}\frac{\sqrt{2}G_F m_t^2 V_{ts}^* V_{tb}}{16\pi^2}\ln\frac{\Lambda^2}{m_t^2}\,, \end{aligned} \tag{159}$$

where $\Lambda = 4\pi\mathfrak{f}$ is the scale of new physics. We ignore the running of the WC to the scale $\mu \sim m_b$ where we do our phenomenology. This is justified in our analysis as the renormalization-group corrections are suppressed by α [163] and so $g_{bs}(\mu_{EW}) \approx g_{bs}(m_b)$. Including the loop term, the onshell ($b \to sa$) and offshell contributions

$(b \to sa \to b \to s\bar{q}q)$, where $q = u, d$, are given by

$$\begin{aligned}
\mathcal{L}^{\text{onshell}} &= g_{bs}(\mu = m_b)\,[\bar{s}P_R b]\,a = [J_{b\to s}]\,a\,, \\
\mathcal{L}^{\text{offshell}} &= [J_{b\to s}]\,\frac{\left[\xi_d \frac{m_d}{\mathfrak{f}}\bar{d}\gamma_5 d + \eta_u \frac{m_u}{\mathfrak{f}}\bar{u}\gamma_5 u\right]}{m_{\pi^0}^2 - m_a^2 + i m_a \Gamma_a}\,.
\end{aligned} \tag{160}$$

6.4 New Physics $B \to \pi K$ fit

To calculate the axion contributions to the $B \to \pi K$ decays we can calculate an onshell and an offshell contribution. In the onshell case we assume there is mixing between the a and the π^0 and so we can define a transformation between the gauge and the mass states as

$$\begin{aligned}
|a\rangle &= \cos\theta\,|a_{\text{phy}}\rangle + \sin\theta\,\left|\pi^0_{\text{phy}}\right\rangle\,, \\
\left|\pi^0\right\rangle &= -\sin\theta\,|a_{\text{phy}}\rangle + \cos\theta\,\left|\pi^0_{\text{phy}}\right\rangle\,.
\end{aligned} \tag{161}$$

The onshell and offshell contributions to the ALP amplitude for $B \to Ka \to K\pi^0$ give

$$\begin{aligned}
\mathcal{A} &= \mathcal{A}^{\text{onshell}} + \mathcal{A}^{\text{offshell}}, \quad \text{where} \\
\mathcal{A}^{\text{onshell}} &= \langle K|\,J_{b\to s}\,|B\rangle\,\langle a\,|\pi^0_{\text{phy}}\rangle = \langle K|\,J_{b\to s}\,|B\rangle \sin\theta\,, \\
\mathcal{A}^{\text{offshell}} &= \frac{m_{\pi^0}^2\,\langle K|\,J_{b\to s}\,|B\rangle}{m_{\pi^0}^2 - m_a^2 + i m_a \Gamma_a}\left[\frac{\eta_u f_\pi}{2\sqrt{2}\mathfrak{f}} - \frac{\xi_d f_\pi}{2\sqrt{2}\mathfrak{f}}\right]\,.
\end{aligned} \tag{162}$$

Here,

$$\langle K|\,J_{b\to s}\,|B\rangle = g_{bs}\,\langle K|\,\bar{s}P_R b\,|B\rangle\,, \tag{163}$$

$$\begin{aligned}
\langle K|\,\bar{s}P_R b\,|B\rangle &= f_+(m_K^2)\frac{m_B^2 - m_K^2}{2(m_b - m_s)} \\
&\quad + f_-(m_K^2)\frac{m_K^2}{2(m_b - m_s)}\,,
\end{aligned} \tag{164}$$

$$\begin{aligned}
\langle K|\,\bar{s}\gamma^\mu b\,|B\rangle &= f_+(q^2)(p_B^\mu + p_K^\mu) \\
&\quad + f_-(q^2)(p_B^\mu - p_K^\mu)\,.
\end{aligned} \tag{165}$$

We use the naive-factorization relations to calculate the offshell effect:

$$\begin{aligned}
\left\langle \pi^0 \right| \bar{d}\gamma_5 d \left|0\right\rangle &= -\frac{f_\pi m_{\pi^0}^2}{2\sqrt{2} m_d}\,, \\
\left\langle \pi^0 \right| \bar{u}\gamma_5 u \left|0\right\rangle &= \frac{f_\pi m_{\pi^0}^2}{2\sqrt{2} m_u}\,, \\
\left|\pi^0\right\rangle &= \frac{\left|\bar{d}d\right\rangle - \left|\bar{u}u\right\rangle}{\sqrt{2}}\,.
\end{aligned} \tag{166}$$

Note that the effect of the offshell contribution can be absorbed in an effective mixing angle,

$$\sin\theta \to \sin\theta + \frac{m_{\pi^0}^2}{m_{\pi^0}^2 - m_a^2} \frac{\eta_u - \xi_d}{2\sqrt{2}} \frac{f_\pi}{\mathfrak{f}}\,. \tag{167}$$

where we have assumed $\Gamma_a \ll |m_{\pi^0} - m_a|$. The term proportional to $m_{\pi^0}^2$ is the same as the $a - \pi^0$ mixing term usually discussed in the chiral Lagrangian description of the interaction of the ALP with mesons, with the ALP-quark couplings induced by the ALP coupling to gluons; see for example Refs. [165, 166]. A similar mixing term proportional to m_a^2 is included in the onshell contribution to $\sin\theta$, i.e, in the first term on the right-hand-side of Eq. (198). If $\mathfrak{f} = 1$ TeV and $\sin\theta \sim 0.1$ with the mixing arising primarily from the second term, then $|\eta_u - \xi_d| \simeq 0.01$ gives $|m_{\pi^0} - m_a| \sim 1$ keV. Detecting an ALP so close in mass to the π^0 will pose a challenge for B factories which have a π^0 mass resolution of a few MeV [167].

With the ALP NP contribution added, we have for the $B \to \pi K$ decays,

$$A^{+0} = -P'_{tc} - P'_{uc} e^{i\gamma} - \frac{1}{3} P'^C_{EW}\,, \tag{168}$$

$$\sqrt{2} A^{0+} = -T' e^{i\gamma} - C' e^{i\gamma} + P'_{tc} - P'_{uc} e^{i\gamma} - P'_{EW} - \frac{2}{3} P'^C_{EW} + \mathcal{A}\,, \tag{169}$$

$$A^{-+} = -T' e^{i\gamma} + P'_{tc} - P'_{uc} e^{i\gamma} - \frac{2}{3} P'^C_{EW}\,, \tag{170}$$

$$\sqrt{2} A^{00} = -C' e^{i\gamma} - P'_{tc} + P'_{uc} e^{i\gamma} - P'_{EW} - \frac{1}{3} P'^C_{EW} + \mathcal{A}\,, \tag{171}$$

which satisfy Eq. (192). We simplify our fit by setting $P'_{uc} = 0$ and taking the QCD-

Parameter	$\lvert C'\rvert/\lvert T'\rvert = 0.2$
χ^2/dof	3.64/3
p-value	30%
$\lvert T'\rvert$	6.4 ± 1.5
$\lvert P'_{tc}\rvert$	50.30 ± 0.47
$\lvert\mathcal{A}\rvert$	6.4 ± 3.4
$\delta_{C'}$	186 ± 54
$\delta_{Ptc'}$	-18.1 ± 5

Table 30: A fit of the SM amplitudes T' and P'_{tc}, the relative phase of C', and the NP amplitude $\mathcal{A}$ with a fixed phase of $\pi/2$. The 8 measurements fit are the 4 branching ratios, $A_{CP}(-+)$, $A_{CP}(0+)$, $A_{CP}(00)$, and $S_{CP}(00)$; we do not fit $A_{CP}(+0)$ since it is independent of all parameters in the table. Magnitudes of the diagrammatic amplitudes are in eV and phases are in degrees. Note that the magnitudes and phases of the electroweak penguin diagrams are obtained using Eq. (155).

factorization inspired value for the ratio $|C'|/|T'| = 0.2$ [168]. Typically to solve the puzzle we need $|\mathcal{A}| \sim P'_{EW} \sim T'$. Notice that T' is not the dominant amplitude as it is suppressed by CKM elements.

A fit of just the SM amplitudes using the 4 branching ratios and the $A_{CP}(-+)$ measurement (which are the most constraining measurements) yields a $\chi^2/\text{dof} = 2.66/1$, and we are left with very large errors in the other A_{CP} measurements. In fact, fitting to all observables other than the $A_{CP}(+0)$, in the SM we obtain $\chi^2/\text{dof} = 11.0/4$ which is a poor fit. This requires us to include the ALP amplitude $\mathcal{A}$. The minimal fit that can be done to extract this amplitude is given in Table 30. Any additional constraints on the system yield central values that differ by just a few percent.

This value of $|\mathcal{A}|$ allows us to evaluate $\sin\theta$ using Eq. (198). Using values of the masses taken from [52], the form factors from [169], and taking $\mathfrak{f} = 1$ TeV, we find

$$|\mathcal{A}| = i\eta_t(\Lambda)\sin\theta\left[5.71 \times 10^{-6}\ \text{GeV}\right] . \tag{172}$$

Using the value for $|\mathcal{A}|$ obtained from the fit, we have

$$\eta_t(\Lambda)\sin\theta = (1.12 \pm 0.60) \times 10^{-3} . \tag{173}$$

We now extract just the $\sin\theta$ term. The coupling $\eta_t(\Lambda)$ is unknown and cannot be properly extracted using this method. Note that if we just consider the branching ratio $B \to Ka$ we have

$$\mathrm{BR}(B \to Ka) = \frac{p_K \tau_B}{8\pi m_B^2} \frac{|\mathcal{A}|^2}{\sin^2\theta} \,. \tag{174}$$

Using $|\mathcal{A}|$ obtained from the fit and branching ratio values 10^{-5} and 2×10^{-5}, we find

$$\sin\theta = 0.188 \pm 0.029 \,, \tag{175}$$

$$\sin\theta = 0.133 \pm 0.021 \,, \tag{176}$$

respectively. Note that a careful search of the decays $B \to K\pi^0$ around the π^0 mass may be able to observe the ALP as a diphoton resonance. We determine the value of $\eta_t(\Lambda)$ by using the value of $\sin\theta = 0.133 \pm 0.021$:

$$\eta_t(\Lambda) = (8.4 \pm 4.7) \times 10^{-3} \,. \tag{177}$$

6.5 $K \to \pi a$ amplitude

We first consider the amplitude of $K^+ \to \pi^+ a$. This can come from $\pi^0 - a$ mixing, so that $K^+ \to \pi^+\pi^0 \to \pi^+ a$. There is also direct production through the weak current [166] which we can make small by an appropriate choice of ALP couplings to the light quarks $\xi_{d,s}$, and η_u. Hence $\mathrm{BR}[K^+ \to \pi^+ a] \sim \sin^2\theta \mathrm{BR}[K^+ \to \pi^+\pi^0]$ and this decay will be swamped by the $K^+ \to \pi^+\pi^0$ decay. This is also the FCNC $s \to d$ transition that arises from a penguin loop (see for example Ref. [170]) that contributes to $K^+ \to \pi^+ a, K_L^0 \to \pi^0 a$ and $K_S^0 \to \pi^0 a$. Using $\eta_t(\Lambda) = (8.4 \pm 4.7) \times 10^{-3}$, we obtain

the branching ratios in the penguin generated $K \to \pi a$ decays:

$$\mathrm{BR}(K^+ \to \pi^+ a) = (4.2 \pm 3.3) \times 10^{-8}\,, \tag{178}$$

$$\mathrm{BR}(K_L^0 \to \pi^0 a) = (1.8 \pm 1.4) \times 10^{-7}\,, \tag{179}$$

$$\mathrm{BR}(K_S^0 \to \pi^0 a) = (5.5 \pm 4.3) \times 10^{-11}\,. \tag{180}$$

Other constraints from the B and the K system are discussed in Ref. [171] in which a model with similar structure and parameters has been considered.

6.6 D system

We now consider the contribution of the ALP to the $D \to K\pi$ system. In our model the ALP enters a meson decay process only via a one-loop penguin diagram when the final state has a π^0. Based on the CKM matrix elements that enter in the amplitude, D-meson decays can be broadly categorized into Cabibbo-favored [$\propto V_{cs}^* V_{ud}$], single-Cabibbo-suppressed (SCS) [$\propto V_{cd}^* V_{ud}$ or $\propto V_{cs}^* V_{us}$], and doubly-Cabibbo-suppressed [$\propto V_{cd}^* V_{us}$]. Of these, a penguin diagram can only appear in the SCS D decays, and only three of these involve a π^0 in the final state ($D^0 \to \pi^0\pi^0, D^+ \to \pi^+\pi^0, D_s^+ \to K^+\pi^0$). The ALP-penguin amplitude $\mathcal{A}$, introduced earlier in B-decays, also contributes to each of these decays. A key difference is that in D decays the bottom quark, rather than the top quark, runs in the penguin loop. We denote this new amplitude by $\mathcal{A}^D$.

Since the penguin diagram here is similar to the diagram that contributes to the B decays, we obtain similar expressions for the ALP contribution in the D system. Key changes appear in the quark flavors, since instead of a $b \to s$ transition, now we

have a $c \to u$ transition:

$$\mathcal{A}^D = g_{cu} \langle P|J_{c\to u}|D\rangle \left\langle a|\pi^0_{\rm phy}\right\rangle , \tag{181}$$

$$\begin{aligned} g_{cu} &= \frac{\xi_b(\Lambda) m_c}{\mathfrak{f}} \frac{\sqrt{2} G_F m_b^2 V_{cb}^* V_{ub}}{16\pi^2} \ln \frac{\Lambda^2}{m_b^2} \\ &= \xi_b(\Lambda) e^{-i\gamma} \left[5.81 \times 10^{-12}\,{\rm GeV}\right] , \end{aligned} \tag{182}$$

$$\langle P|J_{c\to u}|D\rangle = f_+^{D\to P}(m_P^2) \frac{m_D^2 - m_P^2}{2(m_c - m_u)} - f_-^{D\to P}(m_P^2) \frac{m_P^2}{2(m_c - m_u)} , \tag{183}$$

where

$$\langle \pi|J_{c\to u}|D\rangle = 6.52\ {\rm GeV} , \tag{184}$$

$$\langle K|J_{c\to u}|D\rangle = 6.43\ {\rm GeV} , \tag{185}$$

$$\langle K|J_{c\to u}|D_s\rangle = 6.26\ {\rm GeV} . \tag{186}$$

The phase γ arises from the CKM matrix element V_{ub}. Now, with the value of $\sin\theta$ obtained from the B decays, assuming $\xi_b(\Lambda) < \eta_t(\Lambda)$, and $\mathfrak{f} = 1$ TeV, we find that the ALP contribution to the D decays,

$$|\mathcal{A}^D| < 5 \times 10^{-14}\ {\rm GeV} . \tag{187}$$

This amplitude is several orders of magnitude smaller than the typical SM contribution in SCS decays, which are of the order of 10^{-7} GeV [13]. We, therefore, conclude that the ALP contribution does not significantly affect $D \to K\pi$ branching ratios. In Table 31 we provide the experimental values for the magnitudes of the decay amplitudes (calculated from the measured branching ratios) and the direct-CP asymmetries. We now estimate the contribution of the ALP to the direct-CP asymmetries in SCS D-decays as follows. The generic D-decay amplitude in the presence of the ALP can be

Process	Expt. $\lvert A\rvert$ ($\times 10^{-7}$ GeV)	Expt. A_{CP}
$D^0 \to \pi^0\pi^0$	3.54 ± 0.05	0 ± 0.6
$D^+ \to \pi^+\pi^0$	2.738 ± 0.006	2.4 ± 1.2
$D_s^+ \to K^+\pi^0$	1.9 ± 1.1	-26.6 ± 23.8

Table 31: The magnitudes of measured amplitudes and direct-CP asymmetries in SCS D-meson decays. Only included are processes in which the ALP contributes.

expressed as,

$$A_{D\to K\pi} \;=\; |a_{\rm SM}|e^{i\delta}e^{i\phi} + i|\mathcal{A}^D|\,, \tag{188}$$

where $a_{\rm SM}$ is the magnitude of the SM part of the decay amplitude, δ is the relative strong phase, and ϕ is the relative weak phase between the SM part and the ALP contribution. This leads to the direct-CP asymmetry,

$$A_{CP} \;=\; \frac{2x\sin\delta\cos\phi}{1+x^2+2x\cos\delta\sin\phi}\,, \tag{189}$$

where $x = |\mathcal{A}^D|/|a_{SM}| \lesssim 10^{-7}$. Clearly, a nonzero CP asymmetry can appear even if the SM term has a small weak phase. This property is due to the i in the coefficient of the ALP term in Eq. (188) which changes sign under CP conjugation. Also, since $x \lesssim 10^{-7}$, the ALP's contribution to A_{CP} in D-decays is several orders of magnitude below the current sensitivity of flavor experiments.

6.7 $(g-2)_{\mu,e}$ anomalies

Our scenario can be easily extended to explain the anomalies in the anomalous magnetic moments $a_\ell = (g-2)_\ell/2$ of the muon and electron. We consider the 4.2σ a_μ anomaly from a combination of the BNL and Muon g-2 experiments [172] with

$$\Delta a_\mu \;=\; a_\mu^{\rm exp} - a_\mu^{\rm SM} = (251 \pm 59)\times 10^{-11}\,. \tag{190}$$

There are two values of a_e which are inferred from measurements of the fine structure constant, and that are inconsistent with each other. The a_e value obtained from Laboratoire Kastler Brossel [173] and Berkeley [174] measurements of the fine-structure

constant yield [175, 176, 177]

$$\begin{aligned} \Delta a_e^{\rm LKB} &= a_e^{\rm exp} - a_e^{\rm LKB} = (4.8 \pm 3.0) \times 10^{-13}\,, \\ \Delta a_e^{\rm B} &= a_e^{\rm exp} - a_e^{\rm B} = (-8.8 \pm 3.6) \times 10^{-13}\,. \end{aligned} \tag{191}$$

Under our assumption that $\kappa \ll \sin\theta\, g_{\pi\gamma\gamma}$, the couplings of the ALP to the muon and electron must be $\xi_\mu m_\mu/\mathfrak{f} \sim 10^{-5}$ and $\xi_e m_e/\mathfrak{f} \sim 10^{-7}$ for $\Delta a_e^{\rm LKB}$ [178] so the loop-induced $Za\gamma$ coupling remains small. The values of $\xi_\mu m_\mu/\mathfrak{f} \sim 10^{-5}$ and $\xi_e m_e/\mathfrak{f} \sim -10^{-6}$ for $\Delta a_e^{\rm B}$ give a too large $Za\gamma$ coupling.

6.8 Summary

In perhaps a first analysis with ALPs in hadronic B decays, we have proposed a new solution to the $B \to \pi K$ puzzle with an ALP with mass close to the π^0 mass. Our solution preserves the isospin relation in Eq. (192), and is consistent with constraints from B, K, and D decays. We point out that this ALP can also explain the $g-2$ anomalies of the muon and electron. A careful scan of the decay products in $B \to K\pi^0$ around the π^0 mass may reveal the ALP.

7 Exploring an ALP near the π^0 mass

Axions and axion-like particles (ALP) are one of the most well motivated extensions of the standard model (SM). The axion was introduced to solve the strong-CP problem [150, 151, 152, 153]. The phenomenology of ALPs depend on their mass and have have been widely discussed. In a recent publication [179] we pointed out that an ALP with a mass close to the π^0 mass could be responsible for the well known $B \to \pi K$ puzzle while also accounting for the latest electron and muon $g-2$ results.

The $B \to \pi K$ anomaly is in the CP violation measurements in the set of the four $B \to \pi K$ decays, $B^+ \to \pi^+ K^0$ (designated as $+0$ below), $B^+ \to \pi^0 K^+$ ($0+$), $B^0 \to \pi^- K^+$ ($-+$), and $B^0 \to \pi^0 K^0$ (00), that are related by a single isospin relationship,

$$\sqrt{2}A^{00} + A^{-+} = \sqrt{2}A^{0+} + A^{+0}\,. \tag{192}$$

The inconsistencies in the $B \to \pi K$ CP violating measurements has been called the "$B \to \pi K$ puzzle" [112, 113, 114] and one can quantify this puzzle with fits in terms of topological amplitudes representing SM as well as the NP amplitudes [115]. Over the years many such fits were reported in response to new experimental data [141, 129, 116, 117, 118, 180]. One can understand the gist of the $B \to \pi K$ puzzle via a

Decay	BR($\times 10^{-6}$)	A_{CP}	S_{CP}
$B^+ \to \pi^+ K^0$	23.79 ± 0.75	-0.017 ± 0.016	
$B^+ \to \pi^0 K^+$	12.94 ± 0.52	0.025 ± 0.016	
$B_d^0 \to \pi^- K^+$	19.57 ± 0.53	-0.084 ± 0.004	
$B_d^0 \to \pi^0 K^0$	9.93 ± 0.49	-0.01 ± 0.10	0.57 ± 0.17

Table 32: CP-averaged branching ratios, direct CP asymmetries $A_{CP} \equiv [\mathrm{BR}(\bar{B} \to \bar{F}) - \mathrm{BR}(B \to F)]/[\mathrm{BR}(\bar{B} \to \bar{F}) + \mathrm{BR}(B \to F)]$ (with final states $F\,, \bar{F}$), and mixing-induced CP asymmetry S_{CP} (if applicable) for the four $B \to \pi K$ decay modes.

simple examination of the decay amplitudes. Keeping the leading-order diagrams, the

$B \to \pi K$ amplitudes become

$$\begin{aligned} A^{+0} &= -P'_{tc}\,, \\ \sqrt{2}A^{0+} &= -T'e^{i\gamma} + P'_{tc} - P'_{EW}\,, \\ A^{-+} &= -T'e^{i\gamma} + P'_{tc}\,, \\ \sqrt{2}A^{00} &= -P'_{tc} - P'_{EW}\,. \end{aligned} \tag{193}$$

where the various amplitudes are defined in Ref. [115]. The direct CP asymmetry in $B^0 \to \pi^- K^+$ is easily understood as due to the T'-P'_{tc} interference. Naive estimates of these amplitudes based on CKM factors as well as the Wilson co-efficients of the effective Hamiltonian can produce the right sign and the magnitude of the CP asymmetry as shown in Table 32. The puzzle arises in the direct CP asymmetries of $B^+ \to \pi^0 K^+$ where the T'-P'_{tc} interference leads to a direct CP asymmetry. Note that P'_{EW} and P'_{tc} have the same weak phase ($= 0$) and $P'_{EW} \propto T'$ once we neglect C', the color suppressed amplitude, which implies P'_{EW} and T 'have the same strong phase. In other words, $P'_{EW} - P'_{tc}$ and $P'_{EW} - T'$ interferences do not produce any direct CP asymmetry in $B^+ \to \pi^0 K^+$ and we expect $A_{CP}(B^+ \to \pi^0 K^+) = A_{CP}(B^0 \to \pi^- K^+)$. This is clearly not reflected in in Table 32 as not only are $A_{CP}(B^+ \to \pi^0 K^+)$ and $A_{CP}(B^0 \to \pi^- K^+)$ not equal, they are of opposite sign! Experimentally, $(\Delta A_{CP})_{\rm exp} = A_{CP}^{0+} - A_{CP}^{-+} = (10.8 \pm 1.6)\%$ which differs from 0 by 6.5σ.

In Ref. [179] it was proposed that the amplitude $B^+ \to \pi^0 K^+$ receives a new contribution through $B^+ \to aK^+$ with the ALP a mixing with the π^0 thus solving the $B \to \pi K$ puzzle. To briefly review the solution, we start with the ALP Lagrangian,

$$\begin{aligned} \mathcal{L}_a &= \frac{1}{2}(\partial_\mu a)^2 - \frac{1}{2}m_a^2 a^2 - i\sum_{f=d,l} \xi_f \frac{m_f}{\mathfrak{f}} \bar{f}\gamma_5 f a \\ &\quad - i\sum_{f=u} \eta_f \frac{m_f}{\mathfrak{f}} \bar{f}\gamma_5 f a - \frac{1}{4}\kappa a F_{\mu\nu}\widetilde{F}^{\mu\nu}\,, \end{aligned} \tag{194}$$

where $\mathfrak{f}$ is the ALP decay constant, and the dual electromagnetic field tensor is $\widetilde{F}^{\mu\nu} =$

$\frac{1}{2}\epsilon^{\mu\nu\alpha\beta}F_{\alpha\beta}$. The ALP generates the $B^+ \to aK^+$ decay through the $b \to s$ penguin which arises from the usual penguin loop and is divergent. We write a renormalization-group equation for the WC of the FCNC operator [162, 163, 164] and obtain the penguin amplitude at the electroweak scale,

$$\begin{aligned} \mathcal{L}_{bsa}(\mu_{EW}) &= g_{bs}(\mu_{EW})\bar{s}P_R b\, a\,, \quad \text{with} \\ g_{bs}(\mu_{EW}) &= i\frac{\eta_t(\Lambda)m_b}{\mathfrak{f}}\frac{\sqrt{2}G_F m_t^2 V_{ts}^* V_{tb}}{16\pi^2}\ln\frac{\Lambda^2}{m_t^2}\,, \end{aligned} \tag{195}$$

where $\Lambda = 4\pi\mathfrak{f}$ is the scale of new physics. In passing we note that the $B_d \to \pi^0\pi^+$ decay involves a $b \to d$ penguin which is suppressed compared to the dominant tree amplitude and hence the axion contribution will also be suppressed. Hence, if an ALP exist near the π^0 mass then it will be easier to detect it in the $B \to \pi^0 K^+$ decay.

Expressing with the $a - \pi^0$ mixing as

$$\begin{aligned} |a\rangle &= \cos\theta\,|a_{\rm phy}\rangle + \sin\theta\,\left|\pi^0_{\rm phy}\right\rangle\,, \\ \left|\pi^0\right\rangle &= -\sin\theta\,|a_{\rm phy}\rangle + \cos\theta\,\left|\pi^0_{\rm phy}\right\rangle\,, \end{aligned} \tag{196}$$

the onshell and offshell contributions to the ALP amplitude for $B \to Ka \to K\pi^0$ is written as

$$\begin{aligned} \mathcal{A} &= \mathcal{A}^{\rm onshell} + \mathcal{A}^{\rm offshell}\,, \quad \text{where} \\ \mathcal{A}^{\rm onshell} &= \langle K|\,J_{b\to s}\,|B\rangle\,\langle a\,|\pi^0_{\rm phy}\rangle = \langle K|\,J_{b\to s}\,|B\rangle\sin\theta\,, \\ \mathcal{A}^{\rm offshell} &= \frac{m_{\pi^0}^2\,\langle K|\,J_{b\to s}\,|B\rangle}{m_{\pi^0}^2 - m_a^2 + im_a\Gamma_a}\left[\frac{\eta_u f_\pi}{2\sqrt{2}\mathfrak{f}} - \frac{\xi_d f_\pi}{2\sqrt{2}\mathfrak{f}}\right]\,. \end{aligned} \tag{197}$$

The details of the various terms can be found in Ref. [179] and the offshell contribution can be absorbed in an effective mixing angle,

$$\sin\theta \to \sin\theta + \frac{m_{\pi^0}^2}{m_{\pi^0}^2 - m_a^2}\frac{\eta_u - \xi_d}{2\sqrt{2}}\frac{f_\pi}{\mathfrak{f}}\,. \tag{198}$$

where we have assumed $\Gamma_a \ll |m_{\pi^0} - m_a|$. The term proportional to $m^2_{\pi^0}$ is the same as the $a - \pi^0$ mixing term usually discussed in the chiral Lagrangian description of the interaction of the ALP with mesons, with the ALP-quark couplings induced by the ALP coupling to gluons; see for example Refs. [165, 166]. A similar mixing term proportional to m^2_a is included in the onshell contribution to $\sin\theta$ along with any new physics contribution to the mixing. To consider how new physics can contribute to the mixing we consider a specific scenario. We start with the mixing Lagrangian

$$\mathcal{L}_{mix} = m^2_\pi \pi^2 + m^2_a a^2 + 2\delta^2 a\pi. \tag{199}$$

We now introduce a singlet heavy quark D that couple to the axion and mix with the down quark [181]. The Lagrangian is

$$\begin{aligned} \mathcal{L}_{NP} &= ig_D a\overline{D_L}D_R + Y_d \bar{d}_L H D_R + \mu \overline{D}_L d_R + M_D \overline{D}_L D_R \\ &+ h.c. \end{aligned} \tag{200}$$

After electroweak symmetry breaking with $\langle H \rangle = v$ we get $m_d \sim \frac{Y_d v \mu}{M_D}$ [181]. The $a - \pi^0$ mixing in this framework can be written schematically as,

$$\begin{aligned} \delta^2 &\sim \langle \pi^0 \left| \bar{d}d \right\rangle \langle \bar{d}d \left| \bar{D}D \right\rangle \langle \bar{D}D \left| a \right\rangle \\ &\sim g_D g_\pi Y_d v \mu = g_D g_\pi m_d M_D, \end{aligned} \tag{201}$$

where we write the pion quark coupling as $ig_\pi \bar{\psi}_q \gamma_5 \vec{\tau}\cdot\vec{\pi}\psi_q$ (See for example Ref. [182]). For values $m_\pi = 0.135$ GeV, $m_a = 0.131$ GeV and $\sin\theta \sim 0.1$ we find $\delta \sim 10^{-2}$ GeV and therefore with $m_d \sim 10^{-2}$ GeV we get $g_D g_\pi \sim \frac{10^{-2}\text{ GeV}}{M_D}$.

In this paper we explore the experimental signature of the ALP near the π^0 mass. The paper is organized in the following manner. In sec. 1 we discuss a procedure to determine the detector signal of the ALP in $B_d \to \pi^0 K^+$ decay. In Sec. 2 we comment on the detection of the ALP at the Dune near detector, followed by a

discussion of our results.

7.1 ALP in $B_d \to \pi^0 K^+$

The three-body decay process $B \to K\gamma\gamma$ proceed through the intermediate states $B \to K\pi^0$ and the π^0 decays to two photons. Assuming that the π^0 mixes with and axion-like particle, A we reconstruct the momentum-dependent rate distribution for this process.

Utilizing the isobar model, we describe the full decay amplitude as follows,

$$\mathcal{A}_{B\to K\gamma\gamma}(s_{\gamma\gamma}, s) = a_{\rm NR}F_{\rm NR} + a_{\pi^0}F_{\pi^0}(s_{\gamma\gamma}) + a_A F_A(s_{\gamma\gamma}) \ , \tag{202}$$

where $s_{\gamma\gamma} = (k_1+k_2)^2$ is the invariant mass of the diphoton. F_X, where $X = {\rm NR}, \pi^0, {\rm A}$, are the dynamical amplitude for the $B \to K\gamma\gamma$ transition mediated by the intermediate state X. The non-resonant contribution comes from the amplitude given in [183]. The resonant pion and ALP contributions come from the relativistic Briet-Wigner lineshapes. These expressions are given here.

$$F_{\rm NR} = \mathcal{A}(B \to K\gamma\gamma)_{\rm NR} \ , \tag{203}$$

$$F_{\pi^0}(s_{\gamma\gamma}) = \frac{1}{\left(m^2_{\pi^0} - s_{\gamma\gamma}\right) - \imath m_{\pi^0}\Gamma_{\pi^0}} \ , \tag{204}$$

$$F_A(s_{\gamma\gamma}) = \frac{1}{(m^2_A - s_{\gamma\gamma}) - \imath m_A\Gamma_A} \ , \tag{205}$$

where Γ_X is the mass-dependent width of the intermediate particle, $X = \pi^0, A$. These will be fixed at 10 MeV for what follows. Furthermore, we will be considering a flat contribution from the NR part. With this we have that

$$\begin{aligned} s_{\gamma\gamma} = (k_1 + k_2)^2 \ &= \ 2k_1 \cdot k_2 \ , \\ &= m_B^2 + m_K^2 - s_1 - s_2 \ . \end{aligned} \tag{206}$$

The parameters s_1 and s_2 are indistinguishable since the photons are indistin-

guishable, however one will be less than or equal to the other. We define $s_g \geq s_l$. On a Dalitz plot for $B \to K\gamma\gamma$, $s_g = s_l$ is defined by the line

$$y(x) = (m_B^2 + m_K^2 - x)/2 \ , \tag{207}$$

where x represents $s_{\gamma\gamma}$ and y represents s_g. This gives the differential decay width as

$$\frac{d^2\Gamma}{ds_{\gamma\gamma}ds_l} = \frac{1}{(2\pi)^3}\frac{1}{32m_B^3}\left|\mathcal{A}_{B\to K\gamma\gamma}\right|^2 \ . \tag{208}$$

Since we will be interested in the differential decay rate as a function of the diphoton mass we integrate out the s_l dependence and find

$$\frac{d\Gamma}{ds_{\gamma\gamma}} = \frac{E_2\sqrt{E_1^2 - m_1^2}}{128\pi^3 m_B^3}\left|\mathcal{A}_{B\to K(\pi^0\to)\gamma\gamma} + \mathcal{A}_{B\to(Ka\to)\gamma\gamma}\right|^2 + \text{NR} \ , \tag{209}$$

where NR includes all contributions from the non-resonant portion along with the interferences with the non-resonant amplitude, and

$$E_2 = \frac{\sqrt{s_{\gamma\gamma}}}{2} \ , \tag{210}$$

$$E_1 = \frac{m_B^2 - m_K^2 - s_{\gamma\gamma}}{2\sqrt{s_{\gamma\gamma}}} \ . \tag{211}$$

Furthermore, in this case, we have that $m_1 = 0$ and the decay rate simplifies to

$$\frac{d\Gamma}{ds_{\gamma\gamma}} = \frac{\beta\left(m_B^2, m_K^2, s_{\gamma\gamma}\right)}{512\pi^3 m_B^3}\left|\mathcal{A}_{B\to K(\pi^0\to)\gamma\gamma} + \mathcal{A}_{B\to(Ka\to)\gamma\gamma}\right|^2 + \text{NR} \ , \tag{212}$$

where $\beta(a,b,c) = a^2 + b^2 + c^2 - 2ab - 2bc - 2ca$.

7.1.1 Generating a signal

The goal of this section is to generate a semi-real signal that would be measured by a detector. To accomplish this we must convolve the theoretical decay rate with the detector sensitivity and then generate event counts in the bins utilized by the detector.

Using the differential decay rate given in Eq. 212, the assumption that the amplitudes $B \to K\pi^0$ and $B \to Ka$ are equal, and further assume that the non-resonant part is flat, we are able to generate a plot of the decay rate as a function of the invariant diphoton mass near the mass of the pion. Fig. 13 shows a representative example with an ALP mass of $m_\pi - 10$ MeV. Since this is a theoretical construction of the decay rate, we could never hope that a detector would be this sensitive. We must take this signal and smear it with a Gaussian convolution

$$G(x, E) = \frac{1}{w(x)\sqrt{2\pi}} \int_{x_{\min}}^{x_{\max}} dx \; e^{-\frac{(x-E)^2}{2w(x)^2}} \; , \tag{213}$$

where $w(x)$ is the energy-dependent resolution of the detector (in the present case we use the resolution of the Belle II detector [184]), and E is the measured energy. This gives us a smeared decay rate of

$$\begin{aligned} \Gamma_{\text{smear}} = \int_{x_{\min}}^{x_{\max}} dx \int_0^{y_{\max}} dy \; 2y \frac{\beta\left(m_B^2, m_K^2, y^2\right)}{512\pi^3 m_B^3} \frac{1}{w(x)\sqrt{2\pi}} \\ \times e^{-\frac{(x-y)^2}{2w(x)^2}} \left|\mathcal{A}_{B\to K(\pi^0\to)\gamma\gamma} + \mathcal{A}_{B\to(Ka\to)\gamma\gamma}\right|^2 + \text{NR} \; , \end{aligned} \tag{214}$$

where $y = \sqrt{s_{\gamma\gamma}}$, and $y_{\max} = m_B - m_K$. We will perform this smearing for each value of x in the full range of $s_{\gamma\gamma}$ so that we have a theoretical signal for the differential decay rate that incorporates the sensitivity of the detector, performing the integration over y for each value of x. An example of the result of this process is given in Fig. 13. Since the ALP mass is so far from the pion mass we see that there is an additional 'hump' in the distribution. As the masses approach each other, this structure will become less and less pronounced. The goal is to discover the minimum Δm between the ALP and pion that this structure can be distinguished.

We now proceed to construct event counts in each bin. The binning procedure has some degree of arbitrariness in the selection of where the binning begins. We alleviate this by randomizing the binning. For a given binning we determine the partial rates for each bin by integrating over x for that bin. We incorporate the noise

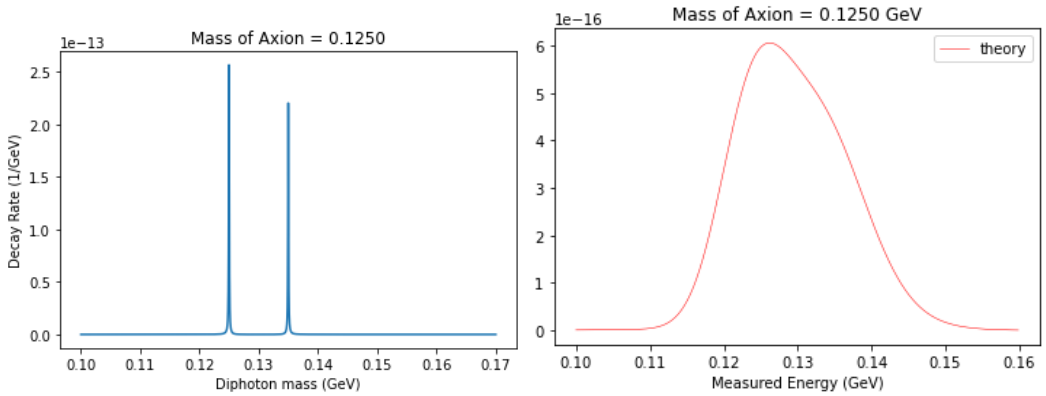

Figure 13: Representative decay rate as a function of diphoton mass. This example uses an ALP mass 10 MeV less than the pion mass. On the left is the pure signal. On the right is the convoluted signal.

of the detector by assuming a normal distribution with a central value equal to the number of events and a width equal to the square root of the number of events in that bin. An example is shown in Fig. 14.

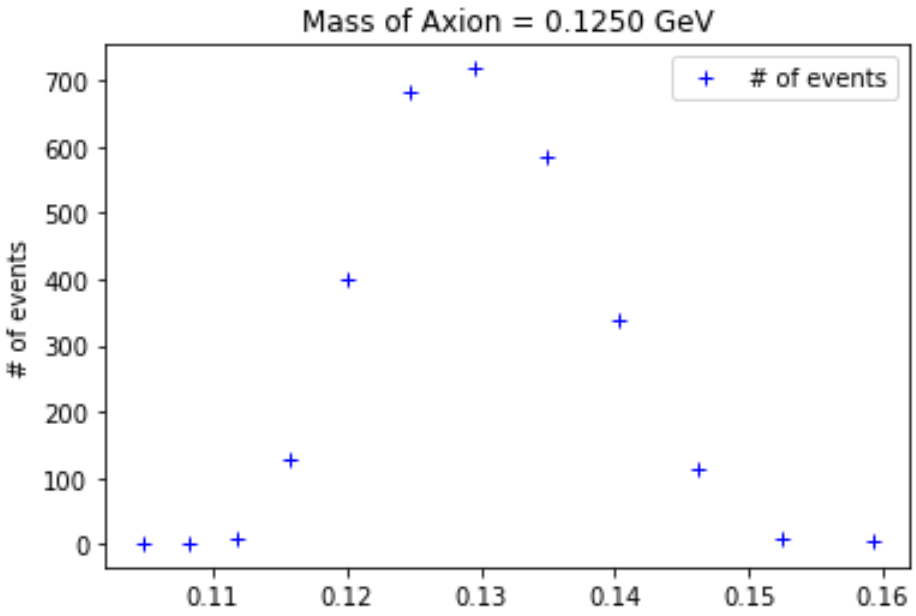

Figure 14: Binned event counts for an ALP mass 10 MeV less than the pion.

7.1.2 Fits

Now that we have generated a rudimentary signal from a detector we now perform a fit on these data. For each set of data we fit a single Gaussian curve and a double

Gaussian curve, both normalized by the total number of events. An arbitrary single normalized Gaussian has 3 parameters: a central value, a width, and a scaling factor. A double Gaussian is determined fully by 6 parameters: 2 centers, 2 widths, 2 scaling factors. Since the double Gaussian fit has more parameters, we expect that fit to be better than the single Gaussian in each case, however, this could be due to a simple increase in the number of parameters. To mitigate this arbitrary improvement we work with the reduced χ^2 value. We begin to compare the fits by calculating the χ^2 value for each of the fits. We take the fitted curves and compare the values at each of the bin centers to the number of events in that bin and sum the squares.

$$\chi^2 = \sum_{i=1}^{N} \left[\frac{\mathcal{O}_i - f(x_i)}{\Delta \mathcal{O}} \right]^2 , \tag{215}$$

where $\mathcal{O}$ is the actual number of events in bin i, and $f(x_i)$ is the value of the fitted gaussian at the bin center, x_i. This gives us a measure of how well the fitted curve fits the available data.

The reduced χ^2 is simply the χ^2 value divided by the number of degrees of freedom, in this case the number of bins minus the number of parameters in each fit. We perform a large number of these fits for various values of ALP mass near the π^0 mass and ALP widths ranging from 10 eV to 1 MeV. What we are looking for is a range of values for these quantities that will allow detection of the ALP to better inform experiments on what to search for.

From the results given in Table 33 we see that for an ALP mass greater than about 3 MeV from the pion mass in either direction shows that the double Gaussian fits the data better by a significant margin. Indicating that the ALP is there but masked by the signal of the π^0. For masses closer to the π^0 mass, the fits are inconclusive as to whether this is the case.

For ALP widths below 0.1 MeV, the results are largely the same as for the 10 eV case and I will forgo presenting those results. When we allow the ALP width to become larger we begin to see some changes in the results. These changes are in part due to

ALP mass (GeV)	Double Gaussian	Single Gaussian
0.1250	0.00066	49.93424
0.1260	0.00071	31.85417
0.1270	0.00072	16.71390
0.1280	0.00065	7.82184
0.1290	0.00047	3.20921
0.1300	0.00027	1.22651
0.1310	0.00012	0.33841
0.1320	0.00004	0.06562
0.1330	0.00001	0.00828
0.1340	0.00142	0.00142
0.1350	0.00133	0.00133
0.1360	0.00000	0.00142
0.1370	0.00001	0.00814
0.1380	0.00004	0.06349
0.1390	0.00012	0.32745
0.1400	0.00027	1.20300
0.1410	0.00046	3.55439
0.1420	0.00063	8.20763
0.1430	0.00070	18.53778
0.1440	0.00071	37.96234
0.1450	0.00070	71.13882

Table 33: Results of fitting to generated data for an ALP width of 10 eV. The table shows the reduced χ^2 values for the Double and Single Gaussian fits.

ALP mass (GeV)	Double Gaussian	Single Gaussian
0.1250	0.46172	29.63386
0.1260	0.38161	19.78123
0.1270	0.44226	11.27217
0.1280	0.50083	6.01653
0.1290	0.55058	3.13126
0.1300	0.45941	1.74267
0.1310	0.48776	1.26604
0.1320	0.52953	1.18116
0.1330	0.32289	1.08032
0.1340	0.09573	1.10454
0.1350	0.04511	1.07320
0.1360	0.01048	1.00571
0.1370	0.03274	0.90346
0.1380	0.25851	1.37520
0.1390	0.81560	1.53908
0.1400	0.68126	2.15146
0.1410	0.43214	3.76306
0.1420	0.92060	7.17909
0.1430	0.80846	13.32697
0.1440	0.68812	23.93668
0.1450	0.55314	40.83630

Table 34: Results of fitting to generated data for an ALP width of 1 MeV. The table shows the reduced χ^2 values for the Double and Single Gaussian fits.

the width of the ALP now becoming comparable to the width of the convolution. This widening of the signal results in the delta function behavior of the width being lost. More of the Breit-Wigner lineshape is bleeding through the smearing and the Gaussian shape that dominated previous models is no longer the only surviving characteristic of the distribution. This results in poorer fits in the double Gaussian scenario. These results are shown in Table 34

7.2 ALP in DUNE near detector

The Deep Underground Neutrino Experiment (DUNE) Near Detector [185] presents an opportunity to possibly detect these ALPs [186, 187]. DUNE utilizes a 120 GeV proton beam fired at a stationary target, yielding proton-proton collisions. The subsequent production of particles yields some number of π^0 (about 2.89 per proton-proton interaction) that will immediately decay into ALPs via mixing. The assumption from

this point is that the ALPs will decay into 2γ inside the near detector located 574m from the interaction point. The near detector is comprised of a Liquid Argon Time Projection Chamber (LArTPC) immediately followed by a Multi-Purpose Detector (MPD). Some number of axions produced via mixing will then decay within the detectors yielding photons that can be detected. The detectors will measure the invariant mass of the diphoton and the opening angle of the pair. For the purposes of our simulation, we include all ALPs that decay inside either detector for an effective detector length of 10m.

Using PYTHIA we can simulate what the distributions will be of the energy of the axion and the opening angle of the photon pair. To determine the ALP production due to meson mixing, we simulate a 120 GeV proton beam colliding with a fixed target using PYTHIA8 [188] with the "SoftQCD:all=on" option. We simulate 10^9 protons-on-target and extract all of the π^0 from the decay products. Since the pions are produced isotropically at the interaction point, we select only those that have a momentum that intersects with the detector, this is about 1% of all pions produced. After mixing, the ALP will have the same 3-momentum as the pion but the energy is scaled to an ALP mass of 200 MeV. The ALP is now directed at the detector and we select various values for the decay width to obtain $a \to \gamma\gamma$ events within the detector. Since we are interested in the invariant mass of the diphoton and the opening angle we make a plot of each. The probability of any of these particles decaying within the detector is given by

$$\mathcal{P}_{\rm det} = e^{-\frac{L_{\rm det}}{c\tau_a\gamma_a\beta_a}} - e^{-\frac{L_{\rm det}+d}{c\tau_a\gamma_a\beta_a}} \ , \tag{216}$$

where $L_{\rm det}$ is the distance from the interaction point to the detector, d is the length of the detector, and τ, γ, β are the lifetime, boost, and velocity of the ALP, respectively.

For a value of $c\tau = 1\text{m} \ll \text{d}_{\rm det}$, we obtain distributions as shown in Fig. 15. For a value of $c\tau = 10000\text{m} \gg \text{d}_{\rm det}$, we obtain distributions as shown if Fig. 16. As is evident in the distributions, there is significant dependence on the width/lifetime of

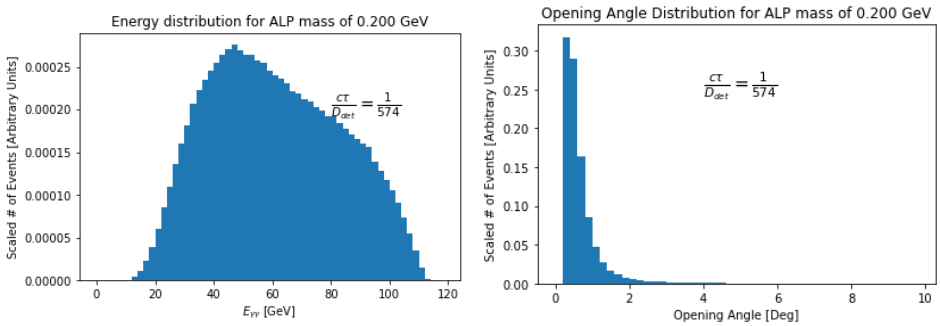

Figure 15: Diphoton energy and opening angle distributions ($c\tau = 1$ m) at the Dune Near Detector facility for an ALP mass of 200 MeV.

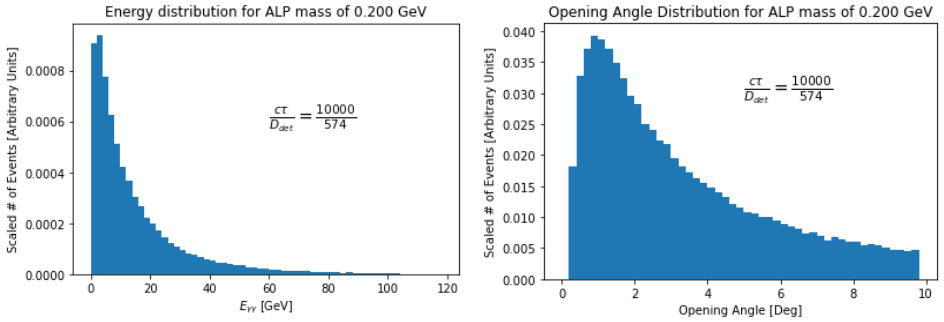

Figure 16: Diphoton energy and opening angle distributions ($c\tau = 10000$ m) at the Dune Near Detector facility for an ALP mass of 200 MeV.

the ALP. We are in the process of determining this dependence.

7.3 Conclusions

We have constructed a signal and soft constraints on the ALP mass and width that will inform particle search experiments on the unique signal characteristics that can be used to identify an ALP. We have also produced the distributions of energy and opening angle of the diphoton decay of an ALP in the Dune Near Detector. A similar construction of the energy and opening angle can be used to construct the distributions that will be produced at the ForwArd Search ExpeRiment (FASER) experiment [189] proposed at the LHC.

8 Summary

In this work I have proposed several solutions to various anomalies within the Standard Model. The $B \to \pi K$ puzzle has been solved in two different ways, using a diquark and an ALP. The $b \to s\mu\mu$ anomaly has also been lifted with the introduction of a leptoquark. The diquark proposed along with the leptoquark have been show to generate neutrino masses as well. The ALP has also been shown to lift the $(g-2)_{\mu,e}$ anomalies as well.

I have also looked a the D meson regime and explicitly determined the connection between the $SU(3)$ matrix elements and diagrammatic approaches. The introduction of R-parity violating SUSY particles has also explained the recent discrepancies in CP asymmetries in that system.

I have begun to apply the characteristics of the ALP to detector simulations to clearly identify the measureable signals that various experiments may be able to utilize in searches for these particles.

Bibliography

References

[1] A. A. Petrov, *Indirect Searches for New Physics*. CRC Press, Boca Raton, 5, 2021, 10.1201/9781351176019.

[2] M. Savage and M. Wise, *SU(3) predictions for nonleptonic B meson decays*, *Phys. Rev. D* **39** (1989) 3346.

[3] B. Grinstein and R. Lebed, *SU(3) decomposition of two-body B decay amplitudes*, *Phys. Rev. D* **53** (1996) 6344 [hep-ph/9602218].

[4] X.-G. He, Y.-J. Shi and W. Wang, *Unification of Flavor SU(3) Analyses of Heavy Hadron Weak Decays*, *Eur. Phys. J. C* **80** (2020) 359 [1811.03480].

[5] X.-G. He and W. Wang, *Flavor SU(3) Topological Diagram and Irreducible Representation Amplitudes for Heavy Meson Charmless Hadronic Decays: Mismatch and Equivalence*, *Chin. Phys. C* **42** (2018) 103108 [1803.04227].

[6] C. Quigg, *Charmed Meson Decays and the Structure of the Charged Weak Current*, *Z. Phys. C* **4** (1980) 55.

[7] T. A. Kaeding, *Tables of SU(3) isoscalar factors*, *Atom. Data Nucl. Data Tabl.* **61** (1995) 233 [nucl-th/9502037].

[8] M. Savage, *SU(3) violations in the nonleptonic decay of charmed hadrons*, *Phys. Lett. B* **257** (1991) 414.

[9] M. Gronau, O. Hernandez, D. London and J. Rosner, *Decays of B mesons to two light pseudoscalars*, *Phys. Rev. D* **50** (1994) 4529 [hep-ph/9404283].

[10] A. J. Buras and L. Silvestrini, *Nonleptonic two-body B decays beyond factorization*, *Nucl. Phys. B* **569** (2000) 3 [hep-ph/9812392].

[11] M. Imbeault, A. Datta and D. London, *Hadronic B decays: A General approach*, *Int. J. Mod. Phys. A* **22** (2007) 2057 [hep-ph/0603214].

[12] B. Bhattacharya, M. Gronau and J. L. Rosner, *Nonleptonic Charm Decays and CP Violation*, in *5th International Workshop on Charm Physics*, 7, 2012, 1207.6390.

[13] B. Bhattacharya, M. Gronau and J. L. Rosner, *CP asymmetries in singly-Cabibbo-suppressed D decays to two pseudoscalar mesons*, *Phys. Rev. D* **85** (2012) 054014 [1201.2351].

[14] D. Zeppenfeld, *SU(3) relations for B meson decays*, *Z. Phys. C* **8** (1981) 77.

[15] S. Müller, U. Nierste and S. Schacht, *Topological amplitudes in D decays to two pseudoscalars: A global analysis with linear $SU(3)_F$ breaking*, *Phys. Rev. D* **92** (2015) 014004 [1503.06759].

[16] L. Wolfenstein, *Parametrization of the Kobayashi-Maskawa matrix*, *Phys. Rev. Lett.* **51** (1983) 1945.

[17] M. Golden and B. Grinstein, *Enhanced CP Violations in Hadronic Charm Decays*, *Phys. Lett. B* **222** (1989) 501.

[18] D. Pirtskhalava and P. Uttayarat, *CP Violation and Flavor SU(3) Breaking in D-meson Decays*, *Phys. Lett. B* **712** (2012) 81 [1112.5451].

[19] H.-Y. Cheng and C.-W. Chiang, *Direct CP violation in two-body hadronic charmed meson decays*, *Phys. Rev. D* **85** (2012) 034036 [1201.0785].

[20] H.-Y. Cheng and C.-W. Chiang, *SU(3) symmetry breaking and CP violation in D -> PP decays*, *Phys. Rev. D* **86** (2012) 014014 [1205.0580].

[21] T. Feldmann, S. Nandi and A. Soni, *Repercussions of Flavour Symmetry Breaking on CP Violation in D-Meson Decays*, *JHEP* **06** (2012) 007 [1202.3795].

[22] G. Hiller, M. Jung and S. Schacht, *SU(3)-flavor anatomy of nonleptonic charm decays*, *Phys. Rev. D* **87** (2013) 014024 [1211.3734].

[23] A. F. Falk, Y. Grossman, Z. Ligeti and A. A. Petrov, *$SU(3)$ breaking and $D^0 - \bar{D}^0$ mixing*, *Phys. Rev. D* **65** (2002) 054034 [hep-ph/0110317].

[24] A. Datta, H. J. Lipkin and P. J. O'Donnell, *Simple relations for two-body B decays to charmonium and tests for eta eta-prime mixing*, *Phys. Lett. B* **529** (2002) 93 [hep-ph/0111336].

[25] A. A. Petrov, *Intrinsic charm of light mesons and CP violation in heavy quark decay*, *Phys. Rev. D* **58** (1998) 054004 [hep-ph/9712497].

[26] Particle Data Group collaboration, *Review of Particle Physics*, *PTEP* **2020** (2020) 083C01.

[27] B. Bhattacharya and J. L. Rosner, *Charmed meson decays to two pseudoscalars*, *Physical Review D* **81** (2010) .

[28] Y. Grossman and D. J. Robinson, *SU(3) Sum Rules for Charm Decay*, *JHEP* **04** (2013) 067 [1211.3361].

[29] A. Khodjamirian and A. A. Petrov, *Direct CP asymmetry in $D \to \pi^-\pi^+$ and $D \to K^-K^+$ in QCD-based approach*, *Phys. Lett. B* **774** (2017) 235 [1706.07780].

[30] LHCb collaboration, *Observation of CP Violation in Charm Decays*, *Phys. Rev. Lett.* **122** (2019) 211803 [1903.08726].

[31] LHCb collaboration, *Evidence for CP violation in time-integrated $D^0 \to h^- h^+$ decay rates*, *Phys. Rev. Lett.* **108** (2012) 111602 [1112.0938].

[32] H.-Y. Cheng and C.-W. Chiang, *Direct CP violation in charmed meson decays within the standard model*, in *11th International Workshop on the CKM Unitarity Triangle*, 12, 2021, 2112.14398.

[33] Q. Qin, C. Wang, D. Wang and S.-H. Zhou, *The factorization-assisted topological-amplitude approach and its applications*, 2111.14472.

[34] I. Bediaga and C. Göbel, *Direct CP violation in beauty and charm hadron decays*, *Prog. Part. Nucl. Phys.* **114** (2020) 103808 [2009.07037].

[35] M. Saur and F.-S. Yu, *Charm CPV: observation and prospects*, *Sci. Bull.* **65** (2020) 1428 [2002.12088].

[36] LHCb collaboration, *Observation of direct CP violation in D^0 meson decays at LHCb*, 1905.05428.

[37] A. Soni, *Resonance enhancement of Charm CP*, 1905.00907.

[38] F. Buccella, A. Paul and P. Santorelli, *$SU(3)_F$ breaking through final state interactions and CP asymmetries in $D \to PP$ decays*, *Phys. Rev. D* **99** (2019) 113001 [1902.05564].

[39] LHCb collaboration, *Mixing and indirect CP violation using two-body decays at LHCb*, *PoS* **CHARM2016** (2016) 071.

[40] A. Dery and Y. Nir, *Implications of the LHCb discovery of CP violation in charm decays*, *JHEP* **12** (2019) 104 [1909.11242].

[41] D. Delepine, G. Faisel and C. A. Ramirez, *Direct CP violation in $D^+ \to K^0(\bar{K}^0)\pi^+$ decays as a probe for new physics*, *Eur. Phys. J. C* **80** (2020) 596 [1903.02422].

[42] P. Santorelli, *CP Violation in nonleptonic two-body decays of D Mesons*, *PoS* **CHARM2016** (2017) 019.

[43] S. Fajfer, *Theoretical perspective on rare and radiative charm decays*, in *7th International Workshop on Charm Physics*, 9, 2015, 1509.01997.

[44] B. Bhattacharya, M. Gronau and J. L. Rosner, *CP asymmetries in singly-Cabibbo-suppressed D decays to two pseudoscalar mesons*, *Phys. Rev. D* **85** (2012) 054014 [1201.2351].

[45] B. Bhattacharya, M. Gronau and J. L. Rosner, *Direct CP Violation in D Decays in view of LHCb and CDF Results*, 1207.0761.

[46] B. Bhattacharya, D. London, M. Gronau and J. L. Rosner, *Shift in weak phase γ due to CP asymmetries in D decays to two pseudoscalar mesons*, *Phys. Rev. D* **87** (2013) 074002 [1301.5631].

[47] J. L. Rosner, *Final state phases in charmed meson two-body nonleptonic decays*, *Phys. Rev. D* **60** (1999) 114026 [hep-ph/9905366].

[48] B. Bhattacharya and J. L. Rosner, *Flavor symmetry and decays of charmed mesons to pairs of light pseudoscalars*, *Phys. Rev. D* **77** (2008) 114020 [0803.2385].

[49] B. Bhattacharya and J. L. Rosner, *Charmed meson decays to two pseudoscalars*, *Phys. Rev. D* **81** (2010) 014026 [0911.2812].

[50] B. Bhattacharya, *Relative phases in dalitz plots for $D^0 \to 3$ pseudoscalars*, Ph.D. thesis, Chicago U., 11, 2011.

[51] M. IMBEAULT, A. DATTA and D. LONDON, *Hadronic b decays: A general approach*, *International Journal of Modern Physics A* **22** (2007) 2057?2092.

[52] Particle Data Group collaboration, *Review of Particle Physics*, *Phys. Rev. D* **98** (2018) 030001.

[53] BESIII collaboration, *Measurements of absolute branching fractions for D mesons decays into two pseudoscalar mesons*, *Phys. Rev. D* **97** (2018) 072004 [1802.03119].

[54] CLEO collaboration, *Measurement of exclusive D meson decays to eta and eta-prime final states and SU(3) amplitude analysis*, *Phys. Rev. D* **77** (2008) 092003 [0802.2664].

[55] Particle Data Group collaboration, *Review of Particle Physics*, *Phys. Rev. D* **98** (2018) 030001.

[56] D. Besson, T. K. Pedlar, J. Xavier, D. Cronin-Hennessy, K. Y. Gao, J. Hietala et al., *Improved measurements of d meson semileptonic decays to π and k mesons*, *Physical Review D* **80** (2009) .

[57] for the ETM Collaboration collaboration, *Scalar and vector form factors of $d \to \pi(k)\ell\nu$ decays with $N_f = 2 + 1 + 1$ twisted fermions*, *Phys. Rev. D* **96** (2017) 054514.

[58] G. Bhattacharyya, *A Brief review of R-parity violating couplings*, in *Workshop on Physics Beyond the Standard Model: Beyond the Desert: Accelerator and Nonaccelerator Approaches*, pp. 194–201, 6, 1997, hep-ph/9709395.

[59] A. Datta, J. M. Yang, B.-L. Young and X. Zhang, *R-parity violating supersymmetry effects and signals in single top production at the Tevatron*, *Phys. Rev. D* **56** (1997) 3107 [hep-ph/9704257].

[60] A. Datta, *R parity violating SUSY and CP violation in B —¿ phi K(S)*, *Phys. Rev. D* **66** (2002) 071702 [hep-ph/0208016].

[61] R. Barbier, C. Berat, M. Besaneon, M. Chemtob, A. Deandrea, E. Dudas et al., *R-parity-violating supersymmetry*, *Physics Reports* **420** (2005) 1?195.

[62] C. Nishi, *Simple derivation of general Fierz-like identities*, *Am. J. Phys.* **73** (2005) 1160 [hep-ph/0412245].

[63] D. Choudhury and P. Roy, *New constraints on lepton nonconserving R-parity violating couplings*, *Phys. Lett. B* **378** (1996) 153 [hep-ph/9603363].

[64] S. Abel, *CP violation in R-parity violating models*, *Phys. Lett. B* **410** (1997) 173 [hep-ph/9612272].

[65] H. Dreiner, M. Kramer and B. O'Leary, *Bounds on R-parity violating supersymmetric couplings from leptonic and semi-leptonic meson decays*, *Phys. Rev. D* **75** (2007) 114016 [hep-ph/0612278].

[66] M. Chemtob, *Phenomenological constraints on broken R parity symmetry in supersymmetry models*, *Prog. Part. Nucl. Phys.* **54** (2005) 71 [hep-ph/0406029].

[67] R. Barbier et al., *R-parity violating supersymmetry*, *Phys. Rept.* **420** (2005) 1 [hep-ph/0406039].

[68] F. Domingo, H. K. Dreiner, J. S. Kim, M. E. Krauss, M. Lozano and Z. S. Wang, *Updating Bounds on R-Parity Violating Supersymmetry from Meson Oscillation Data*, *JHEP* **02** (2019) 066 [1810.08228].

[69] G. Isidori, J. F. Kamenik, Z. Ligeti and G. Perez, *Implications of the LHCb Evidence for Charm CP Violation*, *Phys. Lett. B* **711** (2012) 46 [1111.4987].

[70] J. Liu, N. McGinnis, C. E. M. Wagner and X.-P. Wang, *A Light Scalar Explanation of $(g-2)_\mu$ and the KOTO Anomaly*, 2001.06522.

[71] KOTO collaboration, *Status on the Search for $K_L^0 \to \pi^0\nu\bar{\nu}$ with the KOTO Experiment*, in *Meeting of the Division of Particles and Fields of the American Physical Society (DPF2019) Boston, Massachusetts, July 29-August 2, 2019*, 2019, 1910.07585.

[72] KOTO collaboration, *New results on the search for rare kaon events with the KOTO detector*, 2019, 1910.07148.

[73] A. J. Buras, D. Buttazzo, J. Girrbach-Noe and R. Knegjens, *$K^+ \to \pi^+\nu\overline{\nu}$ and $K_L \to \pi^0\nu\overline{\nu}$ in the Standard Model: status and perspectives*, *JHEP* **11** (2015) 033 [1503.02693].

[74] G. Ruggiero, "New results on $K^+ \to \pi^+\nu\bar{\nu}$ from the NA62 experiment." https://indico.cern.ch/event/769729/contributions/3510938/attachments/1905346/3146619/kaon2019_ruggiero_final.pdf, 10, 2019.

[75] S. Adler et al., *Measurement of the $K^+ \to \pi^+\nu\overline{\nu}$ branching ratio*, *Phys. Rev. D* **77** (2008) 052003.

[76] BNL-E949 collaboration, *Study of the decay $K^+ \to \pi^+\nu\bar{\nu}$ in the momentum region $140 < P_\pi < 199$ MeV/c*, *Phys. Rev.* **D79** (2009) 092004 [0903.0030].

[77] N. Deshpande and X.-G. He, *Consequences of R-parity violating interactions for anomalies in $\bar{B} \to D^{(*)}\tau\bar{\nu}$ and $b \to s\mu^+\mu^-$*, *Eur. Phys. J. C* **77** (2017) 134 [1608.04817].

[78] F. James, *MINUIT Function Minimization and Error Analysis: Reference Manual Version 94.1*, .

[79] H. Dembinski and P. O. et al., *scikit-hep/iminuit*, .

[80] O. C. Kong, *LR scalar mixings and oneloop neutrino masses*, *JHEP* **09** (2000) 037 [hep-ph/0004107].

[81] B. Bhattacharya, A. Datta, D. London and S. Shivashankara, *Simultaneous Explanation of the R_K and $R(D^{(*)})$ Puzzles*, *Phys. Lett.* **B742** (2015) 370 [1412.7164].

[82] A. K. Alok, A. Datta, A. Dighe, M. Duraisamy, D. Ghosh and D. London, *New Physics in b− > sμ+μ−: CP-Conserving Observables*, *JHEP* **11** (2011) 121 [1008.2367].

[83] A. K. Alok, A. Datta, A. Dighe, M. Duraisamy, D. Ghosh and D. London, *New Physics in b -¿ s mu+ mu-: CP-Violating Observables*, *JHEP* **11** (2011) 122 [1103.5344].

[84] LHCb collaboration, *Measurement of Form-Factor-Independent Observables in the Decay $B^0 \to K^{*0}\mu^+\mu^-$*, *Phys. Rev. Lett.* **111** (2013) 191801 [1308.1707].

[85] LHCb collaboration, *Angular analysis of the $B^0 \to K^{*0}\mu^+\mu^-$ decay using 3 fb^{-1} of integrated luminosity*, *JHEP* **02** (2016) 104 [1512.04442].

[86] Belle collaboration, *Angular analysis of $B^0 \to K^*(892)^0\ell^+\ell^-$*, in *Proceedings, LHCSki 2016 - A First Discussion of 13 TeV Results: Obergurgl, Austria, April 10-15, 2016*, 2016, 1604.04042.

[87] ATLAS collaboration, *Angular analysis of $B_d^0 \to K^*\mu^+\mu^-$ decays in pp collisions at $\sqrt{s} = 8$ TeV with the ATLAS detector*, .

[88] CMS collaboration, *Measurement of the P_1 and P_5' angular parameters of the decay $\mathrm{B}^0 \to \mathrm{K}^{*0}\mu^+\mu^-$ in proton-proton collisions at $\sqrt{s} = 8$ TeV*, .

[89] LHCb collaboration, *Differential branching fraction and angular analysis of the decay $B_s^0 \to \phi\mu^+\mu^-$*, *JHEP* **07** (2013) 084 [1305.2168].

[90] LHCb collaboration, *Angular analysis and differential branching fraction of the decay $B_s^0 \to \phi\mu^+\mu^-$*, *JHEP* **09** (2015) 179 [1506.08777].

[91] LHCb collaboration, *Test of lepton universality using $B^+ \to K^+\ell^+\ell^-$ decays*, *Phys. Rev. Lett.* **113** (2014) 151601 [1406.6482].

[92] LHCb collaboration, *Search for lepton-universality violation in $B^+ \to K^+\ell^+\ell^-$ decays*, 1903.09252.

[93] LHCb collaboration, *Test of lepton universality with $B^0 \to K^{*0}\ell^+\ell^-$ decays*, *JHEP* **08** (2017) 055 [1705.05802].

[94] Belle collaboration, *Test of lepton flavor universality in $B \to K^*\ell^+\ell^-$ decays at Belle*, 1904.02440.

[95] A. Datta, M. Duraisamy and D. Ghosh, *Explaining the $B \to K^*\mu^+\mu^-$ data with scalar interactions*, *Phys. Rev.* **D89** (2014) 071501 [1310.1937].

[96] A. Datta, J. Kumar, J. Liao and D. Marfatia, *New light mediators for the R_K and R_{K^*} puzzles*, *Phys. Rev.* **D97** (2018) 115038 [1705.08423].

[97] A. Datta, J. Kumar and D. London, *The B Anomalies and New Physics in $b \to se^+e^-$*, 1903.10086.

[98] A. K. Alok, A. Dighe, S. Gangal and D. Kumar, *Continuing search for new physics in $b \to s\mu\mu$ decays: two operators at a time*, 1903.09617.

[99] M. Ciuchini, A. M. Coutinho, M. Fedele, E. Franco, A. Paul, L. Silvestrini et al., *New Physics in $b \to s\ell^+\ell^-$ confronts new data on Lepton Universality*, 1903.09632.

[100] J. Aebischer, W. Altmannshofer, D. Guadagnoli, M. Reboud, P. Stangl and D. M. Straub, *B-decay discrepancies after Moriond 2019*, 1903.10434.

[101] M. Alguero, B. Capdevila, S. Descotes-Genon, P. Masjuan and J. Matias, *What R_K and Q_5 can tell us about New Physics in $b \to s\ell\ell$ transitions?*, 1902.04900.

[102] L. Calibbi, A. Crivellin and T. Ota, *Effective Field Theory Approach to b?s??(?), B?K(*)?$\overline{?}$ and B?D(*)?? with Third Generation Couplings*, *Phys. Rev. Lett.* **115** (2015) 181801 [1506.02661].

[103] B. Bhattacharya, A. Datta, J.-P. Guevin, D. London and R. Watanabe, *Simultaneous Explanation of the R_K and $R_{D^{(*)}}$ Puzzles: a Model Analysis*, *JHEP* **01** (2017) 015 [1609.09078].

[104] A. Greljo, G. Isidori and D. Marzocca, *On the breaking of Lepton Flavor Universality in B decays*, *JHEP* **07** (2015) 142 [1506.01705].

[105] A. Datta, J. Liao and D. Marfatia, *A light Z' for the R_K puzzle and nonstandard neutrino interactions*, *Phys. Lett.* **B768** (2017) 265 [1702.01099].

[106] A. K. Alok, B. Bhattacharya, A. Datta, D. Kumar, J. Kumar and D. London, *New Physics in $b \to s\mu^+\mu^-$ after the Measurement of R_{K^*}*, *Phys. Rev.* **D96** (2017) 095009 [1704.07397].

[107] A. Datta, B. Dutta, S. Liao, D. Marfatia and L. E. Strigari, *Neutrino scattering and B anomalies from hidden sector portals*, *JHEP* **01** (2019) 091 [1808.02611].

[108] F. Sala and D. M. Straub, *A New Light Particle in B Decays?*, *Phys. Lett.* **B774** (2017) 205 [1704.06188].

[109] W. Altmannshofer, M. J. Baker, S. Gori, R. Harnik, M. Pospelov, E. Stamou et al., *Light resonances and the low-q^2 bin of R_{K^*}*, *JHEP* **03** (2018) 188 [1711.07494].

[110] M. Kohda, H. Sugiyama and K. Tsumura, *Lepton number violation at the LHC with leptoquark and diquark*, *Phys. Lett.* **B718** (2013) 1436 [1210.5622].

[111] S.-Y. Guo, Z.-L. Han, B. Li, Y. Liao and X.-D. Ma, *Interpreting the $R_{K^{(*)}}$ anomaly in the colored Zee–Babu model*, *Nucl. Phys.* **B928** (2018) 435 [1707.00522].

[112] A. J. Buras, R. Fleischer, S. Recksiegel and F. Schwab, *The B —¿ pi K puzzle and its relation to rare B and K decays*, *Eur. Phys. J.* **C32** (2003) 45 [hep-ph/0309012].

[113] A. J. Buras, R. Fleischer, S. Recksiegel and F. Schwab, *B —¿ pi pi, new physics in B —¿ pi K and implications for rare K and B decays*, *Phys. Rev. Lett.* **92** (2004) 101804 [hep-ph/0312259].

[114] A. J. Buras, R. Fleischer, S. Recksiegel and F. Schwab, *Anatomy of prominent B and K decays and signatures of CP violating new physics in the electroweak penguin sector*, *Nucl. Phys.* **B697** (2004) 133 [hep-ph/0402112].

[115] S. Baek, P. Hamel, D. London, A. Datta and D. A. Suprun, *The B —¿ pi K puzzle and new physics*, *Phys. Rev.* **D71** (2005) 057502 [hep-ph/0412086].

[116] N. B. Beaudry, A. Datta, D. London, A. Rashed and J.-S. Roux, *The $B \to \pi K$ puzzle revisited*, *JHEP* **01** (2018) 074 [1709.07142].

[117] R. Fleischer, R. Jaarsma and K. K. Vos, *Towards new frontiers with $B \to \pi K$ decays*, *Phys. Lett.* **B785** (2018) 525 [1712.02323].

[118] R. Fleischer, R. Jaarsma, E. Malami and K. K. Vos, *Exploring $B \to \pi\pi, \pi K$ decays at the high-precision frontier*, *Eur. Phys. J.* **C78** (2018) 943 [1806.08783].

[119] K. S. Babu and C. N. Leung, *Classification of effective neutrino mass operators*, *Nucl. Phys.* **B619** (2001) 667 [hep-ph/0106054].

[120] K. Cheung, T. Nomura and H. Okada, *Three-loop neutrino mass model with a colored triplet scalar*, *Phys. Rev.* **D95** (2017) 015026 [1610.04986].

[121] D. Aristizabal Sierra and M. Hirsch, *Experimental tests for the Babu-Zee two-loop model of Majorana neutrino masses*, *JHEP* **12** (2006) 052 [hep-ph/0609307].

[122] M. Carpentier and S. Davidson, *Constraints on two-lepton, two quark operators*, *Eur. Phys. J.* **C70** (2010) 1071 [1008.0280].

[123] MEG collaboration, *Search for the lepton flavour violating decay $\mu^+ \to e^+\gamma$ with the full dataset of the MEG experiment*, *Eur. Phys. J.* **C76** (2016) 434 [1605.05081].

[124] BaBar collaboration, *Searches for Lepton Flavor Violation in the Decays tau+- —¿ e+- gamma and tau+- —¿ mu+- gamma*, *Phys. Rev. Lett.* **104** (2010) 021802 [0908.2381].

[125] M. Beneke, G. Buchalla, M. Neubert and C. T. Sachrajda, *QCD factorization in B —¿ pi K, pi pi decays and extraction of Wolfenstein parameters*, *Nucl. Phys.* **B606** (2001) 245 [hep-ph/0104110].

[126] G. F. Giudice, B. Gripaios and R. Sundrum, *Flavourful Production at Hadron Colliders*, *JHEP* **08** (2011) 055 [1105.3161].

[127] A. Datta and D. London, *Measuring new physics parameters in B penguin decays*, *Phys. Lett.* **B595** (2004) 453 [hep-ph/0404130].

[128] A. Datta, M. Imbeault, D. London, V. Page, N. Sinha and R. Sinha, *Methods for measuring new-physics parameters in B decays*, *Phys. Rev.* **D71** (2005) 096002 [hep-ph/0406192].

[129] S. Baek, C.-W. Chiang and D. London, *The B —¿ pi K Puzzle: 2009 Update*, *Phys. Lett.* **B675** (2009) 59 [0903.3086].

[130] UTfit collaboration, *Model-independent constraints on $\Delta F = 2$ operators and the scale of new physics*, *JHEP* **03** (2008) 049 [0707.0636].

[131] G. Bhattacharyya, D. Choudhury and K. Sridhar, *R-parity violating SUSY or leptoquarks: Virtual effects in dilepton production*, *Phys. Lett.* **B349** (1995) 118 [hep-ph/9412259].

[132] P. Bandyopadhyay and R. Mandal, *Revisiting scalar leptoquark at the LHC*, *Eur. Phys. J.* **C78** (2018) 491 [1801.04253].

[133] ATLAS collaboration, *Search for scalar leptoquarks in pp collisions at $\sqrt{s}$ = 13 TeV with the ATLAS experiment*, *New J. Phys.* **18** (2016) 093016 [1605.06035].

[134] CMS collaboration, *Search for third-generation scalar leptoquarks decaying to a top quark and a τ lepton at $\sqrt{s}$ = 13 TeV*, *Eur. Phys. J.* **C78** (2018) 707 [1803.02864].

[135] CMS collaboration, *Search for pair production of first and second generation leptoquarks in proton-proton collisions at $\sqrt{s}$ = 8TeV*, *Phys. Rev.* **D93** (2016) 032004 [1509.03744].

[136] CMS collaboration, *Search for Third-Generation Scalar Leptoquarks in the $t\tau$ Channel in Proton-Proton Collisions at $\sqrt{s}$ = 8 TeV*, *JHEP* **07** (2015) 042 [1503.09049].

[137] CMS collaboration, *Search for narrow resonances decaying to dijets in proton-proton collisions at $\sqrt{(s)}$ = 13 TeV*, *Phys. Rev. Lett.* **116** (2016) 071801 [1512.01224].

[138] F. Capozzi, E. Di Valentino, E. Lisi, A. Marrone, A. Melchiorri and A. Palazzo, *Global constraints on absolute neutrino masses and their ordering*, *Phys. Rev.* **D95** (2017) 096014 [1703.04471].

[139] Particle Data Group collaboration, *Review of particle physics*, *Phys. Rev. D* **98** (2018) 030001.

[140] G. Hiller and I. Nisandzic, *R_K and R_{K^*} beyond the standard model*, *Phys. Rev.* **D96** (2017) 035003 [1704.05444].

[141] S. Baek and D. London, *Is There Still a $B \to \pi K$ Puzzle?*, *Phys. Lett. B* **653** (2007) 249 [hep-ph/0701181].

[142] M. Gronau, O. F. Hernandez, D. London and J. L. Rosner, *Electroweak penguins and two-body B decays*, *Phys. Rev. D* **52** (1995) 6374 [hep-ph/9504327].

[143] M. Neubert and J. L. Rosner, *New bound on gamma from $B^\pm \to \pi K$ decays*, *Phys. Lett. B* **441** (1998) 403 [hep-ph/9808493].

[144] M. Neubert and J. L. Rosner, *Determination of the weak phase gamma from rate measurements in $B^\pm \to \pi K, \pi\pi$ decays*, *Phys. Rev. Lett.* **81** (1998) 5076 [hep-ph/9809311].

[145] M. Gronau, D. Pirjol and T.-M. Yan, *Model independent electroweak penguins in B decays to two pseudoscalars*, *Phys. Rev. D* **60** (1999) 034021 [hep-ph/9810482].

[146] G. Buchalla, A. J. Buras and M. E. Lautenbacher, *Weak decays beyond leading logarithms*, *Rev. Mod. Phys.* **68** (1996) 1125 [hep-ph/9512380].

[147] HFLAV collaboration, *Averages of b-hadron, c-hadron, and τ-lepton properties as of summer 2016*, *Eur. Phys. J. C* **77** (2017) 895 [1612.07233].

[148] LHCb collaboration, *Measurement of CP Violation in the Decay $B^+ \to K^+\pi^0$*, *Phys. Rev. Lett.* **126** (2021) 091802 [2012.12789].

[149] LHCb collaboration, *Measurement of CP asymmetries in two-body $B^0_{(s)}$-meson decays to charged pions and kaons*, *Phys. Rev. D* **98** (2018) 032004 [1805.06759].

[150] R. D. Peccei and H. R. Quinn, *CP Conservation in the Presence of Instantons*, *Phys. Rev. Lett.* **38** (1977) 1440.

[151] R. D. Peccei and H. R. Quinn, *Constraints Imposed by CP Conservation in the Presence of Instantons*, *Phys. Rev. D* **16** (1977) 1791.

[152] S. Weinberg, *A New Light Boson?*, *Phys. Rev. Lett.* **40** (1978) 223.

[153] F. Wilczek, *Problem of Strong P and T Invariance in the Presence of Instantons*, *Phys. Rev. Lett.* **40** (1978) 279.

[154] W. Altmannshofer, S. Gori and D. J. Robinson, *Constraining axionlike particles from rare pion decays*, *Phys. Rev. D* **101** (2020) 075002 [1909.00005].

[155] OPAL collaboration, *Multiphoton production in e+ e- collisions at s**(1/2) = 181-GeV to 209-GeV*, *Eur. Phys. J. C* **26** (2003) 331 [hep-ex/0210016].

[156] D. Cadamuro and J. Redondo, *Cosmological bounds on pseudo Nambu-Goldstone bosons*, *JCAP* **02** (2012) 032 [1110.2895].

[157] M. Millea, L. Knox and B. Fields, *New Bounds for Axions and Axion-Like Particles with keV-GeV Masses*, *Phys. Rev. D* **92** (2015) 023010 [1501.04097].

[158] P. F. Depta, M. Hufnagel and K. Schmidt-Hoberg, *Robust cosmological constraints on axion-like particles*, *JCAP* **05** (2020) 009 [2002.08370].

[159] H. Ishida, S. Matsuzaki and Y. Shigekami, *Flavor imprints on axion-like particles at 140 MeV disentangled from pion-like signals*, 2006.02725.

[160] M. Bauer, M. Neubert and A. Thamm, *Collider Probes of Axion-Like Particles*, *JHEP* **12** (2017) 044 [1708.00443].

[161] J. Jaeckel and M. Spannowsky, *Probing MeV to 90 GeV axion-like particles with LEP and LHC*, *Phys. Lett. B* **753** (2016) 482 [1509.00476].

[162] M. Chala, G. Guedes, M. Ramos and J. Santiago, *Running in the ALPs*, *Eur. Phys. J. C* **81** (2021) 181 [2012.09017].

[163] M. Bauer, M. Neubert, S. Renner, M. Schnubel and A. Thamm, *The Low-Energy Effective Theory of Axions and ALPs*, 2012.12272.

[164] J. Martin Camalich, M. Pospelov, P. N. H. Vuong, R. Ziegler and J. Zupan, *Quark Flavor Phenomenology of the QCD Axion*, *Phys. Rev. D* **102** (2020) 015023 [2002.04623].

[165] F. Björkeroth, E. J. Chun and S. F. King, *Flavourful Axion Phenomenology*, *JHEP* **08** (2018) 117 [1806.00660].

[166] M. Bauer, M. Neubert, S. Renner, M. Schnubel and A. Thamm, *Consistent treatment of axions in the weak chiral Lagrangian*, 2102.13112.

[167] Belle-II collaboration, *Detectors for extreme luminosity: Belle II*, *Nucl. Instrum. Meth. A* **907** (2018) 46.

[168] M. Beneke, T. Huber and X.-Q. Li, *NNLO vertex corrections to non-leptonic B decays: Tree amplitudes*, *Nucl. Phys. B* **832** (2010) 109 [0911.3655].

[169] A. Khodjamirian and A. V. Rusov, *$B_s \to K\ell\nu_\ell$ and $B_{(s)} \to \pi(K)\ell^+\ell^-$ decays at large recoil and CKM matrix elements*, *JHEP* **08** (2017) 112 [1703.04765].

[170] E. Izaguirre, T. Lin and B. Shuve, *Searching for Axionlike Particles in Flavor-Changing Neutral Current Processes*, *Phys. Rev. Lett.* **118** (2017) 111802 [1611.09355].

[171] A. Datta, J. L. Feng, S. Kamali and J. Kumar, *Resolving the $(g-2)_\mu$ and B Anomalies with Leptoquarks and a Dark Higgs Boson*, *Phys. Rev. D* **101** (2020) 035010 [1908.08625].

[172] Muon g-2 collaboration, *Measurement of the Positive Muon Anomalous Magnetic Moment to 0.46 ppm*, *Phys. Rev. Lett.* **126** (2021) 141801 [2104.03281].

[173] L. Morel, Z. Yao, P. Cladé and S. Guellati-Khélifa, *Determination of the fine-structure constant with an accuracy of 81 parts per trillion*, *Nature* **588** (2020) 61.

[174] R. H. Parker, C. Yu, W. Zhong, B. Estey and H. Müller, *Measurement of the fine-structure constant as a test of the Standard Model*, *Science* **360** (2018) 191 [1812.04130].

[175] T. Aoyama, M. Hayakawa, T. Kinoshita and M. Nio, *Tenth-Order QED Contribution to the Electron g-2 and an Improved Value of the Fine Structure Constant*, *Phys. Rev. Lett.* **109** (2012) 111807 [1205.5368].

[176] T. Aoyama, T. Kinoshita and M. Nio, *Theory of the Anomalous Magnetic Moment of the Electron*, *Atoms* **7** (2019) 28.

[177] D. Hanneke, S. Fogwell and G. Gabrielse, *New Measurement of the Electron Magnetic Moment and the Fine Structure Constant*, *Phys. Rev. Lett.* **100** (2008) 120801 [0801.1134].

[178] W.-Y. Keung, D. Marfatia and P.-Y. Tseng, *Axion-like particles, two-Higgs-doublet models, leptoquarks, and the electron and muon g-2*, 2104.03341.

[179] B. Bhattacharya, A. Datta, D. Marfatia, S. Nandi and J. Waite, *Axion-like particles resolve the $B \to \pi K$ and g-2 anomalies*, 2104.03947.

[180] A. Kundu, S. K. Patra and S. Roy, *A complete analysis of all $B \to \pi K$ decays*, 2106.15633.

[181] J. D. Bjorken, S. Pakvasa and S. F. Tuan, *Yet another extension of the standard model: Oases in the desert?*, *Phys. Rev. D* **66** (2002) 053008 [hep-ph/0206116].

[182] A. V. Anisovich, V. V. Anisovich, L. G. Dakhno, M. A. Matveev, V. A. Nikonov and A. V. Sarantsev, *The rho —> gamma pi and omega —> gamma pi decays in quark-model approach and estimation of coupling for pion emission by quark*, *Phys. Atom. Nucl.* **73** (2010) 462 [0901.4854].

[183] G. Hiller and A. S. Safir, *Predictions forb→k decays*, *Journal of High Energy Physics* **2005** (2005) 011–011.

[184] I. Adachi, T. Browder, P. Križan, S. Tanaka and Y. Ushiroda, *Detectors for extreme luminosity: Belle ii*, *Nuclear Instruments and Methods in Physics Research Section A: Accelerators, Spectrometers, Detectors and Associated Equipment* **907** (2018) 46.

[185] DUNE collaboration, *Deep Underground Neutrino Experiment (DUNE) Near Detector Conceptual Design Report*, *Instruments* **5** (2021) 31 [2103.13910].

[186] K. J. Kelly, S. Kumar and Z. Liu, *Heavy axion opportunities at the DUNE near detector*, *Phys. Rev. D* **103** (2021) 095002 [2011.05995].

[187] J. M. Berryman, A. de Gouvea, P. J. Fox, B. J. Kayser, K. J. Kelly and J. L. Raaf, *Searches for Decays of New Particles in the DUNE Multi-Purpose Near Detector*, *JHEP* **02** (2020) 174 [1912.07622].

[188] C. Bierlich et al., *A comprehensive guide to the physics and usage of PYTHIA 8.3*, 2203.11601.

[189] FASER Collaboration collaboration, *Faser's physics reach for long-lived particles*, *Phys. Rev. D* **99** (2019) 095011.

Appendix

Appendix

$$\begin{aligned}
\psi^c &= C\overline{\psi}^T \\
\overline{\psi}^c &= (\psi^c)^\dagger\gamma^0 = -\psi^T C^{-1} \\
(\gamma^\mu)^T &= -C^{-1}\gamma^\mu C \\
C^{-1} &= C^\dagger
\end{aligned} \tag{217}$$

$$\begin{aligned}
H &= Y_d^{ij}\overline{d}^c_{i\alpha}P_R d_{j\beta}S^{\alpha\beta} \\
H^\dagger &= Y_d^{ij*}d^\dagger_{j\beta}P_R(-d^T_{i\alpha}C^{-1})^\dagger S^{*\alpha\beta} \\
&= -Y_d^{ij*}\overline{d}_{j\beta}P_L(\gamma^0 C d^*_{i\alpha})S^{*\alpha\beta}
\end{aligned} \tag{218}$$

Integrating out diquark

$$\begin{aligned}
H_{eff} &= -Y_d^{13}\overline{d}^c_\alpha P_R b_\beta S^{\alpha\beta} \otimes Y_d^{12*}s^\dagger_\beta P_R(-d^T_\alpha C^{-1})^\dagger S^{*\alpha\beta} \\
&= -\frac{Y_d^{13}Y_d^{12*}}{m_S^2}\overline{d}^c_\alpha P_R b_\beta \overline{s}_\beta P_L(\gamma^0 C d^*_\alpha) \\
&= \frac{Y_d^{13}Y_d^{12*}}{2m_S^2}\overline{d}^c_\alpha\gamma^\mu P_L(\gamma^0 C d^*_\alpha)\overline{s}_\beta\gamma_\mu P_R b_\beta \\
&= \frac{Y_d^{13}Y_d^{12*}}{2m_S^2}\overline{s}_\beta\gamma_\mu P_R b_\beta\left[-d^T_\alpha C^{-1}\gamma^\mu P_L(\gamma^0 C d^*_\alpha)\right] \\
&= -\frac{Y_d^{13}Y_d^{12*}}{2m_S^2}\overline{s}_\beta\gamma_\mu P_R b_\beta\left[d^T_\alpha\gamma^{\mu T}P_L^T(\gamma^{0T}d^*_\alpha)\right] \\
&= -\frac{Y_d^{13}Y_d^{12*}}{2m_S^2}\overline{s}_\beta\gamma_\mu P_R b_\beta\left[d^\dagger_\alpha\gamma^0 P_L\gamma^\mu d_\alpha\right]^T \\
&= \frac{Y_d^{13}Y_d^{12*}}{2m_S^2}\overline{s}_\beta\gamma_\mu P_R b_\beta\overline{d_\alpha}\gamma^\mu P_R d_\alpha
\end{aligned} \tag{219}$$

Because $S^{\alpha\beta}$ is symmetric/antisymmetric there is an additional factor of 2. In other words S^{12} can contract with S^{12} and S^{21}.

VITA

Education

Master of Science Physics	May 2016	University of Nevada, Las Vegas (UNLV)
Bachelor of Science Mathematics	Aug 2010	University of Maryland, College Park (UMCP)

Employment

Teaching Assistant Ole Miss	Aug 2016-Present	2 years as Engineering Physics Lab TA — 3 semesters PHYS221 — 1 semester PHYS222 4 years as SCALE-UP facilitator PHYS211-212
Instructor Ole Miss	Summer 2020	Instructor of Record for 2 semester Calc-based Physics Course of 14 students —PHYS211 & PHYS212 (Administered virtually via Zoom)
Instructor Ole Miss	Summer 2019	Instructor of Record Calc-based Physics Course of 12 students —PHYS211
Instructor Ole Miss	Summer 2018	Instructor of Record for 2 semester Trig-based Physics Course of 25 students — PHYS213-214
Graduate Assistant UNLV	Aug 2014 - May 2016	2 years as Engineering Physics Lab TA — 2 semesters PHYS180L — 2 semesters PHYS181L
Undergraduate Researcher UNLV	Aug 2013 - May 2014	Computer Simulations of Seifert Surfaces
Undergraduate Researcher UMCP	Fall 2001	Hyperbolic Geometry Simulations using Java

Kitchen Supervisor Rachel's Kitchen Las Vegas, NV	Jan 2013 - Nov 2013	Oversaw kitchen operations and employees
Numismatist Annapolis Coin Exchange	Jan 2010 - Dec 2012	Maintain $2 million inventory
General Manager DP Dough - College Park, MD	Jan 2000 - May 2010	Small Business Operator
Air Transportation Specialist USAF - Andrews AFB	Aug 2003 - Dec 2006	Load and Process Passengers and Cargo in aircraft

Publications/Presentations

Publications

Journal of High Energy Physics	Oct 2021	Flavor SU(3) in Cabibbo-favored D-meson decays
Physical Review D	Sept 2021	Axionlike particles resolve the $B \to \pi K$ and $g-2$ anomalies
Physical Review D	Sept 2019	A unified explanation of $b \to s\mu\mu$ anomalies, neutrino masses, and the $B \to \pi K$ puzzle
Master's Thesis UNLV	May 2016	The Hopf Fibration and Encoding Torus Knots in Light Fields

Presentations

85th annual meeting of Mississippi Academy of Sciences	Aug 2021	Flavor SU(3) in Cabibbo-favored D-meson decays
86th annual meeting of Southeast Section of the American Physical Society	Nov 2019	A unified explanation of $b \to s\mu\mu$ anomalies, neutrino masses, and the $B \to \pi K$ puzzle
Cottrell Scholars Collaborative National TA Workshop	May 2019	Workshop to revamp the methods used to orient and train new TAs in our department. Chosen as the Physics Dept TA representative.
Colloquium Ole Miss	Oct 2019	The $B \to \pi K$ puzzle
LaTeX Workshop Ole Miss	Sept 2017	Taught other graduate students basics of using LaTeX
Colloquium Ole Miss	Oct 2018	Coherent Elastic Neutrino-Nucleon Scattering

Organizations

University of Mississippi Physics Graduate Student Association (PGSA)	Member since 2016	Outreach Coordinator (2018) Student Affairs Coordinator (2017)
Society of Physics Students (SPS)	Member since 2016	Participated in several community outreach events
Pi Mu Epsilon (PME) UMCP Chapter	Aug 2001 - Aug 2010	Activities Coordinator (2002)

Awards/Honors

Dissertation Fellowship	Ole Miss	Spring 2022
Dean's Honors List	UNLV	Spring 2014 Fall 2013
Dean's List	UMCP	Spring 2009 Fall 2008